Investigation of the degradation of LSM-YSZ SOFC cathode by electrochemical impedance spectroscopy

Torres da Silva, Iris Maura; Mogensen, Mogens Bjerg; Hjelm, Johan

Publication date:
2012

Document Version
Publisher's PDF, also known as Version of record

Fuel Cells and Solid State Chemistry Division
Risø National Laboratory for Sustainable Energy
Technical University of Denmark

PhD thesis
Investigation of the degradation of LSM-YSZ SOFC cathode by electrochemical impedance spectroscopy

Iris Maura Torres da Silva

Roskilde, October 2011

ABSTRACT

The aim of this PhD study was to investigate degradation of the LSM-YSZ cathode of anode supported Ni-YSZ/YSZ/LSM-YSZ solid oxide fuel cells.

The chosen cathode materials LSM25 and 8YSZ were investigated for their compatibility and stability, to confirm that expansion/contraction or decreasing conductivity would not be a problem during degradation experiments of the cells. The experiments carried out for this purpose include x-ray diffraction, conductivity and dilatometry.

LSM-YSZ/YSZ/LSM-YSZ symmetrical cells were prepared and investigated by means of electrochemical impedance spectroscopy, at different operating conditions. An equivalent circuit was developed for the symmetrical cell, describing the processes taking place at the LSM-YSZ cathode. This equivalent circuit was applied in degradation studies, where the processes affected by degradation over time could be pinpointed. Furthermore, it was discovered that impurities in air cause significant degradation of the cathode. Humidity was found to increase the degradation rate, but other impurities might also be present and increasing degradation.

Then the anode supported Ni-YSZ/YSZ/LSM-YSZ single cells were prepared and tested. It was found that at the applied operating conditions the impedance data could not be deconvoluted as anode and cathode processes were overlapping. Nonetheless it appeared that at OCV the degradation of the cathode is similar for symmetrical and single cells. Under current degradation was significantly lower, so real performance and degradation data can only be obtained on single cells as symmetrical cells can only be tested at OCV. For single cells degradation caused by impurities from air was also observed.

ACKNOWLEDGEMENTS

This work was supported financially by The Programme Commission on Sustainable Energy and Environment, The Danish Council for Strategic Research, via the SERC project (www.serc.dk), contract no. 2104-06-0011. The work was supervised by Research professor Mogens Mogensen and senior scientist Dr. Johan Hjelm, both at Risø National Laboratory for Sustainable Energy, Technical University of Denmark.

First of all I would like to thank Sune Ebbesen for introducing me to Risø, and recommending me to Mogens Mogensen. Without you this adventure wouldn't even have started!
Thank you, Professor Mogens Mogensen for giving me this opportunity of carrying out a PhD study at Risø DTU at the Fuel Cells and Solid State Chemistry Division. And of course also for being my supervisor over the last three years, you are a true inspiration!
Johan Hjelm, a big big thank you for you. You are the best supervisor any PhD student could wish for; knowledgeable, motivating, inspiring and patient. And much more than just a supervisor! Thank you so much for all the personal help you have also given me outside the PhD arena, without you I don't think I could have coped with the Danish system…
My officemate Ming Chen, I enjoyed our little 'cultural' fights over the amount of sun that should enter our office, but most of all I enjoyed your company, always a positive and content spirit around!
All my colleagues at the division, you are too many to mention separately, but I have enjoyed so much working with all of you and learning more about your cultures. It was great to see how such a diverse multicultural group of people can achieve so many things! Especially to my Danish colleagues: continue opening yourself up to your foreign colleagues; they are definitely worth the effort!
Thank you Ruth and Jake for enjoying many lunches with me, the little bit of extra sunshine we got at the window and sharing all kinds of thoughts, ideas, frustrations and Australian laid-back-ness with you was a hard needed break in the middle of things!

Thanks Ragnar, Ruth, Kristian and Marie for putting up with me in the car driving from København and back! Missing our tiny personality fights Rags, and thanks Ruth and Kristian for keeping us from making it any more than that! Loved sharing the gossip and stroopwafels with you guys ☺.
Thank you Kaska, Shital, Marie, Ruth, Pia, Ragnar, Kristian, Jonathan and Frank for spending quality time outside of work as well! I loved the dinners and hanging out, I wish we would have done that even more. You all have conquered a space in my heart.
'Danish' capoeiristas, thanks for all the training, roda's and good times. Without capoeira and you guys to release some adrenaline my Danish life would have been a lot more boring and tense. Obrigada professor Almiran para me deichar treinar com você sempre. Aprendi muito! Thanks all teachers and students!
Thank you Luca and Damien, for our many coffees, dinners and brunches, it was great to share quality time with you guys and I will be missing you…
A special thanks to Kaska and Gaea, you are just amazing! Sharing hardship and a lot of fun, you have been an amazing support for me, especially my last couple of months in Denmark. The trampoline and capoeira class is waiting for you in the Netherlands!

Mamsie, Titia, Hein, Hein en Sien, dankjulliewel! Eerst 'emigreren' naar Duitsland, dan nog wat verder naar Denemarken! Gelukkig is de cirkel nu doorbroken en kom ik weer jullie richting uit ☺ Mag ik binnenkort eindelijk de tante zijn die ik al die tijd had willen zijn!
Thanks capoeiristas of Cordão de Ouro Holanda, for always keeping in touch, and moreover for taking care of my boy and our teacher, while I was still back in Denmark. Coming back to you all truly feels like a warm bath!

Muito obrigada meu amor, sem você sempre me esforçando realmente eu não consegui este trabalho. Você e a minha vida, nunca mais quero estar/morar/viver sem você.

Best wishes and hugs for every single one of you,
Iris

CONTENTS

1. Introduction…… 7
    1.1 The solid oxide fuel cell…… 8
    1.2 The cathode…… 9
    1.3 Electrochemical Impedance Spectroscopy……. 11
    1.4 Project motivation…….. 14
    1.5 Objectives……... 15
    1.6 References…….. 15
2. LSM25-8YSZ Material studies…….. 17
    2.1 Introduction…… 18
    2.2 Experimental…….. 18
    2.3 Results…… 19
    2.4 Discussion…….. 27
    2.5 Conclusion……. 31
    2.6 References……. 32
3. Characterization of LSM-YSZ SOFC cathodes by Electrochemical Impedance Spectroscopy…… 33
    7.1 Introduction…… 34
    7.2 Experimental…….. 36
    7.3 Results and discussion……... 37
    7.4 Conclusion……. 52
    7.5 References…….. 53
4. The influence of impurities in air on the long-term performance of LSM-YSZ SOFC cathodes……. 56
    4.1 Introduction…… 57
    4.2 Experimental…….. 58
    4.3 Results and discussion…… 60
    4.4 Conclusion……... 73
    4.5 References…….. 74
5. Additional results on symmetrical cells……..76
    5.1 Introduction…… 77
    5.2 Experimental…….. 77
    5.3 Results and discussion…… 78
    5.4 Conclusion……..83

6. Characterisation of anode supported Ni-YSZ/YSZ/LSM-YSZ single cells…….85
    6.1 Introduction…… 86
    6.2 Experimental……...86
    6.3 Results and discussion…… 88
    6.4 Conclusion……..100
    6.5 References…….. 101
7. General discussion, conclusions and outlook…….102
    7.1 General discussion and conclusions……... 103
    7.2 Main conclusions……..... 105
    7.3 Outlook……....106
    7.4 References ……...106

CHAPTER 1

Introduction

1.1 The solid oxide fuel cell

With increasing world wide energy demands, and a call for more sustainable energy solutions, the solid oxide fuel cell (SOFC) could be entering a flourishing market. Preconditions for commercialisation are; (1) the production costs have to be sufficiently low in comparison to competing techniques; (2) durability should be sufficiently long, how long exactly depends on the type of application; (3) reliability of the complete system should be no issue.

In an SOFC a fuel is converted to electricity, the working principle is shown in Figure 1.1.

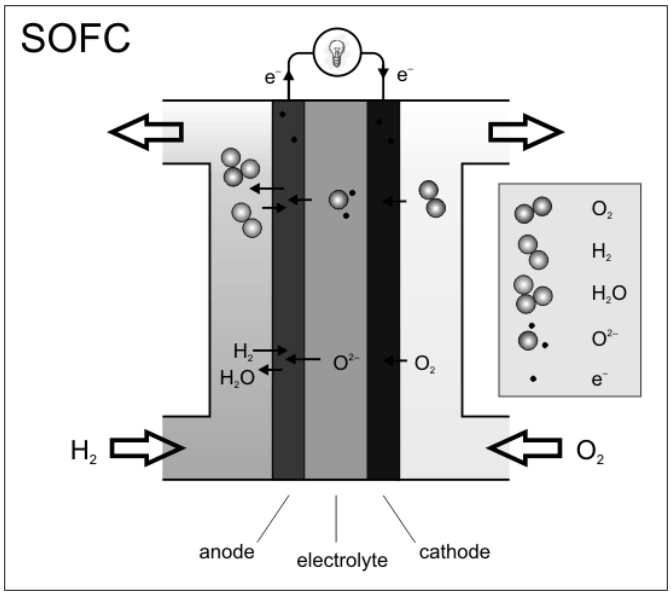

Figure 1.1. Working principle of a solid oxide fuel cell

When applying hydrogen as a fuel the reaction equation will look as follows:

$$2H_2 + O_2 \rightarrow 2H_2O + \Delta G(electricity) + T\Delta S(heat) \qquad [1.1]$$

Some of the advantageous properties of the SOFC are [1]:

- Fuel flexibility: many types of (bio)fuels can be used to produce electricity.
- Minimal emissions: the emissions of a fuel cell are solely water and depending on the fuel also CO_2. If a biofuel is used the energy production can be CO_2 neutral.

- Efficiency: the SOFC is not influenced by the Carnot efficiency that sets a limit to the efficiency of normal engines. Therefore the SOFC can reach higher energy efficiency.
- An SOFC is modular, which makes it easy to deliver the power demanded by any application.
- The SOFC has low noise and does not have any moving parts.

Disadvantages of the solid oxide fuel cell are that high temperatures are required (for anode supported Ni-YSZ/YSZ/LSM-YSZ cells at least 750 °C) and start up times are therefore long. This makes them less suitable for certain applications, like cars [1].
The state-of-the-art SOFC materials are: nickel mixed with yttria stabilised zirconia (Ni-YSZ) for the anode, YSZ for the electrolyte and lanthanum (strontium) manganite (LSM) mixed with YSZ for the cathode.

1.2 The cathode

The cathode, or air electrode, of the SOFC is where oxygen reduction takes place. Oxygen from the atmosphere dissociates and reacts with electrons to form oxygen ions. They will transport to and through the electrolyte, to reach the anode, where oxygen ions react with a fuel, to form, for example, water with hydrogen gas.
The overall reaction taking place at the cathode is:

$$\frac{1}{2}O_2(g) + 2e^- \rightarrow O^{2-} \qquad [1.2]$$

or in Kröger-Vink notation:

$$\frac{1}{2}O_2(g) + 2e^{'} + V_O^{\bullet\bullet} \rightarrow O_O^x \qquad [1.3]$$

Where $V_O^{\bullet\bullet}$ is an oxygen vacancy site and O_O^x is an oxygen ion at a regular oxygen lattice site. Therefore, for oxygen reduction to continuously take place at the cathode, the generated oxygen ions have to be transported away from the reaction site into the bulk of the electrolyte.

In the earliest stages of SOFC development, platinum was used as cathode material. The high cost of platinum led to the search of inexpensive materials with similar properties. Perovskites with crystal structure ABO_3

were found to be suitable as cathode materials. Their basic structure is shown in Figure 1.2.

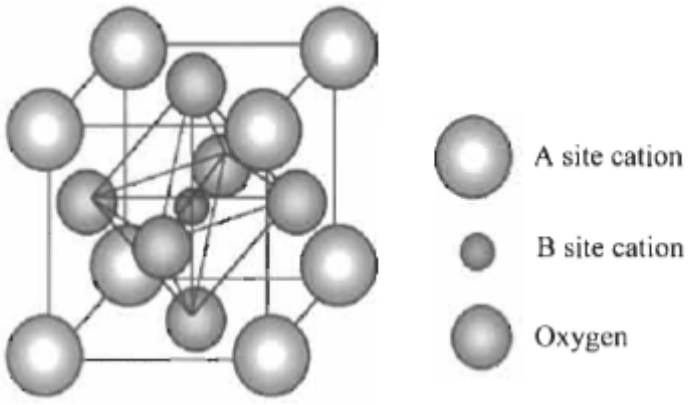

Figure 1.2. Schematic representation of lattice structure of perovskite, ABO_3 [2]

Many factors are involved in designing an optimal cathode. The most important properties a cathode material should have are as follows:

- Cheap
- Low polarisation resistance
- High catalytic activity for oxygen reduction
- High electronic conductivity
- Resistant to high temperatures
- High mechanical strength
- Compatible with the other materials used in the SOFC; specifically the electrolyte and interconnect materials:
    - The thermal expansion coefficient should be similar for each of the SOFC materials applied
    - The materials should be chemically inert, while at the same time having good adhesion to each other.
- The microstructure of the cathode should be good:
    - Porous
    - The triple phase boundary (TPB), the points where gas phase, electronically conducting material and ionically conduction material meet, should be as long as possible.
- Easy to fabricate

Some perovskites tested as cathode material in SOFCs are cobaltites, ferrites and manganites. Cobaltites, for example lanthanum cobaltite and lanthanum strontium cobaltite have shown good initial performances, but show fast degradation due to reactivity with YSZ, the most common electrolyte material. Ferrites, have shown good performance when combined with ceria-based electrolytes. One of the most popular ferrites, LSCF, lanthanum strontium cobalt ferrite, has low polarisation losses due to it being a mixed ionic electronic conductor; however, degradation remains an issue to be resolved. An extensively investigated cathode material for high temperature SOFC application is the lanthanum manganite-based materials. Degradation is found to be less severe for lanthanum manganite and the thermal expansion coefficient matches well with that of YSZ. Nonetheless, several improvements had and have to be made to make lanthanum manganites suitable for application in an SOFC. One of the issues is the fact that lanthanum manganites reacts with YSZ to form zirconates, which posses a low conductivity and therefore cause degradation of the cell, especially at higher temperatures. Approaches to inhibit zirconate formation are lowering of the calcination and operation temperature, and shortening the time of calcination. Furthermore, preparation of slightly A-site deficient LSM perovskites proved to inhibit zirconate formation further.
A second issue was the low electronic conductivity of pure $LaMnO_3$. This was solved by doping $LaMnO_3$ with other cations, of which strontium has shown to increase the electronic conductivity most. Another issue is the fact that lanthanum strontium manganites (LSM) have a high polarisation resistance, especially at lower temperatures. One of the paths to decrease this resistance was to mix the LSM cathode material with the YSZ electrolyte material, to form a composite cathode, showing highly improved performance. By optimising the composition and microstructure of the LSM-YSZ composite cathodes, further improvement can be expected.

1.3 Electrochemical Impedance Spectroscopy

One of the most important techniques to study the performance and degradation of solid oxide fuel cells is electrochemical impedance spectroscopy (EIS). EIS is a very effective technique for basic performance testing of new types of cells, materials in the cell, and reproducibility studies. Moreover, it is a powerful tool for increasing understanding the processes in the cathode, anode and electrode, leading to losses in the fuel

cells performance, and for identification of degradation mechanisms. Another advantage of EIS is that it can, unlike many other techniques, easily be applied in situ, investigating a system while it is in operation. However, EIS should not be used on its own, other techniques like electron microscopy are essential to verify observations made with EIS.

When applying electrochemical impedance spectroscopy, one applies a very small sinusoidal potential or current to any electrochemical system, for example an SOFC, to measure the response of the system. The result will be an impedance spectrum, where both the real and imaginary part of the impedance are measured as a function of the frequency of the applied potential or current:

$$Z(f) = \frac{\Delta V}{\Delta I} = Z_{real} + jZ_{imag} \qquad [1.4]$$

Z is the impedance at a certain frequency f, V being the potential, and I the current. The impedance spectrum will show all processes that are electrically stimulated, for example adsorption, transfer and transport of electrons and diffusion of reactants or ions. Each of these physical processes have their own time constant, which in principle enables separation several processes in one electrochemical system. In this way the magnitude of the processes can often be determined, as well as their activation energies and capacitances.

When applying EIS on an electrochemical system, several things have to be considered. The first one being the size of the perturbation signal; one has to be sure the magnitude of the signal does not interfere with the linearity of the system. Also important are the frequency range required to make sure all processes are included in the spectrum, and the number of points measured within this frequency range. Depending on the analysis to be carried out with the impedance spectrum, e.g. screening of materials or extensive analysis in order to understand the processes in the electrochemical system, the number of data points should be chosen accordingly. Another consideration is the time available to record and impedance spectrum; the time taken should be shorter than the timescale where any changes (degradation) of the system are expected to take place. However, the more time that can be taken, the lower the noise level and the higher the frequency range of measuring can be.

Once an impedance spectrum is recorded the spectrum can be analysed for data quality using the Kramers Krönig technique, which holistically connects the real and imaginary parts of the frequency dependent impedance, ensures that the imaginary impedance and the phase angle cannot be zero over all frequencies, and must vary with all frequencies. Boukamp et. al. developed a linearised form of the Kramers Krönig transforms [3], and the quality of measured data can be conveniently analysed using this technique.

Equivalent circuit

By combining different electrical elements, like resistors, capacitors and inductors, an equivalent circuit can be developed for each electrochemical system, fitting the measured impedance spectrum. One well known example of an equivalent circuit element is the 'RQ' element

$$Z(\omega) = \left(R^{-1} + Q \bullet (i\omega)^{n} \right)^{-1} \qquad [1.5]$$

Where R is the resistance and Q the constant phase element (CPE) and n determines the extent of depression of the arc from a perfect semicircle, as shown in Figure 1.3.

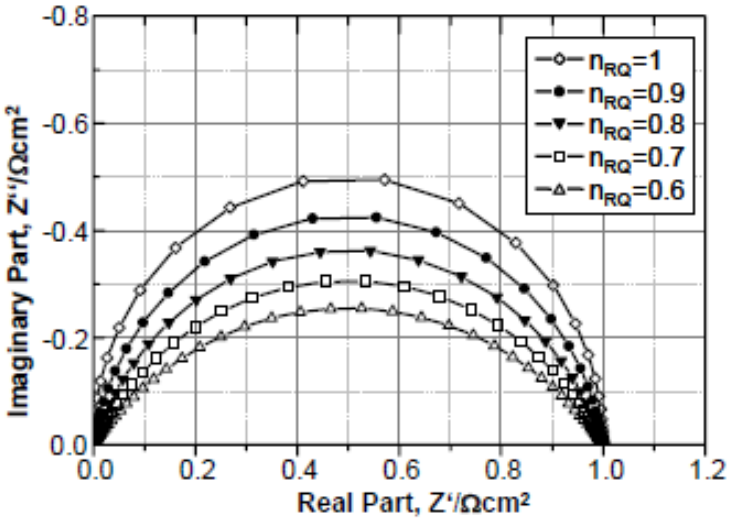

Figure 1.3. Nyquist representation of an RQ element with different n-values [4]

However, often it is possible to design many different equivalent circuits, which all lead to a good fit of the experimental data. Moreover, for SOFCs often different processes are overlapping with respect to time-scale and so the development of an equivalent circuit is a complex matter. Whenever developing an equivalent circuit it is therefore important to be able to ascribe the different elements to certain physical processes. This can be done by recording several impedance spectra at e.g. different temperatures and gas compositions and by examining the system by other techniques besides EIS. Further understanding of the data and development of an equivalent circuit can be reached by several methods. First of all there are many ways of displaying the impedance data, amongst other the Nyquist and Bode plots, in various forms [5]. These plots may each reveal a different feature of the data and therefore it is important to consider which representation(s) are chosen. Secondly, distribution of relaxation times (DRT) is a useful method of analysis to deconvolute impedance data, developed by Schichlein et al. [6]. When applying DRT, a Fourier transform is applied on the data, and the transformed data plot will have a higher degree of separation between the processes. Therefore the resulting plot can be of great help in determination of the number of processes involved in the electrochemical system, and their magnitude. The shape of the peaks reflects the nature of the underlying process, and this information can be used to guide the selection of constituent circuit elements for the equivalent circuit. Another useful analysis technique is called ADIS: analysis of differences in impedance spectra, developed by Jensen et al. [7]. By mathematically comparing two impedance spectra, recorded at different operating conditions, the summit frequency of different processes can be revealed.
Once a satisfactory equivalent circuit is developed the values of each of the element and therefore processes can be fitted using a complex nonlinear least squares (CNLS) fitting procedure, for example using Zview or ZSimpWin.

1.4 Project motivation

Many questions remain on the performance and degradation of SOFCs. Eve though cathode degradation is considered to be smaller than degradation of other parts of the SOFC, it is important to gain more knowledge about this issue and find possibilities to minimise cathode degradation. In this PhD

study LSM25-8YSZ, as part of the anode supported Ni-YSZ/YSZ/LSM-YSZ solid oxide fuel cell, was chosen as the cathode material to be investigated. LSM-YSZ is still the state-of-the-art cathode today, as it is most compatible with other SOFC materials, reliable and relatively durable.

LSM-YSZ cathode materials show some degradation over time. If the degradation processes could be understood and thereby possibly prevented, the LSM-YSZ cathode could have a promising future ahead.

1.5 Objectives

The objectives of this PhD study were:

- To develop an equivalent circuit for the electrochemical impedance response of the LSM25-8YSZ cathode.
- To gain understanding of the processes involved when the performance of the LSM25-YSZ cathode decreases with time.
- To develop ways to minimise degradation of the LSM25-YSZ cathode.

1.6 References

1. R. Steinberger-Wilckens, *5th International Solid Oxide Fuel Cell Summer School, Crete,* (2008).

2. H. Yokokawa and T. Horita, in *High Temperature Solid Oxide Fuel Cells - Fundamentals, Design and Applications*, S. C. Singhal and K. Kendall, Editors, p. 119, Elsevier Ltd. (2003).

3. B. A. Boukamp, *J. Electrochem. Soc.*, **142**(6), 1885 (1995).

4. A. Leonide, V. Sonn, A. Weber and E. Ivers-Tiffée, *ECS Trans.*, **7**(1), 521 (2007).

5. M. E. Orazem, N. Pébère and B. Tribollet, *J. Electrochem. Soc.*, **153**(4), B129 (2006).

6. H. Schichlein, A. C. Müller, M. Voigts, A. Krügel and E. Ivers-Tiffée, *J. Appl. Electrochem.*, **32**(8), 875 (2002).

7. S. H. Jensen, A. Hauch, P. V. Hendriksen, M. Mogensen, N. Bonanos and T. Jacobsen, *J. Electrochem. Soc.*, **154**(12), B1325 (2007).

CHAPTER 2

LSM25-8YSZ Material studies

2.1 Introduction

Many aspects have to be considered when developing a solid oxide fuel cell. Amongst them are the electro catalytic activity of the materials, their chemical inertness, their electrical and ionic conductivities and the thermo mechanical match between the different materials applied in the SOFC [1]. The latter three are subject of investigation in this Chapter. To ensure the compatibility of $(La_{0.75}Sr_{0.25})_{0.95}MnO_{3\pm\delta}$ (LSM25) for use in a solid oxide fuel cell, with 8-YSZ as an electrolyte, LSM25 has to be characterised at operating conditions. To be sure the mismatch between LSM25 and 8-YSZ is minimal under selected test conditions, the thermal expansion of LSM25 was determined, as well as the crystal structure. Furthermore, the conductivity of LSM25 and LSM25-8YSZ will be determined at realistic operating conditions.

2.2 Experimental

2.2.1 LSM and LSM-YSZ bars

A 50 wt% LSM25 – 50 wt% 8-YSZ powder was prepared by weighing 30 g of both $(La_{0.75}Sr_{0.25})_{0.95}MnO_{3\pm\delta}$ (pre-sintered at 950 °C) and 8-YSZ, and ball milling the mixture for 70 hours. Afterwards the powder was dried on a hot plate at 50 °C.

LSM25 and 50 % LSM25 – 50 % 8-YSZ bars (20 in total) were prepared by pressing $(La_{0.75}Sr_{0.25})_{0.95}MnO_{3\pm\delta}$ (~ 3.4 g) and 50 % LSM25 – 50 % 8-YSZ (~ 2.3 g) powders to 5 x 5 x 24 mm^3 bars. The bars were isostatically pressed at 65 ton for 20 seconds and sintered at 1000, 1050 or 1200 °C for 2 hours (the heating/cooling rate was 100 °C/h). After which the bars were cut to 18 mm length where it was ensured the ends of the bars were parallel. The sides of the bars were ground to ensure smooth surfaces. The density of the bars was determined both by the Archimedes method and by weighing each bar and measuring its dimensions.

2.2.2 X-ray diffraction

A Bruker D8 diffractometer was used to characterise both LSM25 powder and eight different LSM25 and LSM25-YSZ bars. The LSM25 powder, sintered at 950 °C, was ground and around 20 wt% of silicon was added as an internal reference. XRD spectra were recorded at room temperature, 750,

800, 850, 900, 950 and 1000 °C. The spectra of the bars were recorded at 2θ from 15 to 80 °, with a 0.05 ° step size and 3 seconds per step. Afterwards, the region of the main peak was recorded again; 2θ from 26 to 33 °, using a 0.05 ° step size and 20 seconds per step.

2.2.3 Dilatometry

A number of bars were characterised by dilatometry at 550 to 950 °C and a pO_2 of 0.21, 0.015 and $1.5 \cdot 10^{-4}$ bar. Partial oxygen pressures were generated by mixing of nitrogen and oxygen at different flow rates. The flow rates were controlled by mass flow controllers. The total flow rate was kept constant at 100 or 250 ml/min. To determine the influence of the flow rate a flow rate variation to 200 ml/min and 50 ml/min was carried out at 850 °C, while keeping all other parameters constant. The pO_2 was determined experimentally using a zirconia potentiometric pO_2 sensor. The isothermal dilatometer used was a Netzsch DIL 402 CD, and an approved standard Al_2O_3 bar was used as a reference.

2.2.4 Conductivity

Platinum wires were wound around the ends of two of the bars that were characterised by dilatometry previously. Furthermore, to ensure good contact with the bars, the ends were painted with platinum paste. The wired bars were sintered at 950_C, with a heating/cooling rate of 100_C, and 1 dwell at 950 °C. The conductivity of the bars was determined from room temperature to 1000 °C, in air. Subsequently the bars were kept at ~ 800 or ~ 850 °C and the change in conductivity with time and/or pO_2 was measured. The conductivity was determined using a 4 point probe DC-technique, using a Keithley 2700 multimeter to measure the resistance. Voltage probes were separated at 0.7 cm from each other on the bar. The pO_2 during the characterisation was determined experimentally using a zirconia potentiometric pO_2 sensor.

2.3 Results

2.3.1 Density of LSM and LSM-YSZ bars

The density of the LSM and LSM-YSZ bars was determined based on dimension and weight of the bars and by the Archimedes method. The

results are shown in Table 2.I. The confidence interval of the average values of the experimental data were calculated at the 95 % level and given in the table along with the number of bars the confidence interval is based on. For the bars sintered at 1200 °C both methods led to the same density, within experimental error. For the bars sintered at 1000 °C and 1050 °C, however, the results of the two methods differed significantly.

TABLE 2.I. Densities of LSM and LSM-YSZ bars, as determined by the Archimedes method and based on dimensions and weight. 95% confidence intervals are calculated with standard deviation, the number of samples used for calculation is shown in brackets.

Sample (bar)	**T sintering °C**	**Density Archimedes g/cm^3**	**Density size/weight g/cm^3**
LSM25	1200	6.0 ± 0.2 (4)	5.9 ± 0.1 (3)
LSM25	1050	5.8 ± 0.7 (4)	4.2 ± 0.3 (4)
LSM25	1000	5.6 ± 0.5 (2)	3.9 ± 0.2 (2)
LSM25-YSZ	1200	5.8 ± 0.1 (4)	5.6 ± 0.9 (4)
LSM25-YSZ	1050	5.2 ± 1.1 (4)	3.6 ± 0.2 (4)
LSM25-YSZ	1000	5.5 ± 0.3 (2)	3.1 ± 0.2 (2)

2.3.2 Crystal structure

The obtained x-ray diffractogram of LSM25 and silicon (internal reference) at room temperature is shown in Figure 2.1. LSM25 was matched with $La_{0.65}Sr_{0.35}MnO_3$ from the ICDD database. In Figure 2.2 the collected x-ray diffractograms for LSM25 and silicon at increasing temperatures from 750 to 1000 °C are plotted. An x-ray diffractogram was obtained for all LSM25 and LSM25-YSZ bars, sintered at 1050 or 1200 °C and both fresh and tested for conductivity and/or dilatometry. The result for the LSM25-YSZ bars, sintered at 1050°C is shown in Figure 2.3. A closer look at the region around 2θ where the main peaks of possible secondary phases; lanthanum- and strontium zirconate, are expected is given in Figure 2.4. The tested LSM25-YSZ bar, sintered at 1050 °C was tested for conductivity: two cycles up to 1000 °C at a heating and cooling rate of 1 °C/min, followed by 430 hours at 850 °C. The diffractograms of the LSM25-YSZ bars sintered at 1200 °C were similar to the ones from the same bar sintered at 1050 °C and are therefore not shown. The diffractograms for the LSM25 bars, both

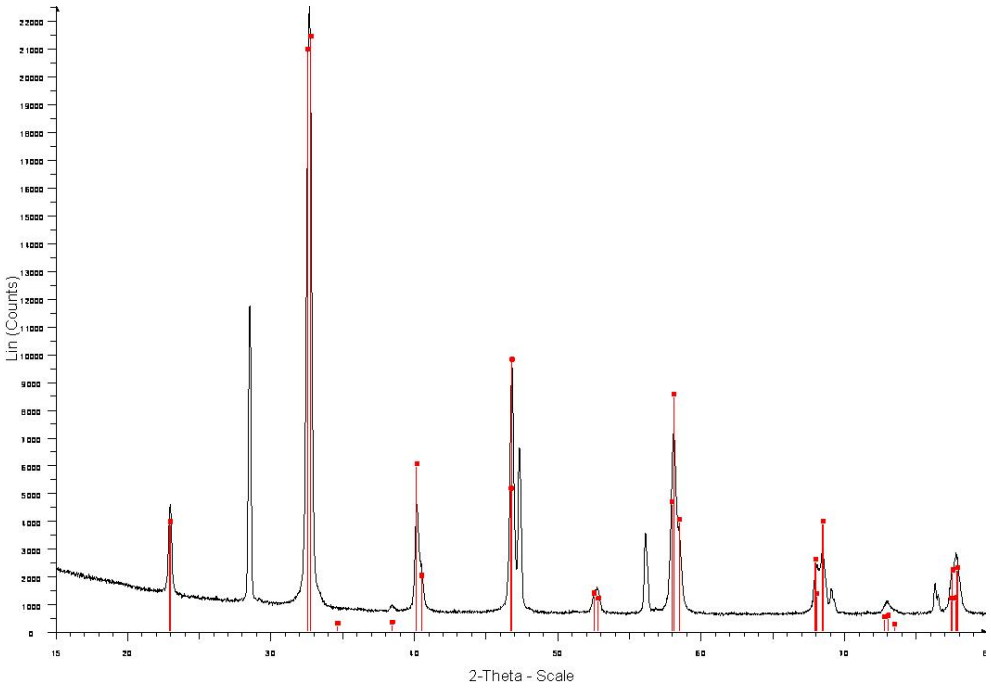

Figure 2.1. X-ray diffractogram of LSM25 and silicon at room temperature, matched with $La_{0.65}Sr_{0.35}MnO_3$ from the ICDD database (red lines).

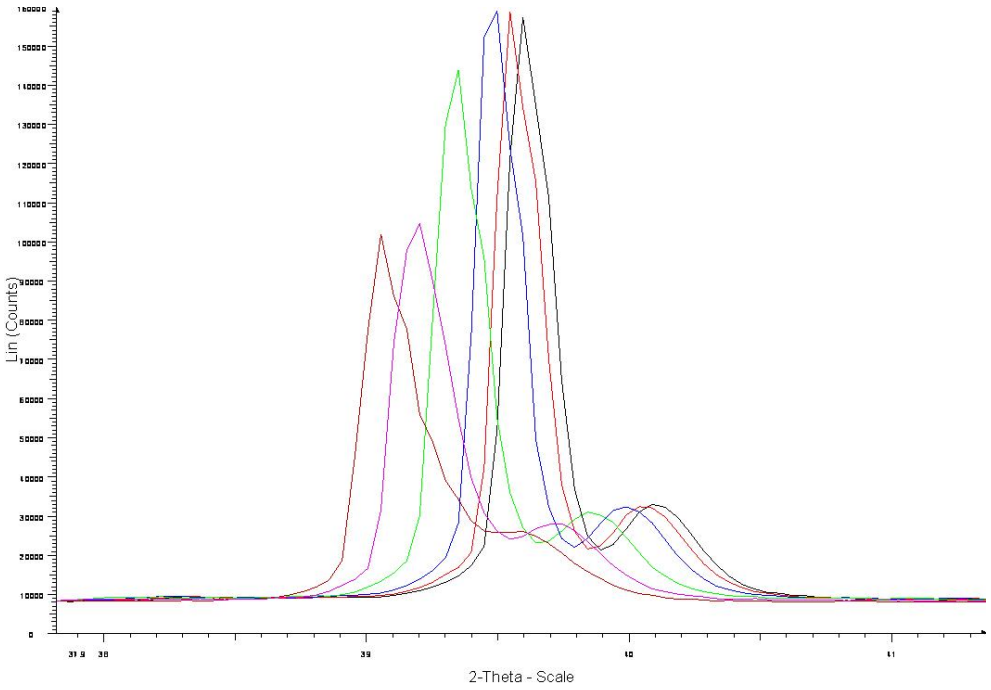

Figure 2.2. Main peak of the X-ray diffractograms obtained for LSM25 and silicon at 750 (black), 800 (red), 850 (blue), 900 (green), 950 (pink) and 1000 °C (brown).

sintered at 1050 and 1200 °C and both fresh and tested were all like the diffractogram of the LSM25 powder (Figure 2.1).

2.3.3 Dilatometry

The thermal expansion coefficient (TEC) was determined for LSM25 and LSM25-YSZ bars in the temperature interval from 50 to 800 °C. The TEC for LSM25 was 12.1 ± 0.5 [$\cdot 10^{-6}$ /K] (based on two bars) and the TEC of LSM25-YSZ was 11.7 [$\cdot 10^{-6}$ /K] (based on one bar). The effect of variations in gas flow during dilatometry experiments was investigated, while all other parameters were kept constant, and the result is shown in Figure 2.5. An almost immediate expansion was observed upon gas flow increase and a contraction was visible upon gas flow decrease. The expansion when increasing the gas flow from 100 to 200 ml/min corresponds with a thermal expansion caused by a temperature increase of 8 °C. Immediately after changing the gas flow a small temperature decrease of ~ 0.1 °C was observed, but this temperature change returned to its initial value rapidly. The length of the bar returned to its initial value when the gas flow was returned to its initial value. Preliminary dilatometry at low pO_2; down to ~ $1.5 \cdot 10^{-4}$ bar, at several temperatures on a LSM25 bar, sintered at 1200 °C was performed. The result at 850 °C is shown in Figure 2.6. A contraction of the bar was observed upon decreasing pO_2.

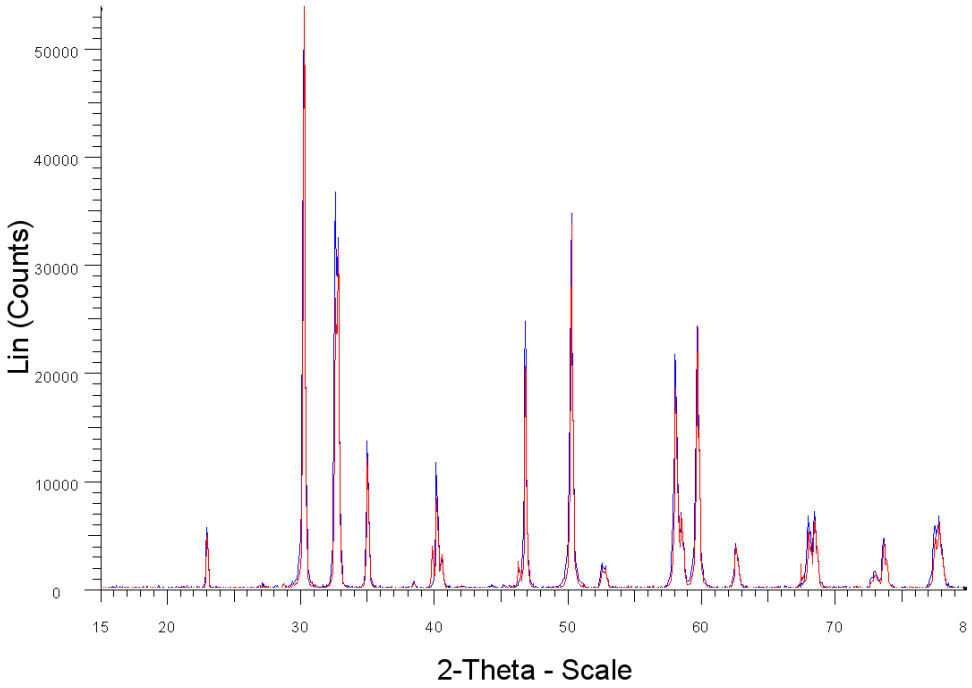

Figure 2.3. X-ray diffractograms of LSM25-YSZ bars at room temperature; fresh bar (blue), tested bar (red).

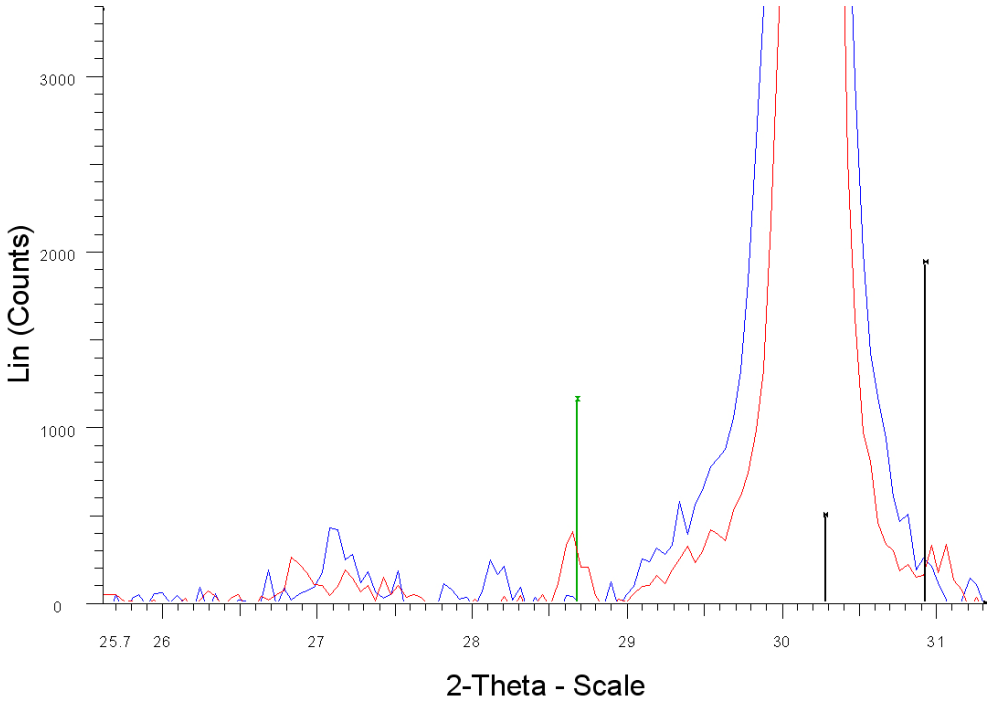

Figure 2.4. Part of the x-ray diffractograms of LSM25-YSZ bars at room temperature; fresh bar (blue), tested bar (red), main peak position of lanthanum zirconate (green), main peak position of strontium zirconate (black).

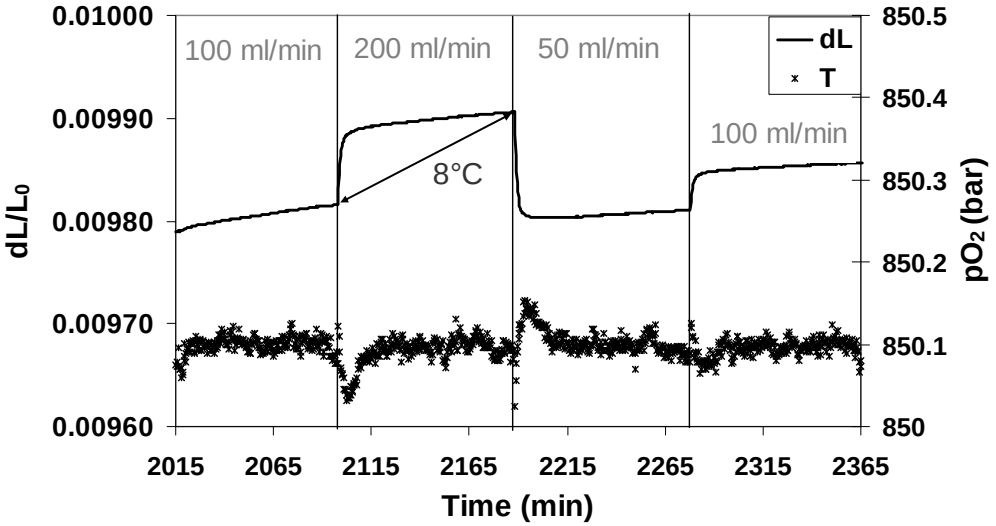

Figure 2.5. Length change of a LSM25 bar (sintered at 1200 °C) at 850 °C, while changing the gas flow (air) from 100 to 200 to 50 and back to 100 ml/min. The green line shows the relative length of the bar, the red line shows the temperature as measured by the thermocouple placed ~ 1 mm above the bars.

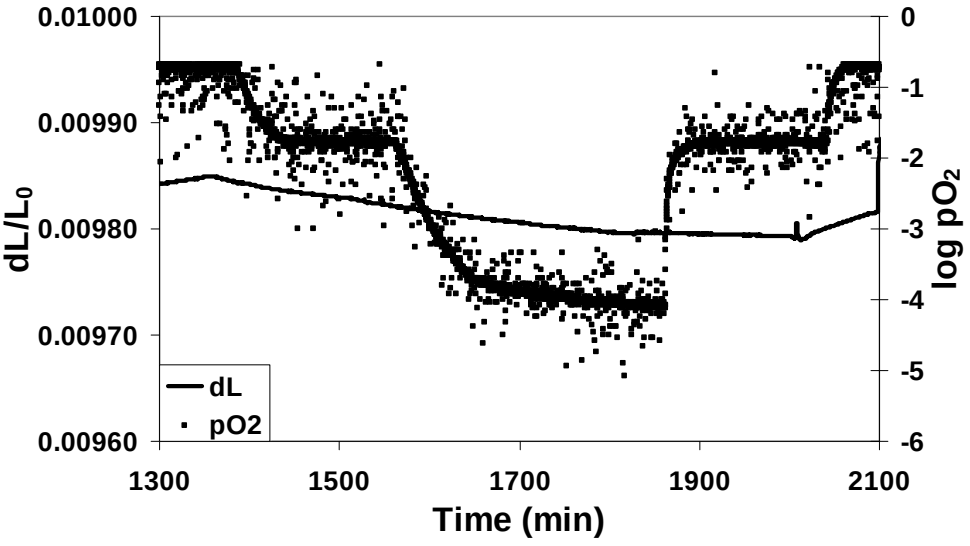

Figure 2.6. Length change of a LSM25 bar (sintered at 1200 °C) at 850 °C, while changing pO_2.

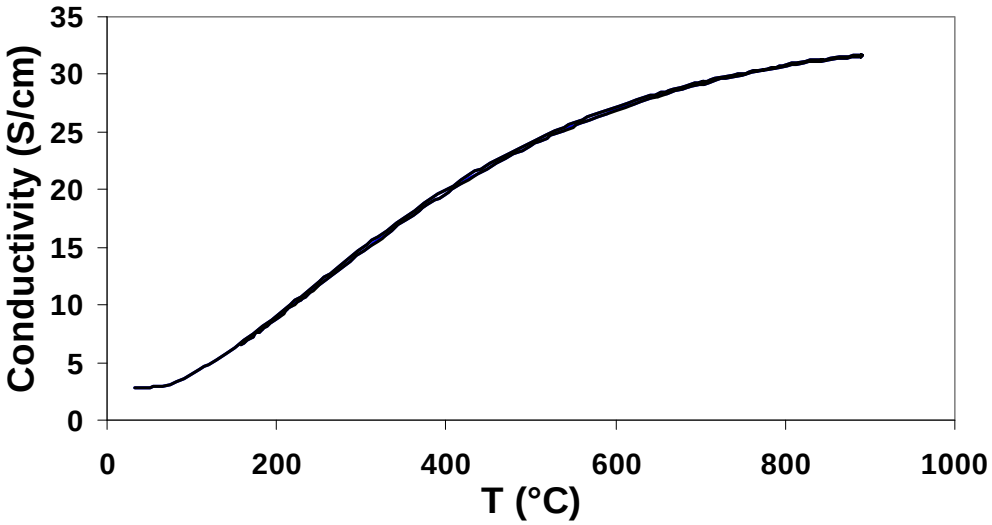

Figure 2.7. Conductivity of a LSM25-YSZ bar (sintered at 1200 °C) in air, as a function of time. Data obtained measuring both the forward and reverse conductivity through the bar.

TABLE 2.II. Conductivity at 850 °C in air, for LSM25 and LSM25-YSZ bars, sintered at 1200 or 1050 °C.

Sample (bar)	**T sintering °C**	**Conductivity** S/cm
LSM25	1200	220
LSM25	1050	111
LSM25-YSZ	1200	31
LSM25-YSZ (repro)	1200	20
LSM25-YSZ	1050	2.4

2.3.4 Conductivity

The conductivity as a function of temperature for the LSM25-YSZ bar, sintered at 1200 °C, is shown in Figure 2.7. A similar trend for the temperature dependence of the conductivity was observed for all LSM25 and LSM25-YSZ bars, although each bar had its own values for the conductivity. The conductivity for each of the tested bars at 850 °C is given in Table 2.II. Furthermore, changes in the conductivity with time were recorded for several hundred hours on the LSM25-YSZ bars. The procentual change in conductivity over time, at several temperatures, for three LSM25-YSZ bars is shown in Figure 2.8.

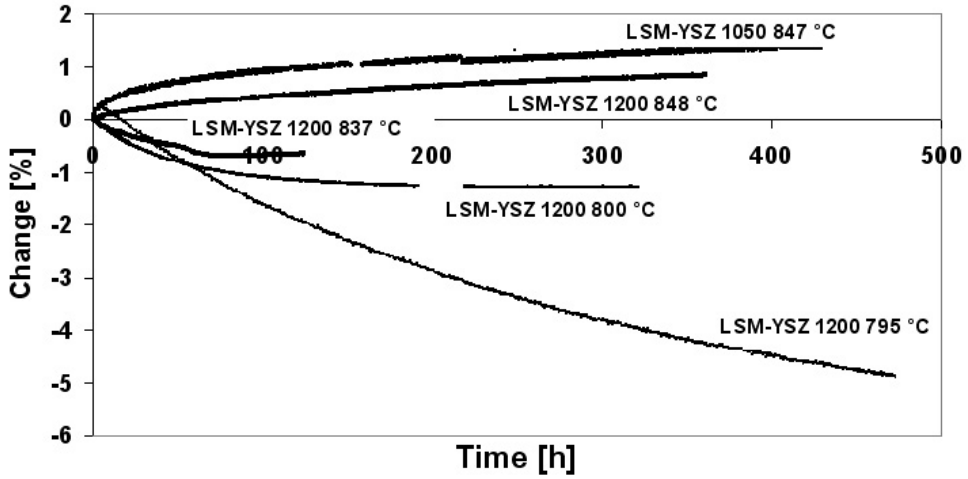

Figure 2.8. Conductivity of LSM25-YSZ bars (sintered at 1050 or 1200 °C), as a function of time, the temperature of conductivity testing is shown at each of the lines.

Two LSM25 bars, one sintered at 1050 °C, the other at 1200 °C, were subjected to changes in partial oxygen pressure. The results are shown in Figure 2.9 and 2.10. A clear, reversible decrease of the conductivity for the LSM25 bar sintered at 1050 °C with decreasing pO_2 was observed. Possible observation of a decreasing conductivity with decreasing pO_2 for the bar sintered at 1200 °C was considered to be within experimental error.

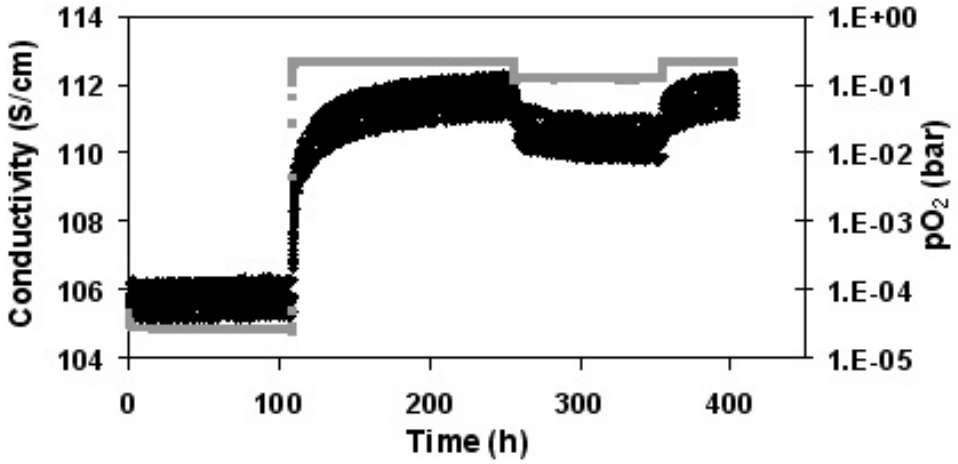

Figure 2.9. Conductivity (black) of a LSM25 bar (sintered at 1050 °C), at 850 °C under different partial oxygen pressures. On the secondary y-axis the pO_2 (grey) is monitored.

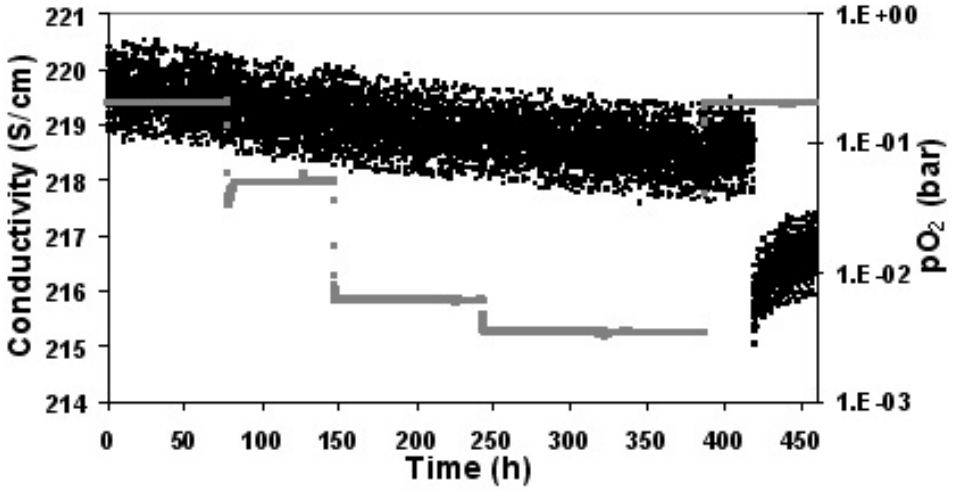

Figure 2.10. Conductivity (black) of a LSM25 bar (sintered at 1200 °C), at 850 °C under different partial oxygen pressures. On the secondary y-axis the pO_2 (grey) is monitored.

2.4 Discussion

2.4.1 Density of LSM25 and LSM25-YSZ bars

The density of both the LSM25 and LSM25-YSZ bar, sintered at 1200 °C, when determined by the Archimedes method and the method based on determination of the dimensions and weight of the bar, was to be same, within experimental error. The fact that both methods led to similar results, indicates that the bars sintered at 1200 °C are dense, at least no significant amount of open pores were accessible for liquid to enter. The bars sintered at 1000 °C and 1050 °C were porous, as the results for the density were different for each of the applied measuring methods. The density determined by the Archimedes method was significantly higher than the one determined based on measuring the dimensions and weight of the bars. The method using the dimension and weight of the bar led to the total porosity of the bars. The density determined by the Archimedes method provided more information on the proportion of open pores that are penetrated by the applied liquid, compared to the closed and non-accessible open pores available in the bar.

2.4.2 X-ray diffraction

The collected x-ray diffractograms for LSM25 and silicon powder showed the expected pattern (Figure 2.1). No phases other than LSM and silicon were observed. Furthermore, when increasing the temperature from 750 to 1000 °C, no phase change for LSM25 occurred. The peaks did however shift to lower angles and their intensity decreased, while increasing the temperature. These changed can be explained, at least for the most part, by expansion of the material at increasing temperature. All four LSM25 bars, both fresh and tested, both sintered at 1050 and 1200 °C, showed the expected x-ray diffraction pattern and were identified as single phase LSM. The LSM25-YSZ bars also showed the expected XRD pattern and were matched with LSM and YSZ single phases. Possibly however for these mixed bars some lanthanum- or strontium zirconate (LZO and SZO) phases might have formed, either during sintering, or during extensive conductivity and/or dilatometry testing. Therefore in Figure 2.4, the part of the XRD pattern is shown in which the main peaks for LZO and SZO are expected. The LSM25-YSZ bars, sintered at 1050 °C, both fresh and tested for conductivity are shown, along with the peak positions of LZO and SZO. LZO and SZO peaks were not observed above background level for either of the bars, indicating that these phases have not formed, at least in sufficient amount to be observed in XRD (>3%). Furthermore, there was no LZO or SZO, nor any other secondary phases observed by XRD for the LSM25-YSZ bars sintered at 1200 °C either.

2.4.3 Dilatometry

The thermal expansion coefficient (TEC) was determined for LSM25 and LSM25-YSZ bars in the temperature interval from 50 to 800 °C. The TEC for LSM25 was 12.1 ± 0.5 [$\cdot 10^{-6}$ /K] (based on two bars) and the TEC of LSM25-YSZ was 11.7 [[$\cdot 10^{-6}$ /K] (based on one bar). In Table 2.III the values for TEC determined in this study and TEC values found in literature are listed. The TEC for LSM25 as determined in this study is at the high end compared to values found in literature [1-4]. As expected from the lower TEC value of YSZ compared to that of LSM25, the LSM25-YSZ mixed bar was determined to have the lower TEC.

TABLE 2.III. Thermal expansion coefficients determined in this study and obtained from literature.

Material	**TEC [10^{-6} /K]**	
	50 – 800 °C	**50 – 1000 °C**
LSM25	**12.1 ± 0.5 (*2 bars*)**	
$La_{0.79}Sr_{0.20}MnO_3$	10.8 [1]	11.1 [1] / 11.3 [2] / 12.4 [2]
$La_{0.8}Sr_{0.2}MnO_3$		11.4 [4] / 12.0[1] [3]
$La_{0.69}Sr_{0.30}MnO_3$	11.7 [1]	11.8 [2] / 12.0 [1, 2] / 12.8 [2]
$La_{0.7}Sr_{0.3}MnO_3$		11.7 [3] / 11.9 [4]
$(La)_{0.95}MnO_3$		11.3 [4]
LSM25-YSZ	**11.7 (*1 bar*)**	
YSZ		10.3 [4] / 10.8 [2] / 10.9 [1]

[1] 50-900 °C

Changes in the gas flow influenced the volume of the bar tested. A length increase, corresponding to thermal expansion by 8 °C temperature increase, was observed when increasing the gas flow from 100 to 200 ml/min, while keeping all other parameters constant. One would expect to see this 8 °C temperature increase also when measuring the temperature on the thermocouple. However, this was not the case. A small temperature decrease (~ 0.1 °C) was observed, which, unlike the length increase, returned to its initial value before the gas flow was returned to 100 ml/min. This discrepancy might possibly be explained by the fact that the thermocouple has a much higher thermal conductivity than the LSM25 bar. The preliminary data on a LSM25 bar, sintered at 1200 °C, at a temperature of 850 °C, while varying the pO_2 (see Figure 2.6), led to the following points of attention:

- The pO_2 monitor does not give satisfactory results. The obtained data show great variation from point to point and therefore the results are not reliable.
- The sample did not have sufficient time to fully equilibrate, both thermally and upon changes in partial oxygen pressure. Longer equilibration times have to be applied in future dilatometry experiments of similar samples.

When extending the dilatometry experiments, it would be very interesting to investigate the stability of the materials when applying several 'redox' cycles of high and low amounts of oxygen in the atmosphere. These experiments can confirm whether or not the SOFC will be stable under harsh operation conditions.

2.4.4 Conductivity

The shape of the curves observed for the change in conductivity with temperature of all LSM25 and LSM25-YSZ bars was similar to that found in literature [5]. Berenov et al. [5] found a conductivity of 190 S/cm at 850 °C for $La_{0.8}Sr_{0.2}MnO_3$ sintered at 1000 °C for 10 hours. In this study the conductivity for LSM25 at 850 °C was observed to be 111 S/cm, for the bar sintered at 1050 °C for 2 hours. The discrepancy compared to literature could be caused by several factors. The first factor is the preparation of LSM, which has a significant influence on the conductivity [3]; for example, Li et. al. [6] have found conductivities for LSM ranging from 40 to 486 S/cm at 1000 °C, depending on the preparation procedure. Another factor is that the density for the bars studied by Berenov et al. [5] was different from the bar studied here, as the preparation of the bars and sintering profiles were different.

When replacing half of the LSM25 by YSZ the conductivity decreased; to 20-31 S/cm, for bars sintered at 1200 °C. This factor ~ 10 decrease in conductivity is caused by the fact that YSZ has a very low electrical conductivity and the percolation of LSM25 in the bar is low due to porosity of the bar. Furthermore, it was observed that the conductivity decreased with decreasing sintering temperature. The conductivity was a factor of 2 lower for the LSM25 bar sintered at 1050 °C, compared to the bar sintered at 1200 °C. In case of the LSM25-YSZ bar the conductivity even decreased by a factor of ~ 10 when decreasing the sintering temperature. The decrease in the conductivity is as expected with increasing porosity. The greater decrease of the conductivity for the LSM25-YSZ bar could be explained by the additional decrease of the percolation of the LSM25 phase with increasing porosity. Observing the change in conductivity over several hundreds of hours (Figure 2.8); the LSM25-YSZ bar, sintered at 1050 °C, showed an increasing conductivity with time at 847 °C. This increase was possibly caused by further sintering of the bar at this temperature, increasing the percolation and thereby the conductivity. It appears that for LSM25-

YSZ bars sintered at 1200 °C had a point around 840 °C, below which the conductivity decreases with time and above which it increases with time. Possibly, below 840 °C, no sintering and therefore, no increasing percolation and hence increasing conductivity occured. Still, the decrease in the conductivity with time below 840 °C cannot be explained. When decreasing the pO_2 a decrease in the conductivity was observed for the LSM25 bar sintered at 1050 °C (see Figure 2.9). However, for the bar sintered at 1200 °C no significant decrease of conductivity was observed (Figure 2.10). A slight decrease was seen, but this was considered to be within experimental error. As the latter bar was dense, the area available for oxygen surface exchange was smaller. Therefore the effect of the oxygen partial pressure was more pronounced in the case of the porous bar, sintered at 1050 °C.

It would be interesting to study the conductivity of several bars (LSM and LSM-YSZ), with a different, known, porosity to further investigate the influence of the porosity on the conductivity. This could lead to a better performance of the SOFC by using an optimised porosity of the materials.

2.5 Conclusions

- No phase change of LSM25 occured in air at temperatures up to 1000 °C.
- There was no LZO or SZO present on the surface of any of the sintered and/or tested LSM25-YSZ bars in amounts detectable by XRD.
- The TEC for LSM25 is 12.1 ± 0.5 [$\cdot 10^{-6}$ /K] (based on two nominally the same bars) and the TEC of LSM25-YSZ is 11.7 [$\cdot 10^{-6}$ /K] (based on one bar).
- The pO_2 had an effect on the expansion of both LSM25 and LSM25-YSZ bars. When decreasing the pO_2 to ~ $1.4 \cdot 10^{-4}$ bar, both materials contracted. This process seems diffusion limited.
- The conductivity of LSM25 and LSM25-YSZ bars increased with increasing sintering temperature, most likely because of decreasing porosity. The decrease was greater in the case of LSM25-YSZ, where a decrease in porosity probably also decreases the percolation of the LSM25 phase.
- The conductivity of LSM25 bars was higher than that of LSM25-YSZ mixed bars, due to the low conductivity of the YSZ phase and poor percolation of the LSM25 phase in the case of a mixed bar.

- The LSM25-YSZ bar sintered at 1050 °C showed a decrease in conductivity with decreasing pO_2, for the LSM25-YSZ bar sintered at 1200 °C however, a slight decrease observed was within experimental error. Possibly the oxygen exchange in the dense bar, sintered at 1200 °C, is minimal, so the material does not change its oxygen deficiency significantly, leading to a minimal decrease in conductivity.

2.6 References

1. F. Tietz, *Ionics,* **5**, 129 (1999).

2. H. Yokokawa and T. Horita, in *High Temperature Solid Oxide Fuel Cells - Fundamentals, Design and Applications*, S. C. Singhal and K. Kendall, Editors, p. 119, Elsevier Ltd. (2003).

3. S. P. Jiang, *J. Mater. Sci.,* **43**, 6799 (2008).

4. M. Mori, Y. Hiei, N. M. Sammes and G. A. Tompsett, *J. Electrochem. Soc.,* **147**, 1295 (2000).

5. A. Berenov, H. Wood and A. Atkinson, *ECS Trans.,* **7**, 1173 (2007).

6. Z. Li, M. Behruzi and D. Stover, *SOFC III,* 171 (1993).

CHAPTER 3

Characterization of LSM-YSZ SOFC cathodes by Electrochemical Impedance Spectroscopy

---

Abstract

This chapter reports a detailed electrochemical study of composite LSM-YSZ solid oxide fuel cell cathodes. LSM-YSZ cathodes were manufactured by screen-printing and tested in a symmetrical cell configuration. Impedance spectra of the symmetrical cells were recorded in the temperature range 450-850 °C, at various oxygen partial pressures. The collected impedance data was analyzed by calculating the distribution of relaxation times (DRT), and the DRT results were used to guide the selection of an equivalent circuit. Non-linear complex least squares fitting of the data, to the chosen equivalent circuit, was used to determine the relevant physical parameters associated with each circuit element. This way the data was separated into impedance contributions assigned to interfacial oxygen ion transfer from YSZ in the cathode to YSZ in the electrolyte, oxygen ion transport in the cathode YSZ matrix, co-limited diffusion and dissociative adsorption of oxygen on LSM, and oxygen gas diffusion. Capacitances were interpreted in terms of interfacial and chemical contributions.

3.1 Introduction

The LSM-YSZ electrode is still one of the most important Solid Oxide Fuel Cell (SOFC) cathode materials, as it is chemically and physically more stable than other candidate materials [1-3].

Much research has been focused on developing the optimal composition of the LSM-YSZ composite cathode [2]. Lanthanum manganite ($LaMnO_3$) is a good electronic conductor, and replacing some of the lanthanum in by strontium enhances the electronic conductivity further; the electronic conductivity showed a maximum at 50 % substitution [4]. The catalytic activity for the oxygen reduction reaction is also enhanced by strontium substitution. However, at 50 % substitution the mismatch of the thermal expansion coefficient (TEC) of LSM and YSZ is large, risking delamination of, or formation of cracks in the electrode upon thermal cycling. The TEC of LSM shows a minimum at an A-site strontium content of around 15 %, where it is closest to the TEC of YSZ [5, 6]. Thus, an optimum stoichiometry of LSM for use in and SOFC cathode will reflect the most relevant trade-off between these properties.

It is well known that adding YSZ (yttria stabilized zirconia) to the LSM cathode enhances its performance significantly, as more active area becomes available for the oxygen reduction reaction, by increasing the triple phase boundary (TPB) length [7, 8]. Compositions with an YSZ content of 50-70 wt% YSZ showed optimal performance as both phases are connected throughout the cathode [9]. A disadvantage of the addition of YSZ is that LSM and YSZ can react with each other. It was found that manganese can diffuse into YSZ, forming La_2O_3 at the surface of LSM. La_2O_3 reacts with YSZ to form $La_2Zr_2O_7$ (LZO), a non conducting phase at the interface between LSM and YSZ. By having an excess of manganese in the LSM; LZO formation can be inhibited or delayed [2, 10]. Furthermore it was found that fully stabilized zirconia (8 mol% Y_2O_3-ZrO_2) is less reactive with LSM than 3YSZ [10].

These observations have led to the choice of using 50 wt% $(La_{0.75}Sr_{0.25})_{0.95}MnO_{3\pm\delta}$ mixed with 50 wt% 8YSZ as the electrodes and 8YSZ as the electrolyte in this study.

Electrochemical Impedance Spectroscopy (EIS) is a powerful tool for the study of performance, deactivation and degradation of SOFC electrodes.

However, understanding the impedance response from electrodes is challenging as several physical processes are limiting the rate of the oxygen reduction reaction. As the timescale of the physical processes often overlap, especially for porous, composite electrodes; they are difficult to separate. Even more difficult is to elucidate the reaction mechanisms involved in the cathode, for which the use of model, dense film or point-contact, electrodes is better suited [1].
Therefore the aim of this study is to establish a physically meaningful description the impedance response from porous LSM-YSZ electrodes at relevant temperatures and partial oxygen pressures, and not to establish the reaction mechanisms taking place in the porous LSM-YSZ electrode. The resulting physically meaningful model will allow pinpointing of the process(es) that lead to the largest losses, or those that are most affected by degradation or deactivation with time. These process(es) can then be placed in focus for the development of improved and more durable cathodes.

In this chapter, LSM-YSZ electrodes were studied by electrochemical impedance spectroscopy, in a symmetrical cell (two-electrode) configuration at open circuit voltage (OCV), and at different temperatures and oxygen partial pressures. The symmetrical cell configuration was chosen to minimize the number of processes to be considered, by investigating the cathode and electrolyte, but not the anode materials. This choice, places this study in the low-overpotential regime, as measurements were carried out at zero dc bias and with a perturbation amplitudes in the range of 0.9-1 mA for a representative sample (0.6 cm^2) at 650-850 °C. It was proposed that the reaction mechanism changes depending on the overpotential applied [11]. At low overpotential, LSM behaves like Pt, where oxygen species are transported via the surface to the triple phase boundary (TPB). At high overpotential LSM becomes reduced, creating oxygen vacancies. Therefore oxygen species can be transported though the bulk of the LSM toward the TPB, and the mechanism becomes like that of mixed ionic and electronic conductors [11].
The obtained EIS data was first analyzed by calculating the distribution of relaxation times (DRT) [12], which was used qualitatively to guide the selection of the number, the type and the relaxation frequency, of elements for the equivalent circuit. Subsequently, analysis of the EIS data was carried

out by applying complex nonlinear least squares (CNLS) fitting of the chosen equivalent circuit.

3.2 Experimental

Cell preparation. LSM25 [$(La_{0.75}Sr_{0.25})_{0.95}MnO_{3\pm\delta}$] powder was received from Topsoe Fuel Cell. The phase purity of LSM25 was confirmed by powder X-ray diffraction. The LSM25 powder was sintered at 950 °C for 2 hours prior to use. For more details on the LSM25 powder, see reference [13]. 8YSZ (ZrO_2 with 8 mol% Y_2O_3) powder was used as supplied by Tosoh. A cathode screen-printing ink was produced by suspending the powders, at a 50-50 wt% ratio, in an organic solvent, together with a dispersant. The suspension was ball milled for 4 h, after which binder and modifiers were added. The ink was screen-printed on either side of a 5 x 5 cm^2 8YSZ or CGO (ceria doped gadolinium) electrode strip (~100 to 200 μm thick) and fired at 1050 °C for 2 hours. The resulting symmetrical cells were cut to 8 x 8 mm^2 pieces and Pt paste (Ferro) was painted onto the cells, serving as a current collection layer. Subsequently the cells were sintered at 850 °C for 2 hours in stagnant air.

Cell characterization. The experimental setup consists of four cell positions, where each symmetrical cell was placed between two Pt-grids used for current collection. The setup was placed in a furnace, applying a 6 l/h gas flow (O_2 (Air liquide, ≥ 99.995 % clean) and/or N_2 (Air liquide, ≥ 99.995 % clean)), the pO_2 was controlled by mixing nitrogen and oxygen gases using thermal mass flow controllers. Impedance spectra were recorded using a Solartron 1260 impedance analyzer, at zero bias. The frequency range measured was from 0.1525 to 707900 Hz, recording 15 points per decade. EIS spectra were recording at 850, 800, 750, 700, 650 and 450 °C, each temperature at several partial oxygen pressures (1, 0.5, 0.21, and 0.1 bar).

Data analysis. The impedance data were checked for consistency with the Kronig-Kramer relations using the "KK test" software developed by Boukamp [14]. The relative errors for the EIS data were determined to be 0.2 % or below, therefore the EIS data are considered of good quality. The KKtest fits produced χ^2 values in the range $7 \cdot 10^{-8}$ to $5 \cdot 10^{-7}$.

DRT spectra were obtained by converting impedance spectra using in house software written based on the DRT method developed by Schichlein et al. [12], using the 'wiener' filter.

Impedance data were analyzed using both Zview 2 and ZSimpWin 3.21. Zview 2 is commercially available software from Scribner Associates, Inzc. and ZSimpWin 3.21 from EChem Software. Both programs include a complex nonlinear least square fitting routine.

3.3 Results and discussion

Nyquist representations of the obtained impedance data at 650 °C are shown in Figure 3.1a. Figure 3.1b shows the corresponding DRT spectra.

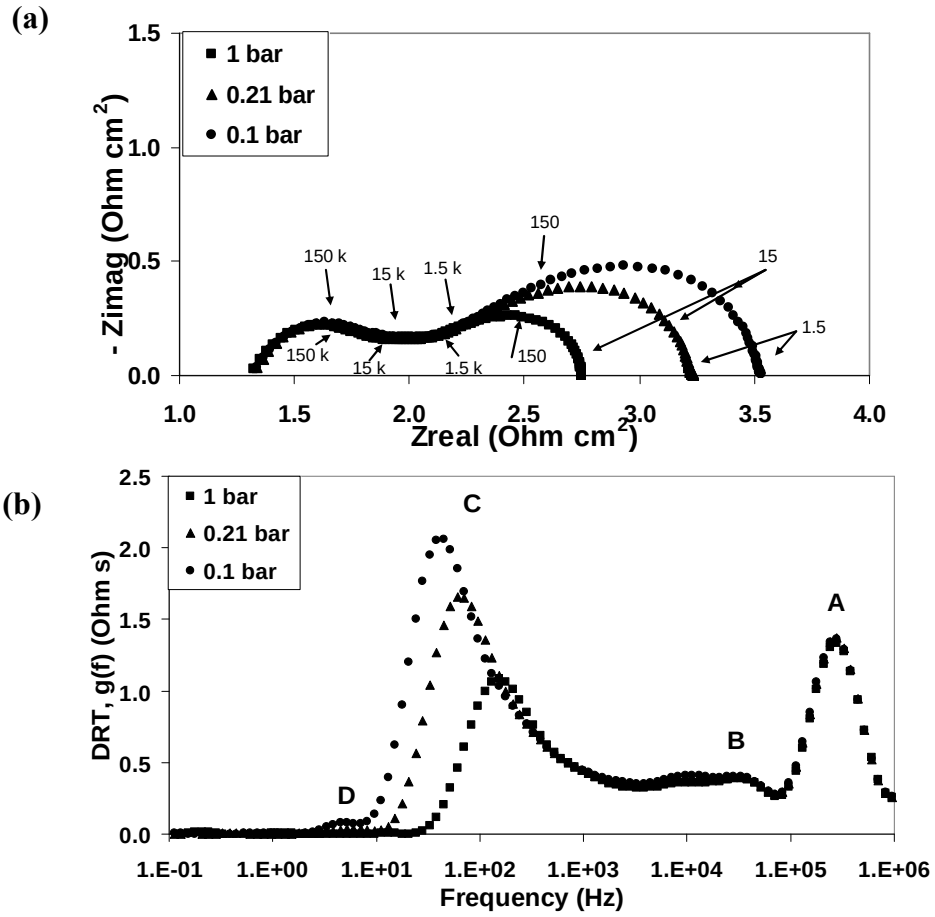

Figure 3.1. Impedance spectra obtained on a LSM-YSZ/YSZ/LSM-YSZ symmetrical cell, at 650 °C and various partial oxygen pressures; (a) Nyquist representation; (b) corresponding DRT spectra.

Equivalent circuit development. An equivalent circuit was developed for the LSM-YSZ/YSZ/LSM-YSZ symmetrical cells. First of all, the inductance, *L*, of the experimental setup was included in the equivalent circuit. Second, the

series resistance, R_s, accounting for the resistance of oxygen ion transport in the YSZ electrolyte, was added.
All other contributions to the cell resistance are part of the electrode polarization resistance, R_p. From the Nyquist representation of the impedance data alone it is hard to distinguish the number and types of processes R_p is consisting of. Therefore, DRT analysis was applied to develop the rest of the equivalent circuit [12]. Using DRT, the number of elements can be determined and moreover the shapes and summit frequencies of the peaks determine the type of element to be used in each case. Up to four relaxation processes were observed from DRT in the measured frequency range, depending on the applied conditions. The arcs were denoted A to D, as proposed previously by Jørgensen et al. [15]. The first arc (A) was observed at frequency increasing with temperature, from 140 kHz at 600 °C to 900 kHz at 750 °C. Arc A was independent of pO_2. Arc A could be described satisfactorily with an *RC* element:

$$Z_{RC} = \frac{R}{1 + RC(j\omega)} \qquad [3.1]$$

As experimental data were obtained up to 708 kHz, arc A could not be fitted at temperatures above 750 °C. Even though the summit frequency of arc A is above the experimentally measured frequency, it was possible to fit arc A at this temperature and obtain reliable values. At 800 °C 11 data points at the high frequency end were removed, so there was no influence of arc A on the rest of the fit. At 850 °C arc A had moved to even higher frequency, so removal of data points was not necessary.
The second arc (B) was observed at a summit frequency of 10 to 100 kHz. The arc was independent of pO_2 but shifted slightly to higher frequencies upon increasing temperature. Arc B could best be described by an *RQ* element:

$$Z_{RQ} = \frac{R}{1 + RQ(j\omega)^n} \qquad [3.2]$$

The *n*-value tended to drop below 0.5 if left to iterate freely, but since an *n*-value below 0.5 cannot be physically explained it was fixed at 0.5. The low

n-value could mean that a finite Warburg or a Gerischer element could describe the arc more accurately; however this was not the case here. Qualitative DRT analysis indicates that the arc possibly consist of two separate arcs, as seen mainly at lower temperatures and pO_2. However, this is possibly a second arc related to arc C. Furthermore, separation into two arcs did not lead to consistent CNLS fits, either because one of the arcs is already described by the Gerischer element for arc C, or because the arcs are small and CNLS fitting is not able to separate them at the right summit frequency. Therefore it was decided to describe the arc by a single RQ element with an *n*-value of 0.5.

A third arc (C) is located in the intermediate frequency region, 50 to 2000 Hz. At most conditions investigated, this arc is the dominant feature in the impedance spectrum. The summit frequency shifts to higher frequencies with both increasing temperature and pO_2. Furthermore, arc C was observed to be asymmetric at all investigated conditions, indicating that the contribution has to be fitted using a more complex equivalent circuit element than an *RC* or *RQ* element [16]. The intermediate frequency contribution becomes more dominant at lower temperatures, so an impedance spectrum of the symmetrical cell was obtained at 450 °C artificial air.

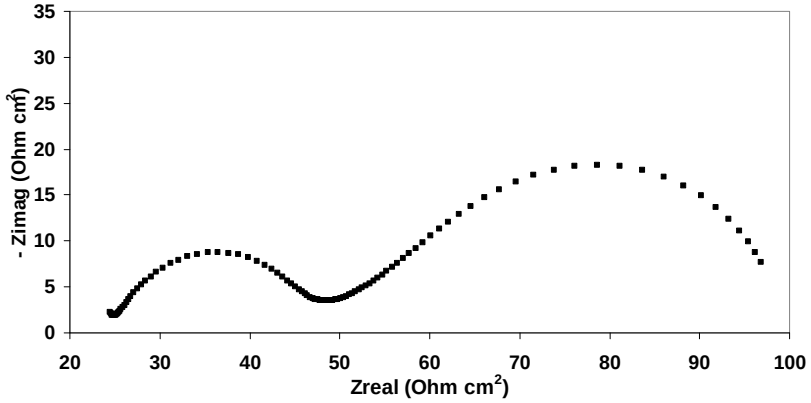

Figure 3.2. Nyquist representation of the impedance spectra obtained on a LSM-YSZ/YSZ/LSM-YSZ symmetrical cell, at 450 °C in 0.21 bar oxygen partial pressure.

The Nyquist representation of this spectrum is shown in Figure 3.2. Two large semicircles are present; the semicircle at the medium frequency range

is asymmetrical and could be described satisfactorily with a Gerischer element:

$$Z_{Ge} = \frac{1}{T_{Ge}\sqrt{P_{Ge} + j\omega}} \qquad [3.3]$$

In which T_{Ge}, often denoted Y_0, is the parameter describing the admittance of the Gerischer impedance, and P_{Ge}, often denoted k, is the rate constant of the Gerischer impedance.

A fourth and final arc (D) was observed at frequencies in the range of 1 to 20 Hz. The size of the arc increases significantly with decreasing pO_2, but is independent of temperature. The arc can be described by an RC element (equation 1). The inductive arc E, observed in some cases by Jørgensen et al. [15], was not observed in this study.

The resulting equivalent circuit is shown in Figure 3.3. Figure 3.4a and b show the resulting CNLS fit when the equivalent circuit was applied, in the Nyquist representation and corresponding DRT, respectively.

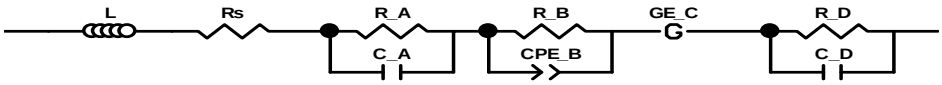

Figure 3.3. Equivalent circuit, developed to deconvolute impedance data obtained on LSM-YSZ/YSZ/LSM-YSZ symmetrical cells. Element R_DC_D, arc D, was not observed and therefore not applied in the measurements in pure oxygen. Element R_AC_A, arc A, is not applied at temperatures above 750 °C, as it is expected at a frequency above the experimentally measured frequency.

(a)

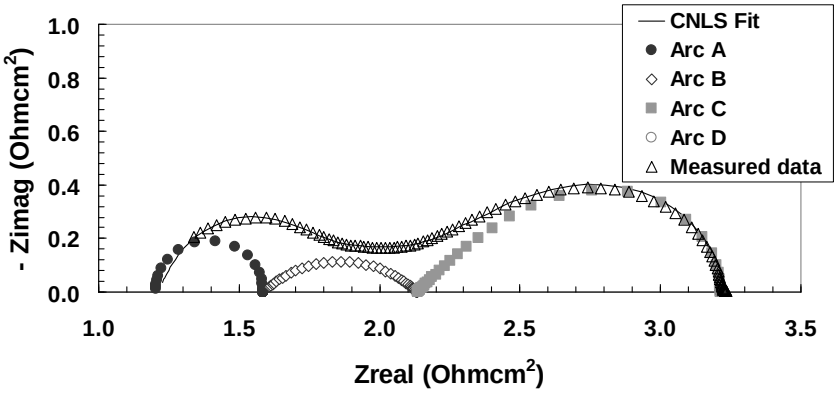

(b)

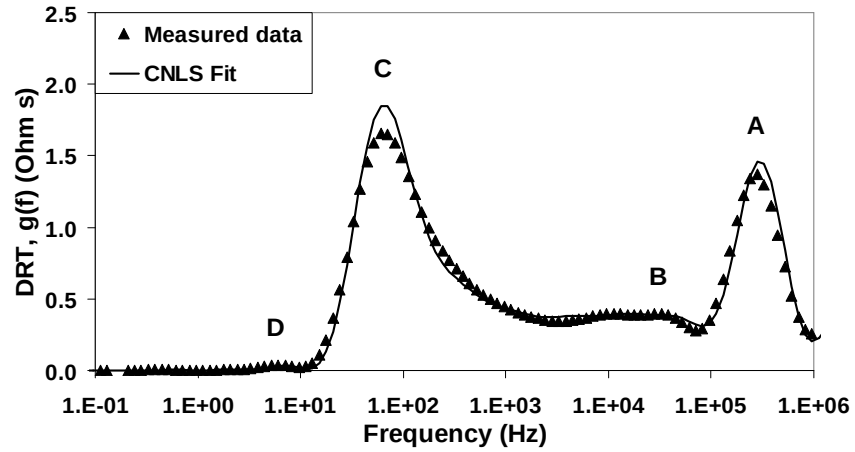

Figure 3.4. Impedance spectra obtained on a LSM-YSZ/YSZ/LSM-YSZ symmetrical cell, at 650 °C and 0.21 bar and the CNLS fits obtained by applying the equivalent circuit depicted in Figure 3.3; (a) Nyquist representation; (b) corresponding DRT.

TABLE 3.I. Fitting results of LSM-YSZ/YSZ/LSM-YSZ symmetrical cell in various partial oxygen pressures and temperatures. Note that R_A-R_D values, and therefore also the R_p value, are based on one electrode only. All values are the average of fitting of three samples.

	$LR_S(R_AC_A)(R_BQ_B)G_C(R_DC_D)$ 650 °C			750 °C	850 °C	
	1 bar	**0.21 bar**	**0.1 bar**	**0.21 bar**	**0.21 bar**	**Remarks**
L /H	$7.4\cdot10^{-8}$	$7.4\cdot10^{-8}$	$7.4\cdot10^{-8}$	$7.4\cdot10^{-8}$	$7.4\cdot10^{-8}$	Fixed
R total /Ωcm²	2.01	2.26	2.41	0.85	0.46	
R_s /Ωcm²	1.23	1.25	1.26	0.60		
R_A /Ωcm²	0.19	0.20	0.20	0.03		
C_A /Fcm⁻²	$5.0\cdot10^{-7}$	$4.9\cdot10^{-7}$	$4.8\cdot10^{-7}$	$9.4\cdot10^{-7}$		$3.5\text{-}5.3\cdot10^{-6}$ [3]
$f_{summit,A}$ /Hz	302069	295486	293133	895538		
R_B /Ωcm²	0.27	0.27	0.28	0.08	0.03	
n_B	0.5	0.5	0.5	0.5	0.5	Fixed
$C_{eq,B}$ /Fcm⁻²	$2.9\cdot10^{-6}$	$3.8\cdot10^{-6}$	$4.4\cdot10^{-6}$	$7.7\cdot10^{-6}$	$1.9\cdot10^{-5}$	10^{-4} [9, 17], 10^{-5} [18]
$f_{summit,B}$ /Hz	37066	27417	23079	45971	56602	
R_C/Ωcm²	0.33	0.53	0.66	0.13	0.03	
$C_{eq,C}$ /Fcm⁻²	$4.2\cdot10^{-4}$	$6.1\cdot10^{-4}$	$7.4\cdot10^{-4}$	$5.2\cdot10^{-4}$	$4.5\cdot10^{-4}$	$5.6\cdot10^{-6}$ [18], $3.4\cdot10^{-4}$ [19]
$f_{summit,C}$ /Hz	88	38	25	174	858	
R_D/Ωcm²	-	0.003	0.009	0.003	0.003	Fixed at each partial pressure
C_D /Fcm⁻²	-	0.91	0.37	0.91	0.91	
$f_{summit,D}$ /Hz	-	9	9	9	9	
chi-squared	$2.4\cdot10^{-5}$	$4.9\cdot10^{-5}$	$7.1\cdot10^{-5}$	$4.6\cdot10^{-5}$	$1.0\cdot10^{-4}$	
R_p total (R_A+R_B+R_C+R_D) /Ωcm²	0.78	1.01	1.15	0.25		

The results of the fitting both equivalent circuits is given in Table 3.I. The summit frequencies of the equivalent circuit elements were calculated as follows:

$$f_{summit,RC} = \left(\frac{1}{2\pi}\right)\left(RC\right)^{-1} \qquad [3.4]$$

$$f_{summit,RQ} = \left(\frac{1}{2\pi}\right)\left(RQ\right)^{-1/n} \qquad [3.5]$$

$$f_{summit,Ge} = \left(\frac{1}{2\pi}\right)\left(P_{Ge}\right)\left(\sin\left(\frac{\pi}{3}\right)\right) \qquad [3.6]$$

The equivalent capacitance for the *RQ*- and Gerischer elements were calculated as follows:

$$C_{eq,RQ} = \frac{(RQ)^{1/n}}{R} \text{ [20]} \qquad [3.7]$$

$$C_{eq,Ge} = \frac{T_{Ge}}{2\sqrt{P_{Ge}}} \qquad [3.8]$$

The resistance for the Gerischer element was calculated as follows:

$$R_{Ge} = \left(\frac{1}{T_{Ge}}\right)\left(P_{Ge}\right)^{-1/2} \qquad [3.9]$$

Activation energies were determined for R_s, each of the resistances adding up to R_p, and R_p itself, using the results from CNLS fitting. The Arrhenius plot is shown in Figure 3.5. The pO_2 dependence of each of the arcs was also determined, as shown in Figure 3.6. Table 3.II and 3.III summarize the values for E_a and the pO_2 dependence of the LSM-YSZ/YSZ/LSM-YSZ symmetrical cells, respectively, along with findings from literature.

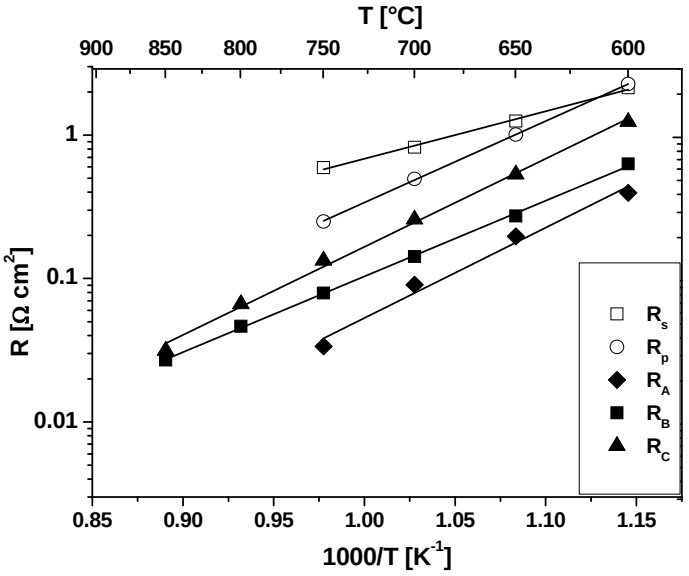

Figure 3.5. Arrhenius plot of the resistances resulting from CNLS fitting, of the LSM-YSZ/YSZ/LSM-YSZ symmetrical cells, from 650 to 850 °C, 21 % O_2 in N_2.

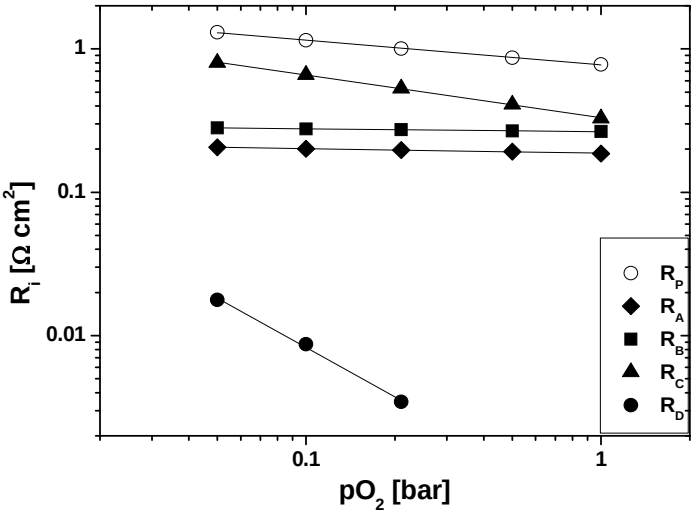

Figure 3.6. pO_2 dependency of the resistances resulting from CNLS fitting, of the LSM-YSZ/YSZ/LSM-YSZ symmetrical cells, at 650 °C and oxygen partial pressures from 0.05 to 1 bar. The pO_2 dependence of arc D was determined from 0.05 to 0.21 bar oxygen partial pressure only, as the resistance of this arc was very small at higher oxygen partial pressures and therefore the value was not reliable for pO_2 dependence determination.

TABLE 3.II. Activation energy of LSM-YSZ/YSZ/LSM-YSZ symmetrical cell

	Ea (eV)					
	this study					literature
***p*O$_2$/bar**	**1**	**0.5**	**0.21**	**0.1**	**0.05**	
R_s	0.65	0.66	0.66	0.66	0.66	0.90 [21]
R_p	1.17	1.14	1.13	1.11	1.10	1.15 [17], 1.1 [22], 1.2-1.6 [23]
R_A	1.27	1.22	1.25	1.25	1.26	
R_B	1.10	1.07	1.05	1.03	1.01	1.13 [3], 1.0 [22], 1.05 [21], 0.7-0.9 [24], 0.9 [25]
R_C	1.21	1.21	1.22	1.23	1.24	3.0 [3], 1.6 [22], 1.49 [21], 2.0-2.2 [24]

TABLE 3.III. pO_2 dependence of LSM-YSZ/YSZ/LSM-YSZ symmetrical cell						
	$R_i \propto pO_2^x$; x =					
	this study					literature
***T*/°C**	**650**	**700**	**750**	**800**	**850**	
R_p	0.17	0.18	0.20	-	-	
R_A	0.03	-0.01	0.04	-	-	
R_B	0.02	0.03	0.05	0.05	0.11	
R_C	0.30	0.32	0.31	0.27	0.24	0.25 [9], 0.5 [22], 0.29 [21], 0.50-0.86 [24]
R_D	1.14	1.14	1.14	1.14	1.14	1 [9], 0.57 [21]

Literature. Several papers have been published on the characterization of LSM-YSZ symmetrical cells using EIS [2, 2, 3, 9, 15, 17, 18, 21-24, 26-31]. Table 3.IV gives an overview of some relevant findings from literature, compared to the finding of this study. Most often, the impedance data were described by two depressed arcs (*RQ* elements). A first *RQ* element was used to describe high frequency behavior (arc B in this study), a second *RQ* element to describe the intermediate frequency behavior (arc C in this study) [2, 2, 9, 17, 18, 22, 23, 26]. The high frequency arc was found to be dependent on temperature, but independent of the partial oxygen pressure, while the intermediate frequency arc was found to depend on both. Literature [3, 9, 18, 21, 22, 24, 26, 27] is in good agreement about the physical explanation of the high frequency arc: it is caused by oxygen ion migration from the LSM-YSZ electrode, or more specifically the triple phase boundary, into vacancies in the YSZ electrolyte lattice. The underlying process(es) causing the arc (C) at intermediate frequency have been discussed heavily in literature. Some authors claim the arc is limited by oxygen dissociation, while others ascribe it to oxygen ion diffusion on the LSM surface or through the LSM bulk. In recent years literature tends to agree on that the arc is a co-limited process of both oxygen dissociation and oxygen ion diffusion [3, 9, 18, 23, 24, 28, 29]. At low overpotentials oxygen ion diffusion is thought to mainly take place on the LSM surface, while at high overpotentials oxygen diffusion shifts more and more to the LSM bulk [1].

Some authors have observed more processes than the two mentioned above. In some cases, a third *RQ* or *RC* element was added to describe low frequency behavior, present especially at low pO_2 [9, 15, 18, 23, 27, 28].

This element was found to depend strongly on pO_2, but to be virtually independent of temperature and is caused by gas-phase diffusion of oxygen, mainly across a stagnant layer outside the electrode. At low frequencies, some authors [15, 23, 27] have also observed an inductive loop. Furthermore, at very high frequencies (above 10 kHz), under certain conditions, another process was observed by Jørgensen et al. [15] and Jiang et al. [3]. Jiang et al. observed that this process has an (almost) pure capacitance, of around 3.5 to $5.3 \cdot 10^{-6}$ F/cm^2 at 700 °C. Mitterdorfer and Gauckler [32] observed the presence of a double layer capacitance of around $1.3 \cdot 10^{-6}$ F/cm^2 for an unsintered YSZ/LSM interface. Sintering the sample would increase the capacitance slightly. Under comparable conditions, YSZ grain boundary resistance has a capacitance of a factor 100 lower [3], and a summit frequency of around 40 MHz [15], excluding it as a possible explanation of the process.

TABLE 3.IV. Summary of cathode properties, testing conditions and observations on the number of arcs and the polarization resistance for this study and by other authors.

Reference	Cathode composition	Sintering T cathode	Particle size	Substrate	Testing conditions	Number of arcs	R_p (Ωcm^2)
This study	$(La_{0.75}Sr_{0.25})_{0.95}MnO_3$ - 8YSZ (1:1 wt ratio)	1050 °C/2h	0.2-2 µm	8YSZ	650-850 °C pO_2 0.1-1 bar	4	0.06 (850 °C) 0.26 (750 °C)
Jiang [3]	$La_{0.72}Sr_{0.18}MnO_3$	1150 °C/2h	0.36 µm	3YSZ	700-900 °C Air	2/3	6.2 (900 °C) 60 (700 °C)
Jiang [24]	$(La_{0.82}Sr_{0.18})_{0.82}MnO_3$	1150 °C/2h		3YSZ	850-1000 °C Various pO_2	2	
Brant [18]	$La_{0.65}Sr_{0.35}MnO_3$ (porous) $La_{0.45}Sr_{0.55}MnO_3$ (dense)	1100 °C/2h	0.2 µm	8YSZ	900 °C - Air	3	4.16 (900 °C)
Østergård [27]	$La_{0.85}Sr_{0.15}MnO_3$			YSZ	1000 °C Various pO_2	3	
van Heuveln [29]	$La_{0.85}Sr_{0.15}MnO_3$	1100-1300 °C/2h	0.29-2 µm	YSZ	945 °C – Air	2	
Belardi [30]	$La_{0.8}Sr_{0.2}MnO_3$	1150 °C/6h	0.1 µm	8YSZ	850 °C – Air	2	15 (850 °C)
Kim [31]	$(La_{0.85}Sr_{0.15})_{0.9}MnO_3$	1350 °C/30 min		8YSZ	900-1000 °C Various pO_2	2	
la O' [19]	$La_{0.8}Sr_{0.2}MnO_3$ (dense)			8YSZ	570-790 °C Air	4	
Wang [22]	$La_{0.8}Sr_{0.2}MnO_3$-YSZ (1:0, 8:2, 6:4 wt ratios)	1300 °C/ 2.5h		YSZ	750-950 °C Various pO_2	1/2	1 (950 °C)
Choi [26]	$La_{0.9}Sr_{0.1}MnO_3$-YSZ (1:0 and 1:1 wt ratio)	1000-1300 °C/2h	Submicron to few micron	8YSZ	900 °C - Air	2	1.03 (900 °C)
Perry Murray [21]	$La_{0.8}Sr_{0.2}MnO_3$-8YSZ (1:0 and 1:1 wt ratio)	1100 °C/2h		YSZ	550-850 °C Various pO_2	2/3	1.4 (750 °C)
Kim [9]	LSM-8YSZ (1:1 wt ratio)	1000 °C/2h		8YSZ	800-950 °C Various pO_2	3	0.06 (950 °C) 0.075 (800 °C)
Kim [28]	LSM-8YSZ (6:4 wt ratio)	1200 °C/2h	LSM: 0.97 µm YSZ: 0.6-4.8 µm	8YSZ	600-900 °C Air	2	1.86 (700 °C)
Bebelis [17]	$La_{0.65}Sr_{0.3}MnO_3$-8YSZ (1:1 wt ratio)	1100 °C/3h	0.39 µm	CGO/YSZ	600-850 °C 21 % O_2 in He	2	0.02 (850 °C) 0.1 (750 °C)
Co [23]	$(La_{0.8}Sr_{0.2})_{0.98}MnO_3$-8YSZ (1:1 vol ratio)	1150 °C/2h	0.2-0.9 µm	YSZ	600-900 °C Various pO_2	2/3	0.73 (800 °C) 3.6 (700 °C)
Jørgensen [15]	$(La_{0.75}Sr_{0.25})_{0.9}MnO_3$-3YSZ (1:1 wt ratio) + $(La_{0.85}Sr_{0.15})_{0.9}MnO_3$-3YSZ (6:4 wt ratio) + $(La_{0.75}Sr_{0.25})_{0.95}MnO_3$-8YSZ (1:1 wt ratio)	1100-1300 °C		8YSZ	800-1000 °C Air	5	

Physical explanation of the equivalent circuit

Arc A was observed at very high frequency, increasing upon temperature increase, its summit frequency found at 140 kHz at 600 °C up to 900 kHz at 750 °C. At temperatures above 750 °C the arc moved outside the frequency range determined experimentally. The activation energy was calculated to be 1.22 to 1.27 eV. However, the slope of the Arhennius plot (Figure 3.5) was not linear. Possibly this was caused by an error in the fitting of the arc. Like arc B it was independent of pO_2. Only Jørgensen et al. [15] and Jiang [3] have observed arc A previously. Jørgensen points out that arc A is often overlapping with arc B, the latter being more dominant. Also, as observed here, arc A shifts to higher frequencies with increasing temperatures and simultaneously decreases in size. These factors might explain the absence of the arc in other literature. Jiang however, has observed and modeled the arc at 700 °C. As in this study, an *RC* element was found appropriate to describe arc A. An equivalent capacitance of around $5 \cdot 10^{-6}$ $F \cdot cm^{-2}$ was found by Jiang, while in this study a value of $5 \cdot 10^{-7}$ $F \cdot cm^{-2}$ was observed. Both values are too high to be related to the grain boundary resistance of YSZ [24]. To improve understanding of the physical process related to Arc A, symmetrical cells were produced with CGO as the electrolyte instead of YSZ. Scanning electron microscopy images comparing the LSM-YSZ/YSZ/LSM-YSZ with the LSM-YSZ/CGO/LSM-YSZ are shown in Figure 3.7. The EIS obtained from the LSM-YSZ/CGO/LSM-YSZ cell at 650 °C in oxygen is shown in Figure 3.8. It was observed that arc A decreased significantly by replacing the YSZ electrolyte by CGO, while all other arcs remain constant. From the SEM images it appears as if the contact between the LSM/YSZ cathode and the electrolyte was better or smoother in case of the CGO compared to the YSZ electrolyte. In case the coverage/contact area of the cathode on the electrolyte is not optimal current constriction can occur causing not only an increase of the electrolyte resistance, but also the appearance of arc A. This was described previously by Fleig et. al [33]. Furthermore, Jørgensen et al. [15] mentioned the importance of the cathode microstructure on the magnitude of Arc A. Refining the microstructure is likely to improve the cathode-electrolyte interface as well.

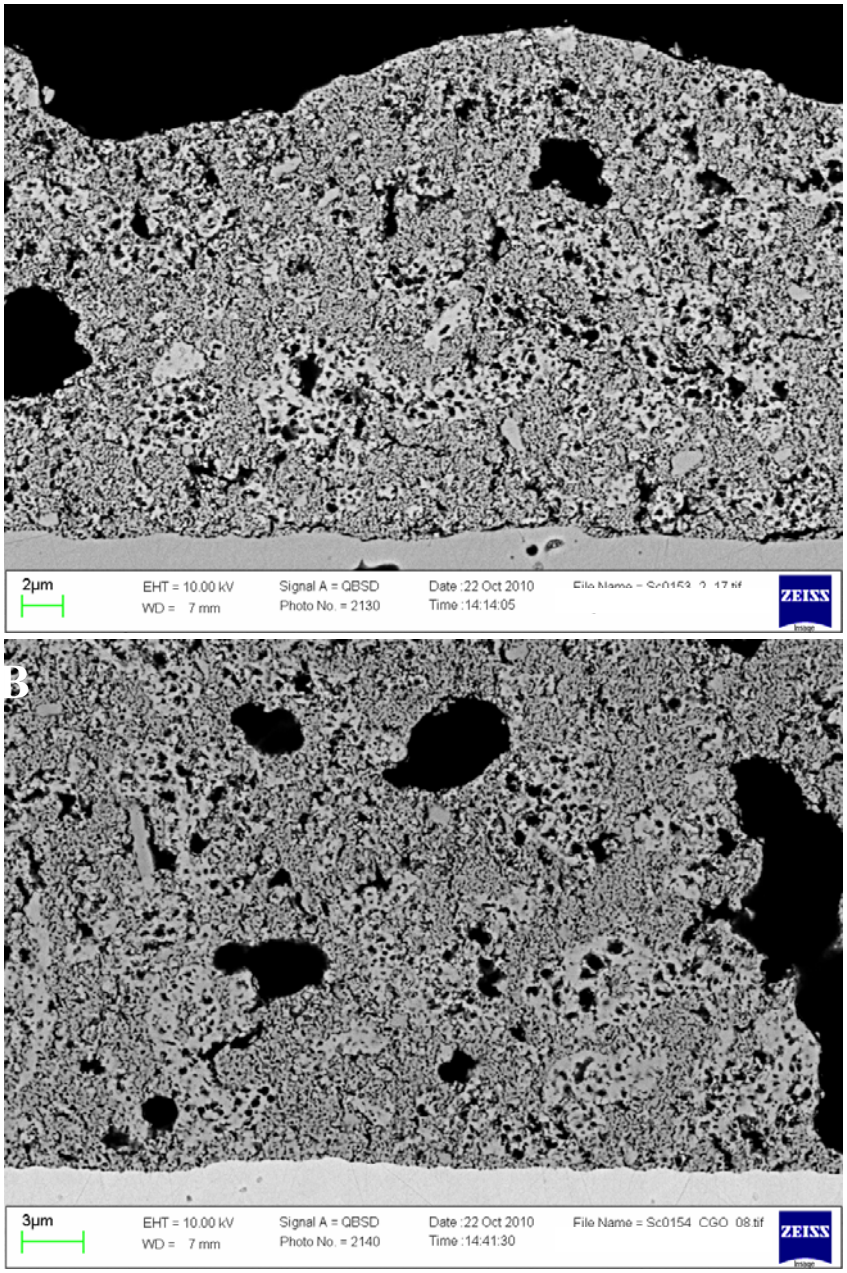

Figure 3.7. Scanning electron microscopy (SEM) images of LSM-YSZ cathode interface with (a) YSZ electrolyte; (b) CGO electrolyte.

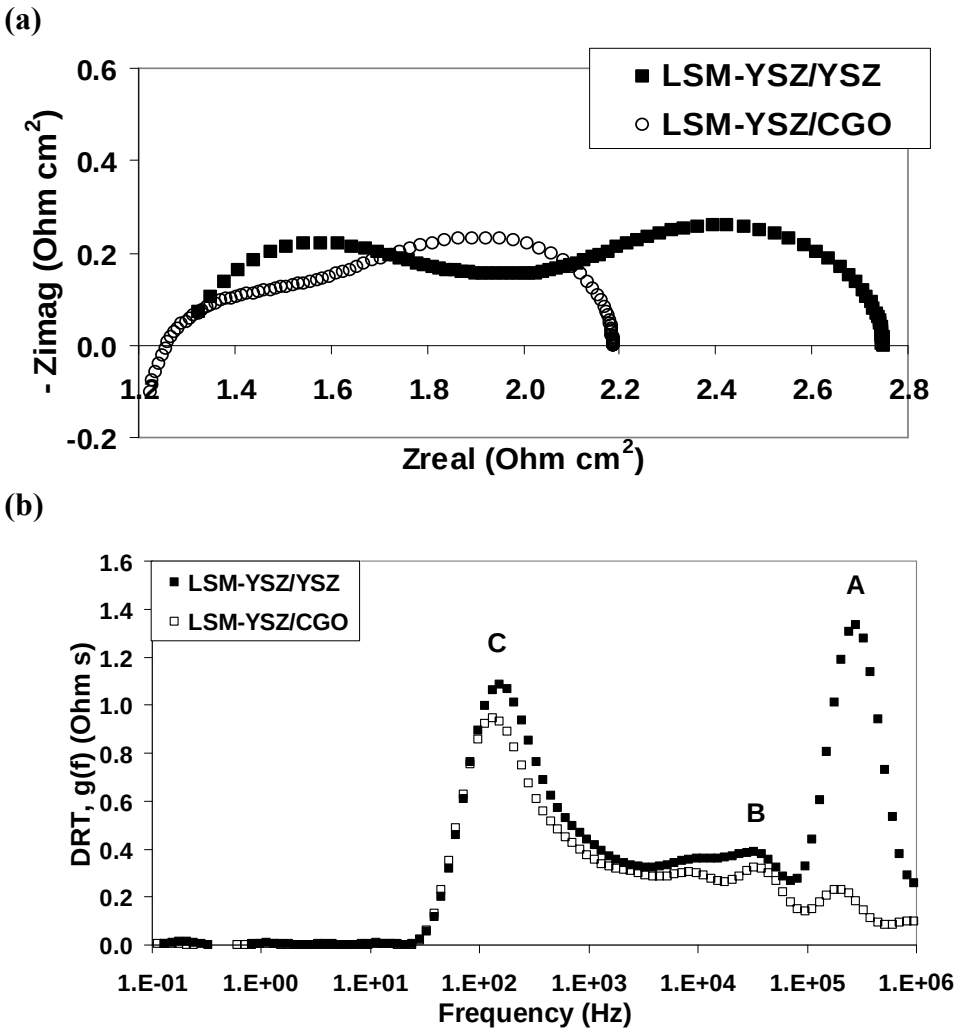

Figure 3.8. Impedance spectra obtained on LSM-YSZ/YSZ/LSM-YSZ and LSM-YSZ/CGO/LSM-YSZ symmetrical cell, at 650 °C in oxygen; (a) Nyquist representation; (b) corresponding DRT spectra.

Arc B, the high frequency contribution observed around 30 kHz at 650 °C, has an equivalent capacitance in the order of 10^{-5}-10^{-6} F·cm^{-2}, and was also observed by other authors [15, 18, 25]. Jørgensen et al. [15] observed that there are two arcs at high frequencies, arc A and B, as found in this study. However, the arcs were not well separable at the conditions applied in the study by Jørgensen et al [15]. The arcs were ascribed to transport of oxide ions and/or oxygen intermediates across LSM/YSZ interfaces and transport through the YSZ phase of the composite. As the capacitance value is too high to be YSZ grain boundary resistance [21, 22], Brant et al. [18] ascribe the arc to the diffusion of oxide ions from the interface LSM/YSZ to the

oxide ion vacancies located at the electrolyte surface. However, it is not clear what process is meant with this exactly; ionic transport in the YSZ matrix from the TPB to the electrode/electrolyte interface, and/or ion transfer across the electrode/electrolyte interface. The latter is found at a higher frequency, and arc A was assigned to this process. Another assignment for an arc similar to arc B in this study, was made by Sonn et al. [25], who have observed a similar high frequency arc at ~25 kHz for Ni/8YSZ cermet electrodes at 750-950 °C. The arc was ascribed to ionic transport in the YSZ matrix. It is likely that the ionic transport in YSZ in the LSM/YSZ cathode leads to a similar impedance response. Furthermore the activation energy of 1.05 eV found in this study corresponds well with the activation energy of the ionic conductivity of 8YSZ, which was found to be between 0.85 eV (at 850-1000 °C) and 1.11 eV (at 400-500 °C) [34]. Therefore arc B was either a double layer effect, or the process of ionic transport in the YSZ matrix.

Arc C, observed at intermediate frequencies, has been the subject of much discussion in literature, generally with respect to its nature and description. Authors have ascribed the arc to either (dissociative) adsorption of oxygen, bulk or surface diffusion of oxygen species or a combination of these. Often an *RQ* element was applied to describe the arc. However, some authors suggested that a Gerischer element might be more appropriate [1, 15, 30, 31]. Boukamp and Bouwmeester noted that the use of a Gerischer element implies the coupling of a diffusion process with a 'chemical reaction' [35]. In this study, 850 °C was the maximum applied temperature, and a clear asymmetrical peak shape was observed from both DRT analysis at all temperatures, and a Nyquist plot at 450 °C, indicating that a finite-length Warburg or Gerischer type circuit element can describe the process most accurately. A Gerischer element was found to describe arc C better than a Warburg element, indicating that co-limited processes are indeed involved. For the case of mixed ionic electronic conductors, Adler et al. [36] derived that a Gerischer element describes the competition between dissociative adsorption of oxygen and bulk diffusion of oxygen ions. LSM however, is known to have a very low ionic conductivity, so bulk diffusion is negligible compared to surface diffusion. Moreover, the relatively low summit frequency, chemical capacitance of 10^{-4} $F \cdot cm^{-2}$, low activation energy of 1.20 eV and pO2 dependency of 0.24-0.32 of the Gerischer element, point to surface diffusion as opposed to bulk diffusion of oxygen species to the

TPB [9, 19, 21, 32]. Atangulov et al. [37] derived Gerischer impedance for a slow adsorption process competing with surface diffusion, which was observed for platinum electrodes on YSZ electrolytes under certain conditions. Therefore, arc C was assigned to the coupled processes of dissociative adsorption of oxygen and surface diffusion of oxygen species.
Arc D. Several, but not all, authors have observed an arc at low frequency, similar to arc D observed in this study [9, 15, 18, 23, 27, 28, 38]. The arc is virtually independent of temperature. However, arc D became more visible at higher temperatures, as other contributions to the impedance spectrum became smaller with increasing temperature. Furthermore, the arc decreased in size with increasing pO_2, becoming absent in a pure oxygen atmosphere. Therefore, depending on the applied conditions, arc D might be absent or very small compared to the other contributions to R_p, so many authors have not included it in their respective equivalent circuits. Because of its strong pO_2 dependence, independence of temperature, peak shape and location arc D is assigned to oxygen gas diffusion.

With a satisfying equivalent circuit, resulting an error smaller than 0.5 %, the polarization resistance of the LSM-YSZ/YSZ/LSM-YSZ was deconvoluted into a number of process specific contributions represented by four circuit elements. The development of the equivalent circuit was carried out by qualitative analysis of the distribution of relaxation times in conjunction with CNLS fitting for quantification of the process contributions. With this equivalent circuit and the knowledge about the physical processes involved in the cell, we will be able to study the symmetrical cell further, and improve understanding of the nature of the processes involved in degradation. Furthermore, we will continue work by extending it to more complex systems, like a single anode supported SOFC, working under OCV or at current load.

3.4 Conclusion

An equivalent circuit used for breakdown of losses in a LSM-YSZ/YSZ/LSM-YSZ symmetrical cell was developed. This was achieved by analysis of impedance spectra from 450 to 850 °C and in oxygen partial pressures from 0.1 to 1 bar. All elements in the equivalent circuit were physically explained by the processes taking place in the symmetrical cell. The maximum error found when fitting the equivalent circuit was less then

0.5 % over the whole frequency range. The equivalent circuit can now be applied to study degradation of the symmetrical cell. Furthermore, the method of pre-analysis of the data using DRT followed by conventional CNLS fitting to develop and validate an equivalent circuit will be extended to a single anode supported SOFC, to study performance and degradation both at OCV and under current load.

3.5 References

1. S. B. Adler, *Chem. Rev.,* **104**, 4791 (2004).
2. S. P. Jiang, *J. Mater. Sci.,* **43**, 6799 (2008).
3. S. P. Jiang, *Solid State Ionics,* **146**, 1 (2002).
4. J. Mizusaki, Y. Yonemura, H. Kamata, K. Ohyama, N. Mori and H. Takai, *Solid State Ionics,* **132**, 167 (2000).
5. M. Mori, Y. Hiei, N. M. Sammes and G. A. Tompsett, *J. Electrochem. Soc.,* **147**, 1295 (2000).
6. F. Tietz, *Ionics,* **5**, 129 (1999).
7. T. Kenjo and M. Nishiya, *Solid State Ionics,* **57**, 295 (1992).
8. M. Mogensen and S. Skaarup, *Solid State Ionics,* **86-88**, 1151 (1996).
9. J.-D. Kim, G.-D. Kim, J.-W. Moon, Y.-I. Park, W.-H. Lee, K. Kobayashi, M. Nagai and C.-E. Kim, *Solid State Ionics,* **143**, 379 (2001).
10. van Roosmalen, J. A. M. and E. H. P. Cordfunke, *Solid State Ionics,* **52**, 303 (1992).
11. E. Siebert, A. Hammouche and M. Kleitz, *Electrochim. Acta,* **40**(11), 1741 (1995).
12. H. Schichlein, A. C. Müller, M. Voigts, A. Krügel and E. Ivers-Tiffée, *J. Appl. Electrochem.,* **32**(8), 875 (2002).
13. K. Kammer Hansen, M. Menon, J. Knudsen, N. Bonanos and M. Mogensen, *J. Electrochem. Soc.,* **157**(3), B309 (2010).
14. B. A. Boukamp, *J. Electrochem. Soc.,* **142**(6), 1885 (1995).
15. M. J. Jørgensen and M. Mogensen, *J. Electrochem. Soc.,* **148**(5), A433 (2001).
16. A. Leonide, V. Sonn, A. Weber and E. Ivers-Tiffée, *ECS Trans.,* **7**(1), 521 (2007).
17. S. Bebelis, N. Kotsionopoulos, A. Mai, D. Rutenbeck and F. Tietz, *Solid State Ionics,* **177**, 1843 (2006).
18. M. C. Brant, T. Matencio, L. Dessemond and R. Z. Domingues, *Solid State Ionics,* **177**, 915 (2006).

19. G. J. la O', B. Yildiz, S. McEuen and Y. Shao-Horn, *J. Electrochem. Soc.,* **154**(4), B427 (2007).
20. T. Jacobsen, B. Zachau-Christiansen, L. Bay and S. Skaarup, in *High Temperature Electrochemistry: Ceramics and Metals*, F. W. Poulsen, N. Bonanos, S. Linderoth, M. Mogensen and B. Zachau-Christiansen, Editors, p. 29, Riso Nat. Lab (1996).
21. E. Perry Murray, T. Tsai and S. A. Barnett, *Solid State Ionics,* **110**, 235 (1998).
22. S. Wang, Y. Jiang, J. Yan and W. Li, *Solid State Ionics,* **113-115**, 291 (1998).
23. A. C. Co, S. Jiang Xia and V. I. Birss, *J. Electrochem. Soc.,* **152**(3), A570 (2005).
24. S. P. Jiang, J. G. Love and Y. Ramprakash, *J. Power Sources,* **110**, 201 (2002).
25. V. Sonn, A. Leonide and E. Ivers-Tiffée, *J. Electrochem. Soc.,* **155**(7), B675 (2008).
26. J. H. Choi, J. H. Jang and S. M. Oh, *Electrochim. Acta,* **46**, 867 (2001).
27. M. J. L. Østergård and M. Mogensen, *Electrochim. Acta,* **38**(14), 2015 (1993).
28. J.-S. Kim, S.-I. Pyun and H.-C. Shin, *J. Electrochem. Soc.,* **156**(5), B620 (2009).
29. F. H. van Heuveln and H. J. M. Bouwmeester, *J. Electrochem. Soc.,* **144**(1), 134 (1997).
30. R.-M. Belardi, J. Deseure, M. C. Brant, T. Matencio and R. Z. Domingues, *Ionics,* **15**, 227 (2009).
31. J.-S. Kim, S.-I. Pyun, J.-W. Lee and R.-S. Song, *J. Solid State Electrochem.,* **11**, 117 (2007).
32. A. Mitterdorfer and L. J. Gauckler, *Solid State Ionics,* **111**, 185 (1998).
33. J. Fleig and J. Maier, *J. Electrochem. Soc.,* **144**(11), L302 (1997).
34. F. T. Ciacchi, K. M. Crane and S. P. S. Badwal, *Solid State Ionics,* **73**, 49 (1994).
35. B. A. Boukamp and H. J. M. Bouwmeester, *Solid State Ionics,* **157**, 29 (2003).
36. S. B. Adler, J. A. Lane and B. C. H. Steele, *J. Electrochem. Soc.,* **143**(11), 3554 (1996).
37. R. U. Atangulov and I. V. Murygin, *Solid State Ionics,* **67**, 9 (1993).

38. R. Barfod, M. Mogensen, T. Klemensø, A. Hagen, Y.-L. Liu and P. V. Hendriksen, *J. Electrochem. Soc.,* **154**(4), B371 (2007).

CHAPTER 4

The influence of impurities in air on the long-term performance of LSM-YSZ SOFC cathodes

Abstract

The influence of impurities in air on composite LSM-YSZ solid oxide fuel cells is reported in this paper. LSM-YSZ/YSZ/LSM-YSZ symmetrical cells were prepared by screen-printed and tested for at least 250 hours at 750 °C in different atmospheres; compressed air, 21 % oxygen in nitrogen, cleaned compressed air I and cleaned compressed air II. The performance of the cells was recorded by means of Electrochemical Impedance Spectroscopy. A clear increase in the polarization resistance of the LSM-YSZ cathode caused by impurities in air was observed, mainly affecting the coupled processes of dissociative adsorption of oxygen and surface diffusion of oxygen species.

The increase of the polarization resistance was less when cleaning the air before entering the test setup. Moreover, the initial performance could be recovered to a large extent by heating the symmetrical cells to 850 °C for a few hours. Humidity in air was found to increase degradation significantly, while the addition of CO_2 had no influence.

4.1 Introduction

Long lifetime is an important requirement for commercialization of Solid Oxide Fuel Cells (SOFCs). It was observed that for an anode supported Ni-YSZ/YSZ/LSM-YSZ single cell, degradation of the cathode can be the dominant contribution to the degradation, especially at lower temperature and high cathode overpotential [1]. Several processes are known to limit the lifetime of SOFC LSM-YSZ composite cathodes; processes can be either intrinsic; i.e. caused by internal sources; chemical reaction between materials, phase changes or segregation of elements/impurities, or extrinsic; i.e. caused by external sources, like impurities in the gas phases. The formation of zirconates at the LSM-YSZ interface is the most well described intrinsic degradation mechanism at the cathode [2]. Zirconates like $La_2Zr_2O_7$ (LZO) and $SrZrO_3$ (SZO) are less conducting than YSZ, by an order of magnitude of 2 to 3 [3]. Consequently, their formation decreases the performance of the cathode/electrolyte interface. It was shown in literature that an A-site deficient cathode composition can prevent or at least retard zirconate formation [2]. Moreover a 'safe' operation regime was determined; to prevent zirconate formation a relatively low sintering temperature has to be applied, and relatively low cathode overpotential has to be ensured during operation [4].

Different kinds of impurities were also found to cause degradation of SOFCs. The source of these impurities can be their presence in raw materials, system components or applied gases. Trace elements, like SiO_2, TiO_2, Fe_2O_3, Na_2O and other oxides are always present in raw materials. During sintering or operation at high temperature some of the trace elements segregate to the surface of the materials. These segregated oxides might block the active triple phase boundary (TPB), or even cause delamination between the electrolyte and electrode [5, 6]. Impurities originating from system components, like metallic interconnect metals and sealing glasses were also observed at the cathode. One of them includes LSM poisoning by chromium species [7, 8]. Chromium species are known to be deposited mainly at the TPB, thereby poisoning the active TPB for the oxygen reduction reaction. The gas phase also contains impurities; the most described impurity is sulfur present in fuel gases [9-11]. Impurities in air, causing degradation on the LSM cathode have been described less, but recently research groups from EPFL, Switzerland [10] and AIST, Japan [11-14], have addressed this topic. Impurities like S, Na, Al, Si and P were

observed at the SOFCs cathode after long-term operation of a SOFC stack, even if the impurities were present in very low concentration levels in the gas (ppb up to a few ppm) [12-15].
Another extrinsic degradation mechanism at the cathode was related to humidity in air. Some of the impurities coming from system components, like Cr, are known to become more volatile in the presence of humidity, causing increased degradation [16]. Also, segregation of impurities from the bulk of the raw material to the surface was reported to be enhanced in humid atmospheres [17]. Moreover, humid air in itself was also found to cause passivation (reversible increase of the polarization resistance) and degradation of the LSM cathode [18-20].
Recently, a method to clean supplied gases was developed in our group [21]. It was shown that for a Solid Oxide Electrolysis Cell (SOEC), no degradation was observed when the gases were cleaned [22, 23]. However, as the supplied gas at the LSM electrode was O_2, no significant degradation of this electrode was expected, as high pO_2 was maintained and the supplied gas was of high purity [24].

The aim of this study was to investigate the influence of impurities in air on the increase of the LSM/YSZ cathode polarization resistance with time, determining which processes at the cathode are affected.
The influence of impurities in air on LSM-YSZ/YSZ/LSM-YSZ symmetrical cells was investigated by Electrochemical Impedance Spectroscopy (EIS). The tests were carried out at 750 °C and OCV, applying different air compositions: compressed air, a mixture of 21 % O_2 in N_2 and cleaned compressed air (I and II). Furthermore the addition of H_2O and CO_2 to the air mixture was investigated.

4.2 Experimental

Cell preparation. LSM25 [$(La_{0.75}Sr_{0.25})_{0.95}MnO_{3\pm\delta}$] powder was received from Topsoe Fuel Cell. The phase purity of LSM25 was confirmed by powder X-ray diffraction. The LSM25 powder was calcined at 950 °C for 2 hours prior to use. For more details on the LSM25 powder, see reference [25]. 8YSZ (ZrO_2 with 8 mol% Y_2O_3) powder was used as supplied by Tosoh. A cathode screen-printing ink was produced by suspending the powders, at a 50-50 wt% ratio, in an organic solvent, together with a dispersant. The suspension was ball milled for 4 h, after which binder and

modifiers were added. The ink was screen-printed on either side of a 5 x 5 cm^2 8YSZ electrolyte strip (~100 to 200 μm thick) and fired at 1050 °C for 2 hours. The resulting symmetrical cells were cut to 8 x 8 mm^2 pieces and Pt paste (Ferro) was painted onto the cells, serving as a current collection layer. Subsequently the cells were sintered at 850 °C for 2 hours in stagnant air.

Cell characterization. The experimental setup consists of four cell positions, where each symmetrical cell was placed between two Pt-grids used for current collection. The setup was placed in a furnace, applying different qualities of air: ambient air (no flow), 6 l/h compressed air, 6 l/h mixture of 21 % O_2 (Air liquide, ≥ 99.995 % clean) and 79 % N_2 (Air liquide, ≥ 99.995 % clean), the pO_2 was controlled by mixing nitrogen and oxygen gases using thermal mass flow controllers. In two experiments the compressed air was cleaned, applying two different methods, I and II: the cleaning methods are subject to a pending patent application [21]. It is expected that cleaning method II results in the cleanest air. In two other experiments CO_2 and/or H_2O were added to 21 % O_2 in N_2; 0.3 l/h CO_2 was added by using a thermal mass flow controller, H_2O by feeding the gas through a bubble flask at ~30 °C, leading to ~3 % humidified air. Impedance spectra were recorded using a Solartron 1260, at OCV, applying an AC voltage, ensuring a maximum current density amplitude of 1.7 mA/cm^2 at all frequencies. The frequency range measured was from 0.1525 to 707900 Hz, recording 15 points per decade.

Data analysis. The impedance data were checked for consistency with the Kronig-Kramer relations using the "KK test" software developed by Boukamp [26]. The relative errors for the EIS data were determined to be 0.2 % or below, therefore the EIS data are considered of good quality. The KKtest fits produced χ^2 values in the range $9 \cdot 10^{-8}$ to $1 \cdot 10^{-7}$.

Impedance data were analyzed using Zview 2. Zview 2 is commercially available software from Scribner Associates, Inc., and includes a complex nonlinear least square fitting routine. The EIS data were fitted to the equivalent circuit depicted in Figure 4.1. The *n*-value for arc B was fixed at 0.5.

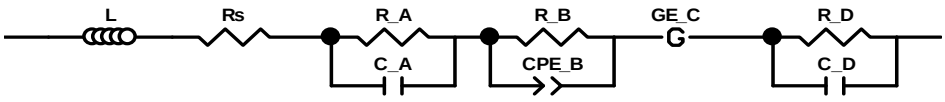

Figure 4.1. Equivalent circuit applied, see Chapter 3.

The inductance of the test equipment was determined by fitting of the EIS data recorded at 850 °C, where its contribution is relatively large. Thereafter the EIS data where corrected for inductance (L) before plotting:

$$-Z_{imagcorr} = -Z_{imag} + (L \cdot f \cdot 2\pi) \qquad [4.1]$$

For all types of air 4 samples were tested, of which 2 or 3 samples resulted in reliable results. These samples were fitted as described above. The results shown in this study are the averaged values from the samples.
The Analysis of Differences in Impedance Spectra (ADIS) method [27] is a method to plot the difference in derivative with respect to ln(f) of the real part of the impedance of two different impedance spectra, A and B. The method was shown to be helpful in separating overlapping processes in impedance data. It was applied in this study to get further insight in which frequency ranges are affected as the polarization resistance (R_p) increased over time. The method for calculating ADIS is as follows:

$$\Delta Z_{real}(\omega) \cong \frac{\left[Z_{realB}(\omega_{n-1}) - Z_{realA}(\omega_{n-1})\right] - \left[Z_{realB}(\omega_{n+1}) - Z_{realA}(\omega_{n+1})\right]}{\left[\ln(\omega_{n+1}) - \ln(\omega_{n-1})\right]} \qquad [4.2]$$

4.3 Results and discussion

The development of the R_p of the LSM-YSZ/YSZ/LSM-YSZ symmetrical cells in different qualities of air is shown in Figure 4.2. The initial values of R_p for the samples varied between samples, probably caused by slight differences in cathode microstructure and thickness. However, the trend of *Rp* increase over time is the same for all samples tested in the same conditions. All of the samples showed significant increase of R_p over time, and there is a clear difference between the different atmospheres applied. While overall degradation of R_p is similar for the symmetrical cells tested in

compressed and cleaned compressed air I, a clear decrease in degradation of R_p was observed when applying 21 % oxygen in nitrogen and even more so when applying cleaned compressed air II. As the latter two qualities of air are expected to be cleaner than the first three qualities of air, this indicates that impurities in air are causing a major part of the increase of R_p of the LSM-YSZ/YSZ/LSM-YSZ symmetrical cells.

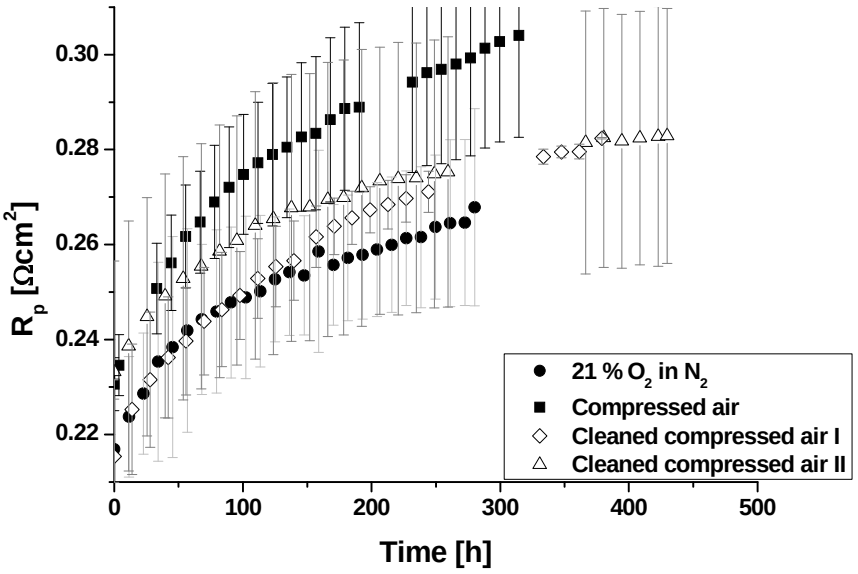

Figure 4.2. Development of polarization resistance with time at 750 °C in different qualities of air, the values shown are averages of 2 or 3 cells tested at the same time.

To determine which of the processes in the tested symmetrical cells were affected by degradation caused by impurities in air, the obtained impedance spectra were fitted to the equivalent circuit shown in Figure 4.1. An example of the fitted impedance spectra, in 21 % oxygen in nitrogen, initially and after 280 hours of testing is shown in Figure 4.3. Figure 4.4 shows the Bode and ADIS plots for the same spectra as shown in Figure 4.3 [27]. The development of the magnitude of the different processes with time in 21 % O_2 in N_2 is shown in Figure 4.5a. Figure 4.5b and 4.5c show the development of arc C with time in all qualities of air applied in this study. In Table 4.I the initial values and degradation rates of the resistances in the equivalent circuit are given for each of the tests.

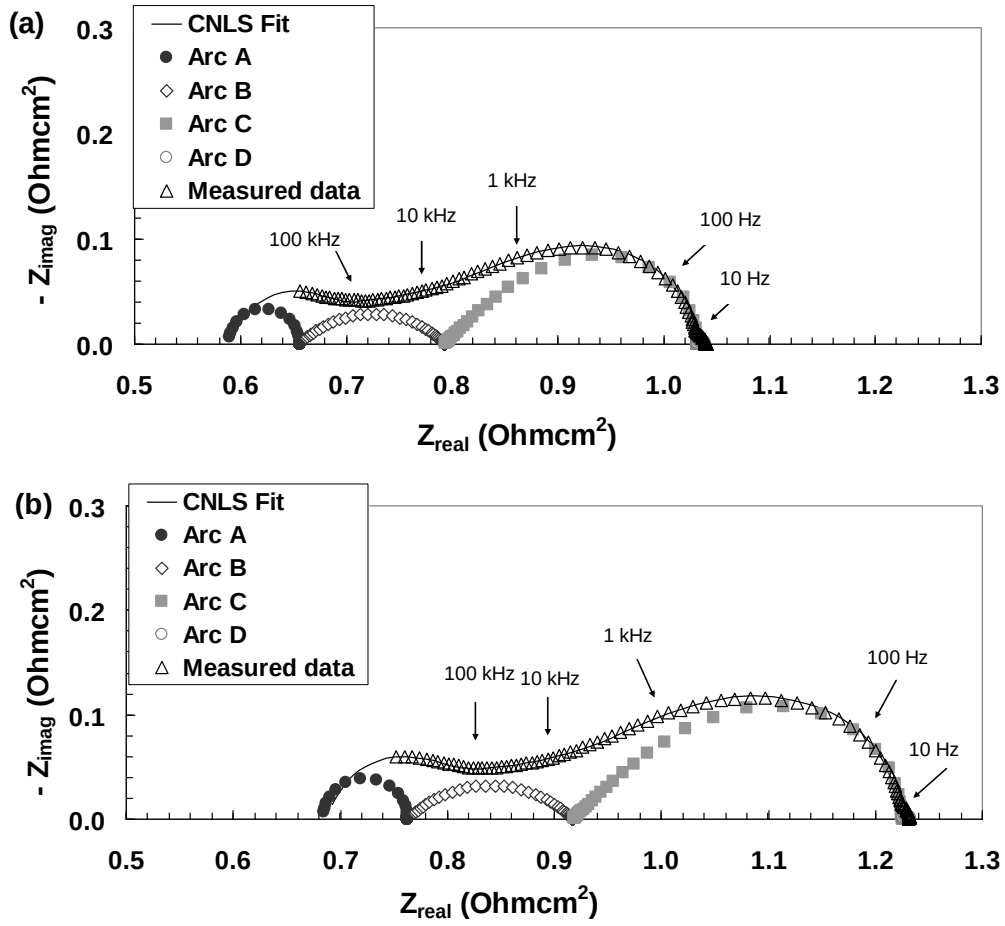

Figure 4.3. Breakdown of (inductance corrected) impedance spectra, in 21 % O_2 in N_2 atmosphere, by use of the equivalent circuit shown in Figure 4.1. (a) Spectrum recorded at 0 hours; (b) spectrum recorded at 280 hours.

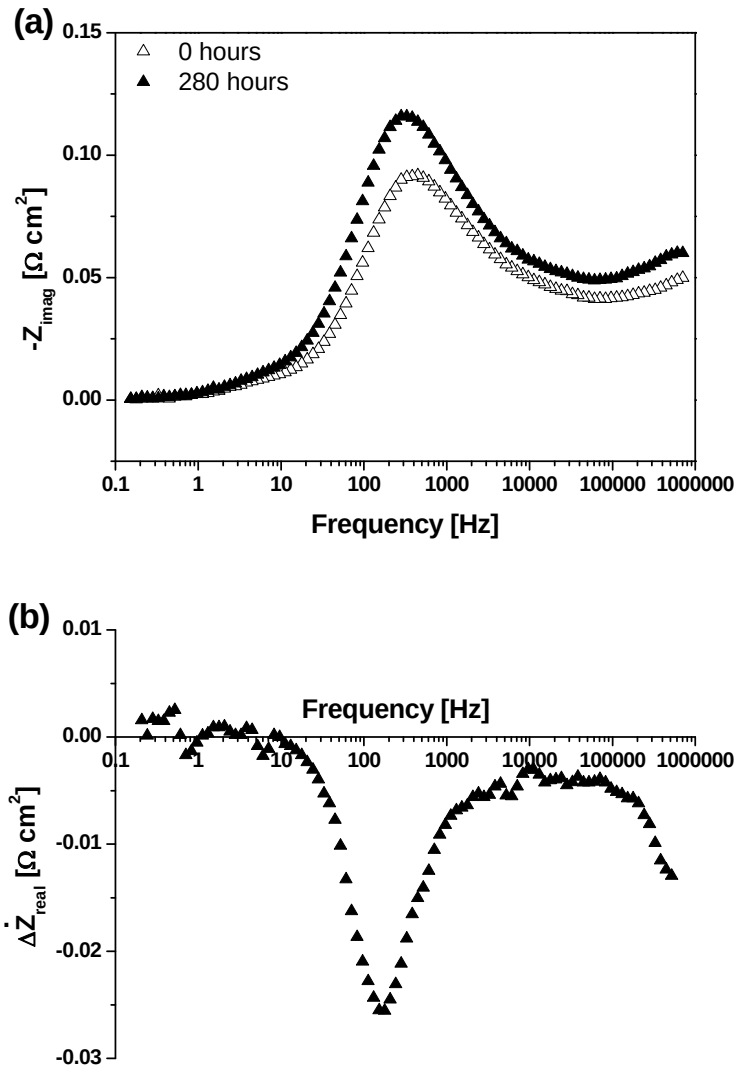

Figure 4.4. (a) Bode and (b) ADIS plots of impedance spectra, corrected for inductance, in 21 % O_2 in N_2 atmosphere, 280-0 hours.

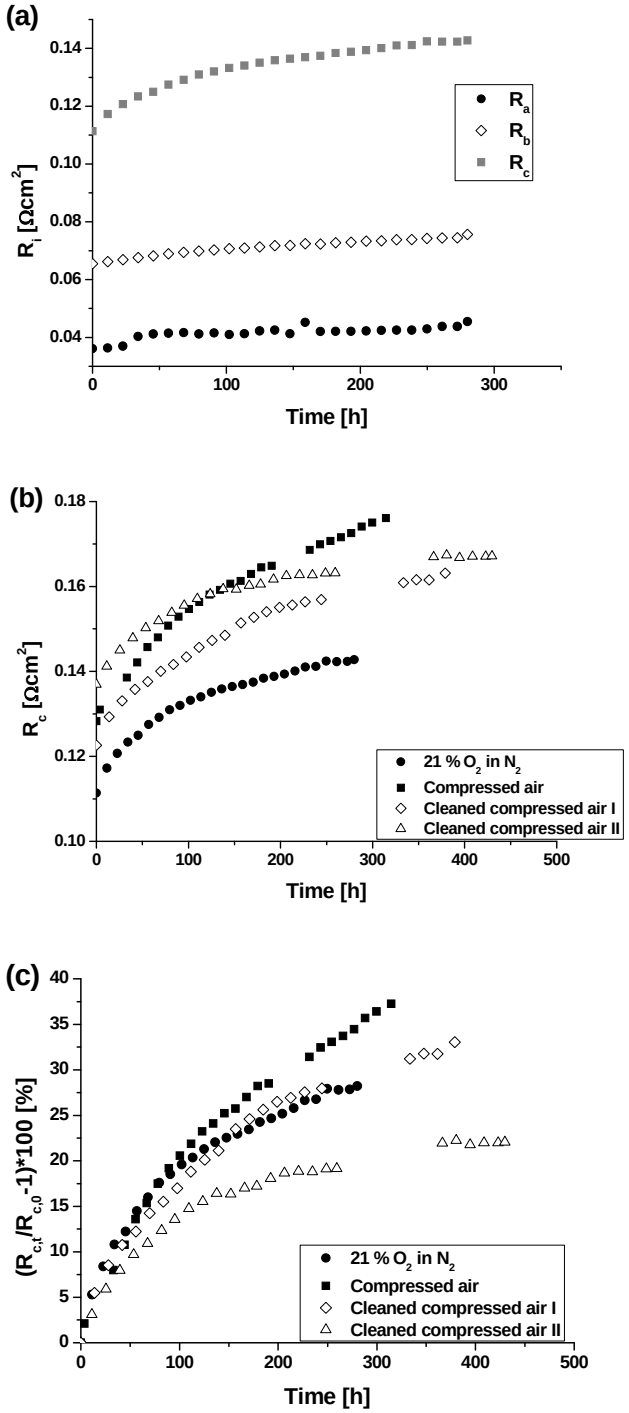

Figure 4.5. (a) Development of $R_{a\text{-}c}$ with time at 750°C and in 21 % O_2 in N_2, as found by fitting to the equivalent circuit of Figure 4.1. (b) Development of R_c with time at 750 °C in different qualities of air. (c) Change of R_c in percentage from the initial R_c with time at 750°C in different qualities of air.

TABLE 4.I. Degradation of LSM-YSZ/YSZ/LSM-YSZ symmetrical cell at 750 °C in different qualities of air. All values are the average of fitting of two or three samples. Note that R_A-R_D values, and therefore also the *Rp* value, are divided by two, so they are based on one average electrode only. Degradation rates were calculated based on the period from 0 to ~ 250 hours.

	$LR_S(R_AC_A)(R_BQ_B)G(R_DC_D)$			
Quality of air	**Compressed air**	**21 % O_2 in N_2**	**Cleaned compressed air I**	**Cleaned compressed air II**
Initial R_p *(Ωcm^2)* ($R_p = R_A+R_B+R_C+R_D$)	0.23	0.21	0.22	0.23
Degradation ***R_p*** *($m\Omega cm^2/1000h$)*	270	182	228	167
Degradation ***R_p*** *(%/1000h)*	117	87	106	72
Initial R_A *(Ωcm^2)*	0.03	0.03	0.03	0.03
Degradation ***R_A*** *($m\Omega cm^2/1000h$)*	52	27	53	34
Degradation ***R_A*** *(%/1000h)*	164	78	194	114
Initial R_B *(Ωcm^2)*	0.07	0.06	0.06	0.06
Degradation ***R_B*** *($m\Omega cm^2/1000h$)*	46	39	35	28
Degradation ***R_B*** *(%/1000h)*	68	54	56	44
Initial R_C *(Ωcm^2)*	0.13	0.11	0.12	0.14
Degradation ***R_C*** *($m\Omega cm^2/1000h$)*	171	122	140	105
Degradation ***R_C*** *(%/1000h)*	134	112	115	77
Initial R_D *(Ωcm^2)*	0.002	0.004	0.002	0.002

Figure 4.4 shows that the main frequency range affected by degradation over time was around 100 Hz. Furthermore, the peak located around 1 MHz changed with time, and a smaller effect was observed in the frequency range around 5-50 kHz. These frequency ranges correspond with arc C, arc B and arc A, as described in Chapter 4, respectively.

Figure 4.3 and Table 4.I also show that the increase of R_p affected all processes, except for arc D, which describes the oxygen gas diffusion (Chapter 4). The latter is as expected, as the oxygen gas diffusion arc is only affected by degradation over time if the porosity of the electrode changes, which is not expected for LSM/YSZ cathodes operated below 900 °C [14].

Arc A was most likely caused by current constriction due to bad contacting at the electrode/electrolyte interface. The increased resistance of this process can possibly be explained by the formation of either a zirconate layer at the interface, segregation of impurities from the raw materials to the interface, or migration of impurities from the gas phase to the interface, all leading to increased current constriction. The latter two are more likely at the conditions applied in this experiment, as the conditions were in the 'safe' operation regime, where zirconate formation is not expected to occur [4].

Deposition of impurities from the gas phase, and their migration to the electrode/electrolyte interface has possibly increased the resistance of Arc A, as the increase of R_A was lower for the samples tested in cleaner air (21 % oxygen in nitrogen and cleaned compressed air II).
Arc B describes the ionic transport in the YSZ matrix. This process could be affected over time if the ionic conductivity of the YSZ decreases with time. This might be the case if for example Mn dissolves from LSM into YSZ, which was observed earlier by Yokokawa et al. [14]. The process should not directly be affected by impurities from the gas phase, but could be slightly affected indirectly as the rest of the spectrum changes. This agrees with the experiments in this study, showing that arc B passivated/degraded slightly with time, but no significant difference was observed depending on the quality of air applied.
Arc C describes the coupled processes of dissociative adsorption of oxygen and surface diffusion of oxygen species. This process is expected to be affected by degradation over time, as impurities from air could cover the LSM surface and/or the TPB. The experiments in this study showed a successively reduced degradation as the purity of the oxidant gas increased.

Reactivation of the LSM-YSZ/YSZ/LSM-YSZ symmetrical cell
Passivation of the LSM-YSZ/YSZ/LSM-YSZ symmetrical cell by deposition of impurities at the cathode surface/TPB/cathode-electrolyte interface is possibly reversible if the impurities could be desorbed again. One method to achieve this is to increase the temperature of the symmetrical cell. Therefore, the temperature was increased from 750 °C to 850 °C in the tests in 21 % oxygen in nitrogen and cleaned compressed air I, for a short period of time (~24 hours). The influence on R_p for the case of 21 % oxygen in nitrogen is shown in Figure 4.6.

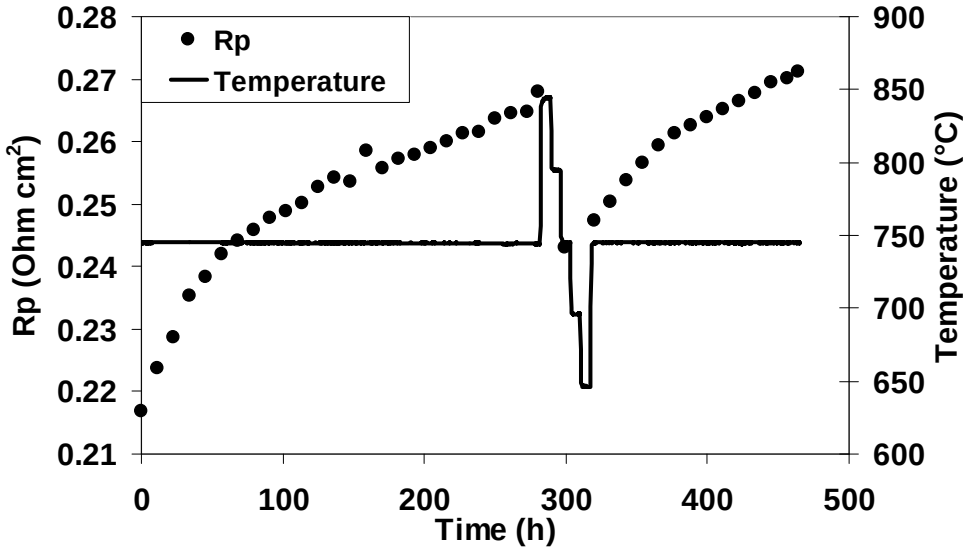

Figure 4.6. Partial recovery of the polarisation resistance after a short period of time at a higher temperature (850 °C), all in 21 % O_2 in N_2 atmosphere.

A partial recovery of R_p was observed; recovering 40 % (20 mΩcm^2) of the passivation in the case of 21 % oxygen in nitrogen, and 64 % (43 mΩcm^2) in the case of cleaned compressed air I. Clearly, the symmetrical cells in the atmosphere with most impurities (cleaned compressed air I) had recovered most, indicating that the recovery was, at least in part, due to desorption of some of the impurities.

It was determined which processes were affected in the recovery by making an Bode and ADIS plot from EIS data before and after partial recovery of R_p, which are shown in Figure 4.7. Moreover the recovery of each of the processes was determined by fitting the impedance spectra before and after heating to 850 °C. The recovery of each of the resistances is given in Table 4.II.

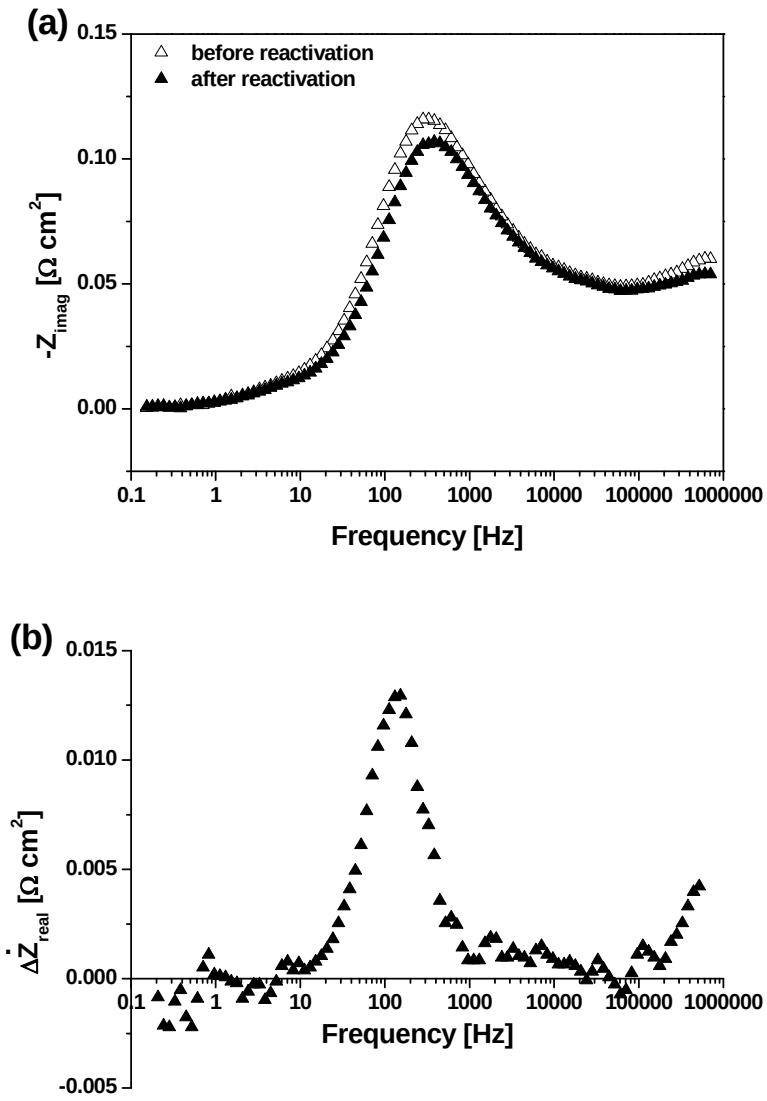

Figure 4.7. (a) Bode and (b) ADIS of impedance spectra, corrected for inductance, in 21 % O_2 in N_2 atmosphere, before and after partial recovery at 850 °C.

TABLE 4.II. Recovery of LSM-YSZ/YSZ/LSM-YSZ symmetrical cells after a few hours at elevated temperature; 850 °C in different qualities of air. Note that R_A-R_D values, and therefore also the R_p value, are based on one electrode only. All values are the average of fitting of two or three samples.

		$LR_S(R_AC_A)(R_BQ_B)G(R_DC_D)$	
	Quality of air	**21 % O_2 in N_2**	**Cleaned compressed air I**
Recovery			
R_p	$m\Omega cm^2$	20	43
	%	40	64
R_A	$m\Omega cm^2$	7	10
	%	73	64
R_B	$m\Omega cm^2$	2	2
	%	16	18
R_C	$m\Omega cm^2$	12	31
	%	38	76

From the Bode and ADIS plots it is clear that the processes in the frequency ranges around 100 Hz (Arc C) and 1 MHz (Arc A) were reactivated upon heating the symmetrical cells to 850 °C. This is confirmed by fitting of the cells, which showed a significant recovery of arc A and C, while Arc B shows only a minor recovery. As described in the previous section, the processes involved in Arc C are likely affected by deposition of impurities, and can be reactivated partially upon desorption of these impurities. Degradation of the Arc B, ionic transport in the YSZ matrix, was not caused by impurities and did therefore, as expected, not recover upon heating the symmetrical cells. Arc A, was found to degrade with time, current constriction might be increased by the degradation of arc C, causing arc A to degrade along with arc C.

Influence of humidity and CO_2 on the increase of the polarization resistance of LSM-YSZ/YSZ/LSM-YSZ symmetrical cells

One difference between 21 % oxygen in nitrogen and compressed air is that the first does not contain CO_2. Furthermore, compressed air is likely to contain more humidity than 21 % oxygen in nitrogen or cleaned air, even though the humidity of compressed air in our laboratory was tested to be below 0.1 % [24]. Therefore, two experiments were carried out in 21 % oxygen in nitrogen, adding H_2O, CO_2 or both to the gas mixture. The first experiment was carried out in 21 % oxygen in nitrogen; where after 50 hours of testing H_2O was added to the gas mixture by leading the gas at through a bubble flask at ~30 °C. 180 hours into the test the H_2O was turned off again. The second experiment was also carried out in 21 % oxygen in nitrogen. After 24 hours CO_2 was added (0.3 l/h) to the gas mixture. At 160 hours H_2O was also added to the gas mixture, until 230 hours where the humidity was turned off again. The result of the two experiments is shown in Figure 4.8.

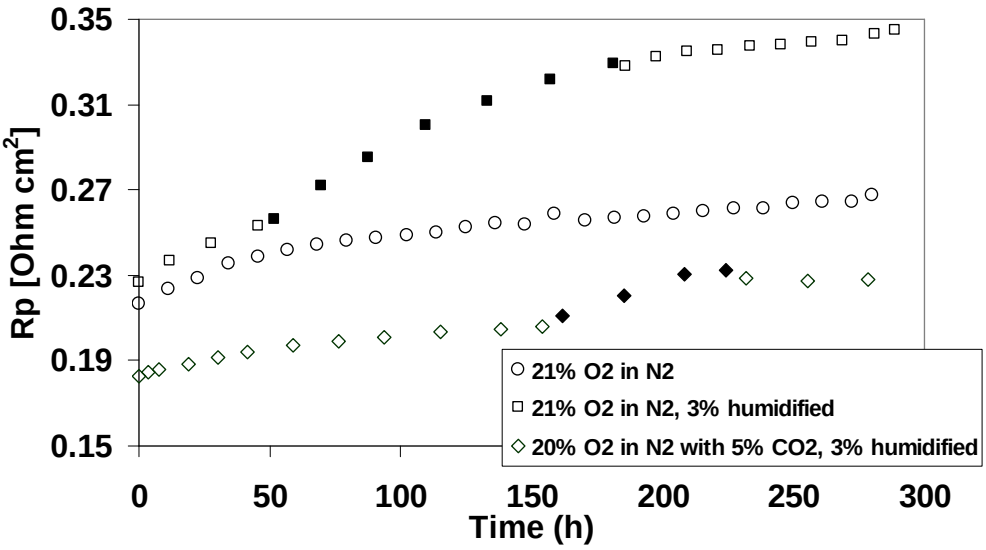

Figure 4.8. Influence of humidity and addition of CO_2 to 21 % O_2 in N_2 atmosphere on the degradation of Rp. 'Open' symbols, dry gas; 'closed' symbols ~3 % humidified gas.

The addition of 3 % humidity to the 21 % oxygen in nitrogen gas mixture caused a significant increase in R_p. When the humidity was turned of a small

reactivation was observed, followed by a lower degradation rate, similar to the degradation rate in the experiment which was entirely carried out in 21 % oxygen in nitrogen. Previously, humidity air was applied to anode supported Ni-YSZ/YSZ/LSM-YSZ single cells [19, 20]. Nielsen et al. [20] did not observe an increased degradation rate at OCV for single cells. Nonetheless, both authors observed an increased degradation rate of the LSM/YSZ cathode caused by humidity in air when current load was applied. Addition of CO_2 had no influence, or even decreased the degradation rate of R_p slightly.

To verify which processes were affected by the addition of humidity, the ADIS plot of the end minus start of the humid period is shown in Figure 4.9. The degradation rates in 21 % oxygen in nitrogen are compared with those in 21 % oxygen in nitrogen containing 3 % humidity in Table 4.III. Values are calculated after fitting the impedance spectra to the equivalent circuit in Figure 4.1. The ADIS plot in Figure 4.8 shows that the increase of R_p caused by humidity was observed around 100 Hz, which corresponds to Arc C. This observation is confirmed by the degradation rates from Table 4.III; while the degradation rates of Arc A and Arc B increase only slightly when the 21 % oxygen in nitrogen gas mixture was humidified, Arc C increased by a factor of almost 3. Arc C describes the coupled processes of dissociative adsorption of oxygen and surface diffusion of oxygen species.

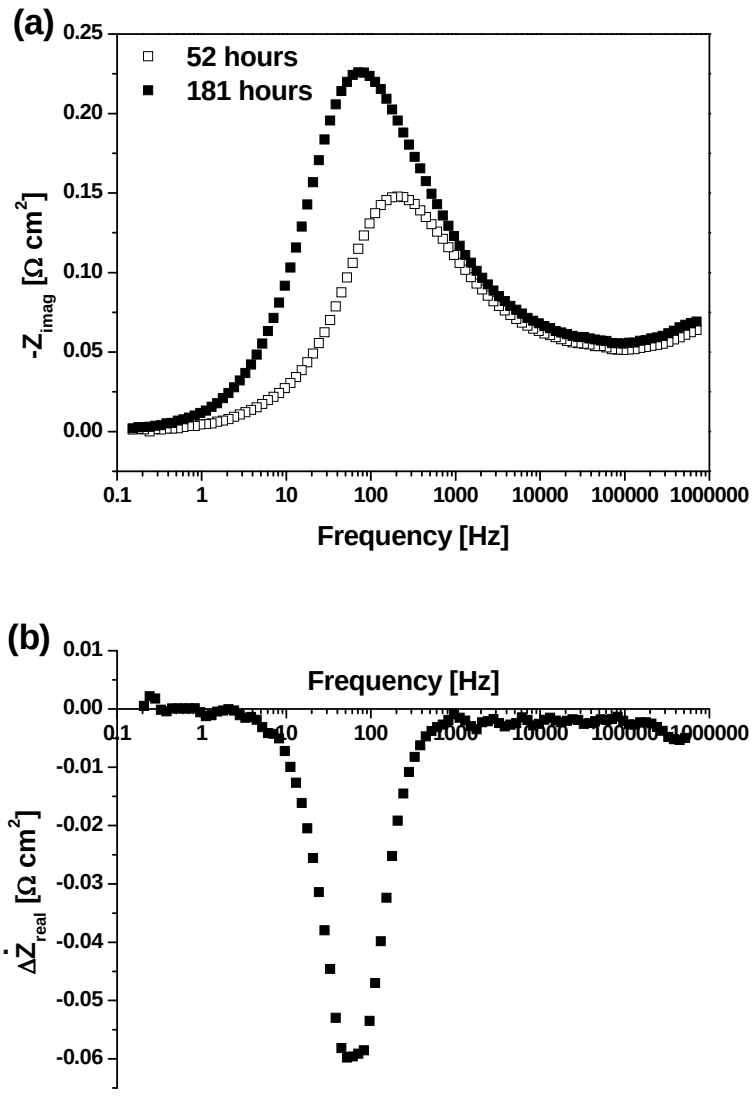

Figure 4.9. (a) Bode and (b) ADIS of impedance spectra, corrected for inductance, in humidified 21 % O_2 in N_2 atmosphere, 181-52 hours.

Microscopy studies on the under humidity degraded YSZ/LSM-YSZ interface of anode supported Ni-YSZ/YSZ/LSM-YSZ [4, 19, 20] showed changes of the YSZ interface, mainly at the 'craters' where YSZ and LSM were contacted. Ripples and sometimes also nanoparticles were noted on the surface, the 'craters' where flattened out and increased Si, Ca, Mn and S concentrations were detected at the YSZ/LSM contact areas and around the

nanoparticles. These observations explain that the processes of Arc C are affected by humidity, as the processes take place at the electrode/electrolyte interface, preferably around the TPB.

TABLE 4.III. Degradation of LSM-YSZ/YSZ/LSM-YSZ symmetrical cell at 750 °C in 21 % O_2 in N_2, with and without 3 % humidity. Note that R_A-R_D values, and therefore also the *Rp* value, are based on one electrode only. All values are the average of fitting of two or three samples.

	$LR_S(R_AC_A)(R_BQ_B)G(R_DC_D)$	
Quality of air	**21 % O_2 in N_2**	**21 % O_2 in N_2, 3 % humidity**
Time period	0-250 h	51-182 h
Degradation		
R_s *(mΩcm²/1000h)*	55	83
R_s *(%/1000h)*	8	14
R_p *(mΩcm²/1000h)*	182	565
R_p *(%/1000h)*	87	221
R_A *(mΩcm²/1000h)*	27	40
R_A *(%/1000h)*	78	91
R_B *(mΩcm²/1000h)*	39	60
R_B *(%/1000h)*	54	77
R_C *(mΩcm²/1000h)*	122	504
R_C *(%/1000h)*	112	291

4.4 Conclusion

Impurities in air were the cause of a significant part of the increase over time of R_p of LSM-YSZ/YSZ/LSM-YSZ symmetrical cells tested at 750 °C at OCV. Cleaning preheated compressed air before entering the test-setup was found to decrease the increase of R_p by at least one third. Impedance analysis showed that the main cathode processes affected by impurities were the coupled processes of dissociative adsorption of oxygen and surface diffusion of oxygen species, indicating that impurities were accumulating on the LSM/YSZ surface and at the triple phase boundary. When increasing the temperature from 750 °C to 850 °C for a few hours, the activity of the symmetrical cell was partially recovered. Humidity in air increased the passivation or degradation rate significantly, whilst the addition of CO_2 to air had no influence.

4.5 References

1. A. Hagen, R. Barfod, P. V. Hendriksen, Y. -. Liu and S. Ramousse, *J. Electrochem. Soc.,* **153**(6), A1165 (2006).
2. A. Mitterdorfer and L. J. Gauckler, *Solid State Ionics,* **111**, 185 (1998).
3. F. W. Poulsen and N. van der Puil, *Solid State Ionics,* **53-56**, 777 (1992).
4. Y. L. Liu, A. Hagen, R. Barfod, M. Chen, H. J. Wang, F. W. Poulsen and P. V. Hendriksen, *Solid State Ionics,* **180**, 1298 (2009).
5. M. Mogensen and K. V. Hansen, in *Handbook of Fuel Cells - Fundamentals, Technology and Applications. Vol 5, Advances in Electrocatalysis, Materials, Diagnostics and Durability.*, Volume 5 ed., W. Vielstich, A. Lamm, H. A. Gasteiger and H. Yokokawa, Editors, Wiley-Blackwell (2009).
6. D. Kuscer, J. Holc, M. Hrovat, S. Bernik, Z. Samardzija and D. Kolar, *Solid State Ionics,* **78**, 79 (1995).
7. J. W. Fergus, *Int. J. Hydrogen Energ.,* **32**, 3664 (2007).
8. N. H. Menzler, A. Mai and D. Stöver, in *Handbook of Fuel Cells - Fundamentals, Technology and Applications*, Volume 5: Advances in Electrocatalysis, Materials, Diagnostics and Durability ed., W. Vielstich, H. Yokokawa and H. A. Gasteiger, Editors, p. 566, John Wiley & Sons, Ltd. (2009).
9. Y. Matsuzaki and I. Yasuda, *Solid State Ionics,* **132**, 261 (2000).
10. A. J. Schuler, Z. Wuillemin, A. Hessler-Wyser and J. Van herle, *ECS Trans.,* **25**(2), 2845 (2009).
11. Y. Xiong, K. Yamaji, T. Horita, H. Yokokawa, J. Akikusa, H. Eto and T. Inagaki, *J. Electrochem. Soc.,* **156**(5), B588 (2009).
12. H. Yokokawa, T. Watanabe, A. Ueno and K. Hoshino, *ECS Trans.,* **7**(1), 133 (2007).
13. T. Horita, H. Kishimoto, K. Yamaji, M. E. Brito and H. Yokokawa, *ECS Trans.,* **26**(1), 349 (2010).
14. H. Yokokawa, H. Tu, B. Iwanschitz and A. Mai, *J. Power Sources,* **182**, 400 (2008).
15. H. Yokokawa, N. Sakai, T. Horita and K. Yamaji, in *Handbook of Fuel Cells - Fundamentals, Technology and Applications*, Volume 6: Advances in Electrocatalysis, Materials, Diagnostics and Durability ed., W. Vielstich,

H. Yokokawa and H. A. Gasteiger, Editors, p. 979, John Wiley & Sons, Ltd. (2009).
16. S. P. S. Badwal, R. Deller, K. Foger, Y. Ramprakash and J. P. Zhang, *Solid State Ionics,* **99**, 297 (1997).
17. A. Hauch, S. H. Jensen, J. B. Bilde-Sørensen and M. Mogensen, *J. Electrochem. Soc.,* **154**(7), A619 (2007).
18. S. H. Kim, K. B. Shim, C. S. Kim, J. T. Chou, T. Oshima, Y. Shiratori, K. Ito and K. Sasaki, *J. Fuel Cell Sci. Tech.,* **7**, 021011-1 (2010).
19. A. Hagen, K. Neufeld and Y. L. Liu, *J. Electrochem. Soc.,* **157**(10), B1343 (2010).
20. J. Nielsen, A. Hagen and Y. L. Liu, *Solid State Ionics,* **181**, 517 (2010).
21. S. D. Ebbesen and M. Mogensen, (Patent Pending).
22. S. D. Ebbesen and M. Mogensen, *Electrochem. Solid-State Lett.,* **13**(9), B106 (2010).
23. S. D. Ebbesen, C. Graves, A. Hauch, S. H. Jensen and M. Mogensen, *J. Electrochem. Soc.,* **157**(10), B1419 (2010).
24. A. Hagen, Y. L. Liu, R. Barfod and P. V. Hendriksen, *J. Electrochem. Soc.,* **155**(10), B1047 (2008).
25. K. Kammer Hansen, M. Menon, J. Knudsen, N. Bonanos and M. Mogensen, *J. Electrochem. Soc.,* **157**(3), B309 (2010).
26. B. A. Boukamp, *J. Electrochem. Soc.,* **142**(6), 1885 (1995).
27. S. H. Jensen, A. Hauch, P. V. Hendriksen, M. Mogensen, N. Bonanos and T. Jacobsen, *J. Electrochem. Soc.,* **154**(12), B1325 (2007).

CHAPTER 5

Additional results on symmetrical cells

5.1 Introduction

The performance and degradation of SOFCs is known to be very sensitive to several factors, like preparation method, testing conditions, time on shelf, and even on the person preparing and testing the cell. During this PhD study two different batches of LSM-YSZ/YSZ/LSM-YSZ symmetrical cells were prepared, using slightly different LSM-YSZ screen printing inks, to compare the difference in response. Cells from batch I, used for obtaining the results on symmetrical cells in Chapter 3 and 4, are compared with cells from batch II in this Chapter.

One major degradation mechanism at the LSM-YSZ cathode / YSZ electrolyte interface is the formation of zirconate species; lanthanum zirconate (LZO) and strontium zirconate (SZO). Zirconate species are hardly conducting, and their formation is therefore responsible for degradation of SOFCs. It is known that excess manganese in the cathode can prevent or at least retard zirconate formation. Possibly, addition of a small amount of manganese to the electrolyte could generate the same effect. Therefore 2 mol% of manganese was added to the YSZ electrolyte and the performance and degradation of the LSM-YSZ/Mn-YSZ/LSM-YSZ cells were investigated.

Finally, as seen in Chapter 4, the increase of the polarisation resistance of LSM-YSZ/YSZ/LSM-YSZ symmetrical cells was enhanced by impurities in air. In an attempt to investigate which impurities were causing this R_p increase, some fresh and tested symmetrical cells were investigated by applying x-ray photoelectron microscopy (XPS).

5.2 Experimental

YSZ electrolytes (110-180 μm thick) were prepared by tape casting 8YSZ powder and cut to 5 x 5 cm squares. Mn-YSZ electrolytes were prepared by mixing 2 mol% of MnO powder with 8YSZ powder by ball milling overnight. The obtained powder was made into a ~180 μm thick electrolyte by tape casting, and the tape was also cut to 5 x 5 cm squares. Two different LSM-YSZ screen printing inks were prepared. For both inks the same LSM25 and 8YSZ powders were used, 50 wt% of each, for preparing the inks. The difference between the inks was the extent of milling and the solvents/dispersant and binders that were applied.

The cells were tested in home build cathode symmetrical cell testing rigs.

Scanning electron microscopy (SEM) images where obtained on a FEG-SEM Supra-35 (Zeiss) and a TM1000 (Hitachi) microscope.
Several fresh and tested symmetrical cells where investigated by x-ray photo electron spectroscopy (XPS), to look for impurities at the surface. In case of the tested cells the platinum current collector paste was scratched off by means of a knife to reach the cathode.

5.3 Results and discussion

5.3.1. Comparison of LSM-YSZ/YSZ/LSM-YSZ symmetrical cells of batch I and II

In Figures 5.1 and 5.2 the difference in cathode microstructure between the LSM-YSZ/YSZ/LSM-YSZ batch I and II is shown and visible. Both cathodes showed some bigger YSZ lumps, although it was worse in the case of batch II. Batch I showed several larger round shaped holes in the cathode, while batch II showed crack-like defects in the microstructure. Figure 5.3 shows the impedance data for both batches at 650 °C in 21 % O_2 in N_2. In Figure 5.3a the Nyquist representation is shown; Figure 5.3b shows the corresponding DRT plots. From the impedance data it was clear that the microstructure of the cathode has a great influence on the performance of the cathode. It appears that the processes involved were the same for both cathodes, but the magnitude is different, and some of the summit frequencies were also shifting slightly. Arc A is much less visible in batch II than in batch I, indicating that the contacting between the electrolyte and the cathode was better in batch II. Possibly this is the case because there are much less holes at the electrolyte/cathode interface in batch II. On the other hand, arc C, describing the coupled process of oxygen dissociation and surface diffusion was much larger in the case of batch II. This may indicate that the triple phase boundary (TPB) length was smaller for of batch II. This could be explained by the observation that the cathode is less well mixed, showing big lumps of YSZ in the cathode microstructure of batch II. The degradation of the two batches was also different. While the initial performance was best for batch I, degradation was worse in this case. At 280 hours of testing the polarisation resistance of batch I had increased by 67 mΩ cm^2, while Rp of the cell from batch II only increased by 27 mΩ cm^2 after 280 hours.

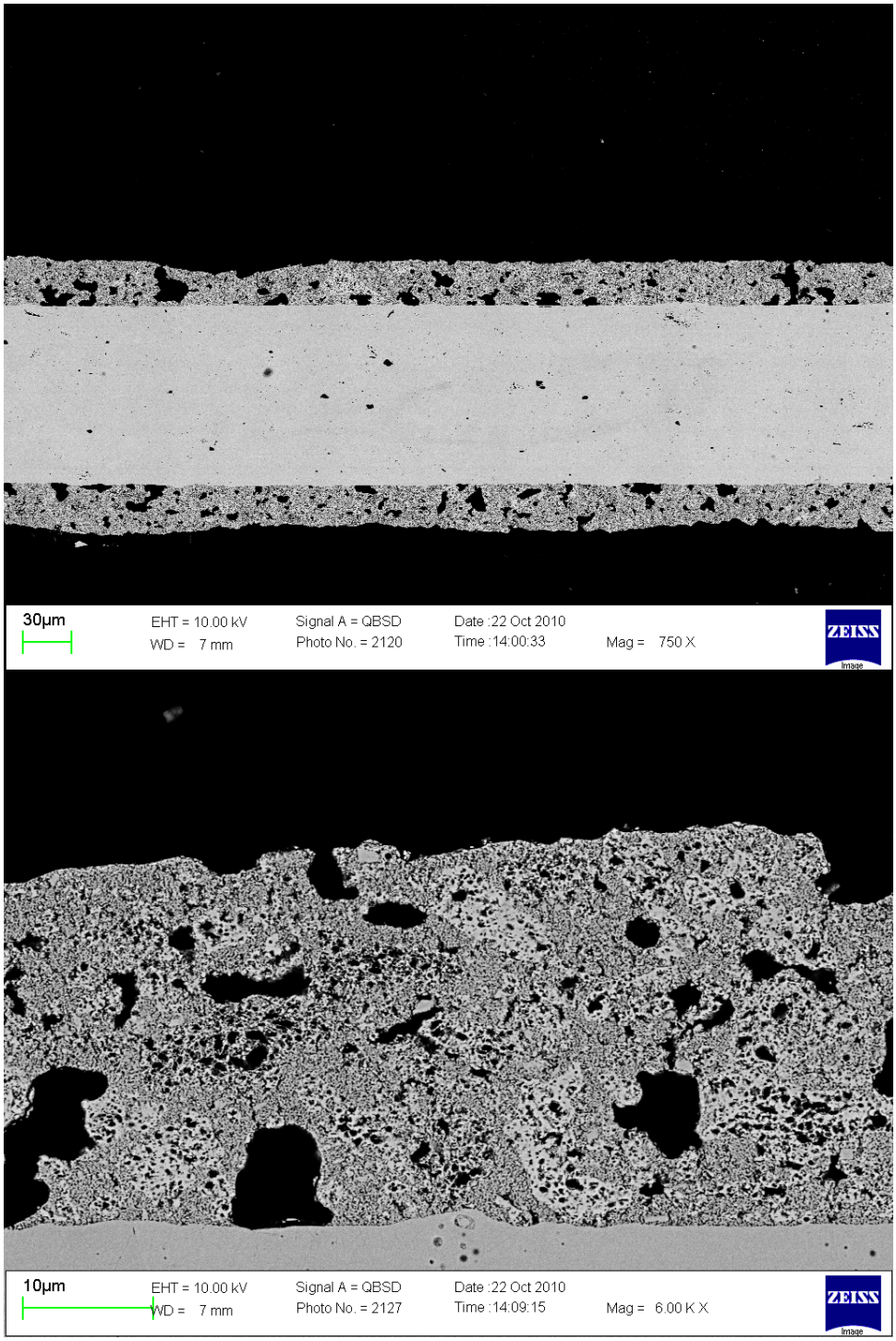

Figure 5.1. Scanning electro microscopy images of the LSM-YSZ/YSZ/LSM-YSZ symmetrical cell of batch I.

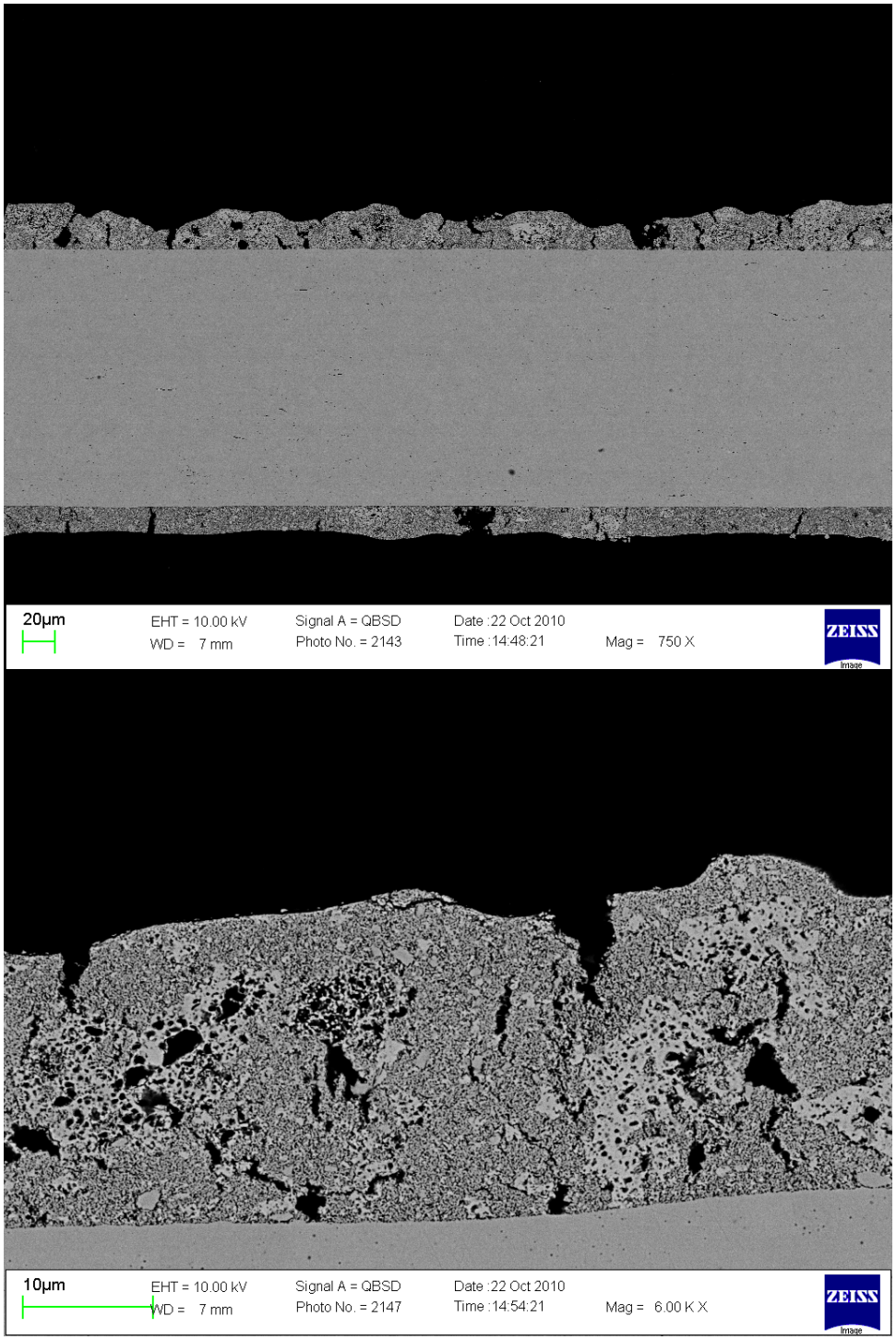

Figure 5.2. Scanning electro microscopy images of the LSM-YSZ/YSZ/LSM-YSZ symmetrical cell of batch II.

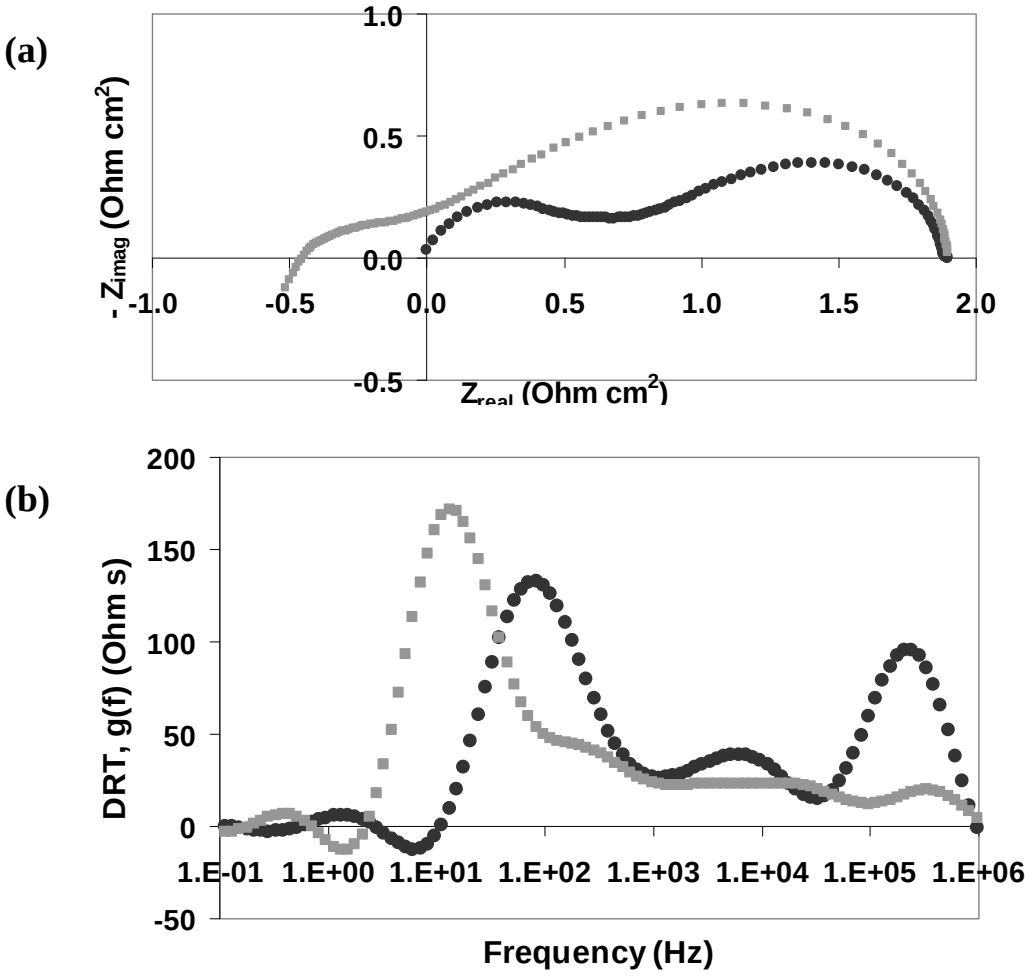

Figure 5.3. Impedance spectra obtained on LSM-YSZ/YSZ/LSM-YSZ symmetrical cells, at 650 °C and in 21 % O_2 in N_2 (●) batch I, (■) batch II; (a) Nyquist representation; (b) corresponding DRT spectra.

5.3.2. Performance and degradation of LSM-YSZ/Mn-YSZ/LSM-YSZ symmetrical cells

When testing the LSM-YSZ/Mn-YSZ/LSM-YSZ symmetrical cell impedance data showed that R_s was a factor 2 bigger than for similar LSM-YSZ/YSZ/LSM-YSZ symmetrical cells. This means that the ionic conductivity of the YSZ electrolyte has decreased. Looking at the SEM image (Figure 5.4) showed that the Mn-enriched electrolyte was less dense than a normal YSZ electrolyte (Figures 5.1 and 5.2). Furthermore, R_p had

also increased by a factor of 1.4. Possibly the contacting between the Mn-YSZ electrolyte and the cathode was worse than for the YSZ electrolyte cells, although this does not show in the SEM image (at the used resolution). Degradation of both R_s and R_p was similar for both symmetrical cells. Therefore the path of manganese enrichment of the electrolyte was not pursued any further.

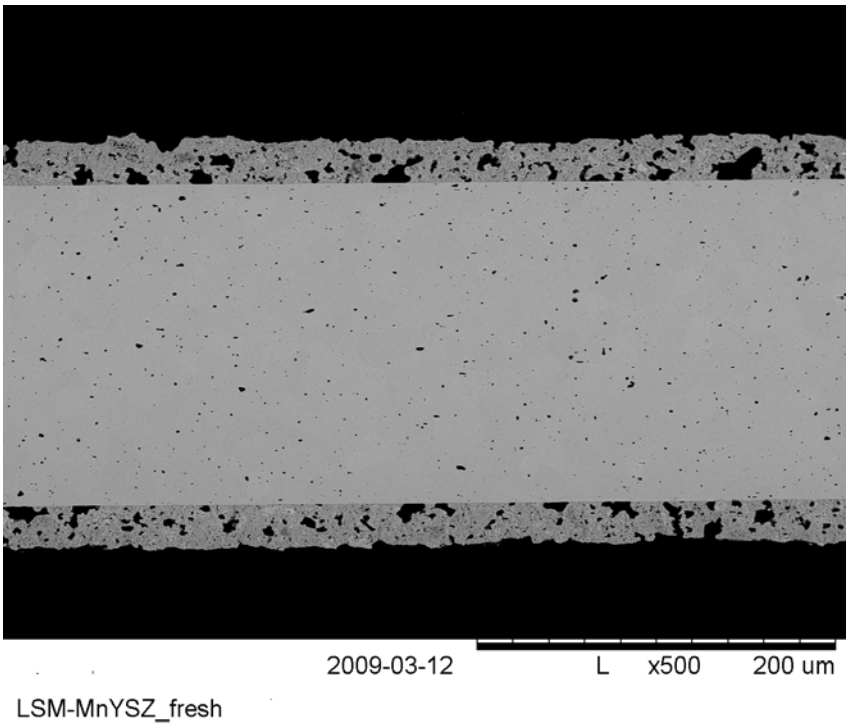

Figure 5.4. Scanning electro microscopy image of the LSM-YSZ/Mn-YSZ/LSM-YSZ symmetrical cell.

5.3.3. Investigation of impurities on the LSM-YSZ surface

Tabel 5.I shows the compositions obtained with XPS for the different samples. In all cases the YSZ content was found to be higher than expected from theory, while the LSM content was lower than expected. It is possible that by scratching off the platinum paste, some of the cathode also came off, so the XPS was measured close to the electrolyte surface, explaining the higher YSZ concentration. Also as the cathode was porous and had some bigger holes as seen in Figure 5.1, this could also mean that part of the XPS is measured at the electrolyte surface.

Few impurities were identified from XPS. Platinum peaks were found for the tested cells, coming from the platinum paste that was apparently not completely removed. At a concentration of less than 1 atomic percent some impurities were found that could be cobalt, barium or iron. The latter seems most likely, the source being the knife with which the platinum paste was removed from the cells. In the sample tested in cleaned compressed air 3 atomic percent of silicon was found. Silicon is known to be present in small amounts in the raw material, which could explain why it was found here. However, no obvious impurities coming from air have been observed by XPS. One explanation could be that no impurities were actually present, and what was causing enhanced degradation was humidity in air only. Another option is that the impurities were present in very small amounts, and localized at the TPB, so they were not detectable by XPS.

TABLE 5.I. Compositions of surface layer as recorded by XPS, all cells came from batch I. Carbon has been disregarded and the resulting compositions are corrected for this.

Sample/ Component	**Theoretical composition**	**Untested**	**Tested in 21 % O_2 in N_2**	**Tested in cleaned compressed air**	**Tested in compressed air**
O	63.8	63.4	63.5	65.9	64.0
Zr	14.7	24.7	23.7	21.4	23.8
La	6.8	2.8	3.1	3.8	3.2
Y	2.8	4.7	4.4	4.9	4.7
Mn	9.6	4.1	4.1	3.0	3.6
Sr	2.3	0.3	1.2	1.0	0.8

5.4 Conclusion

The microstructure of the cathode had a major impact on both the performance and degradation of the symmetrical cell, confirming once more that optimisation of the microstructure can improve performance.

Adding manganese to the electrolyte in order to prevent zirconate formation led to increased series and polarisation resistances, while the degradation rate did not decrease.

No impurities from air were observed when applying x-ray photoelectron spectroscopy to both untested and tested symmetrical cells. Either they were

so much localised that they were never detected, or the only impurity affecting degradation was the humidity in air.

CHAPTER 6

Characterisation of anode supported Ni-YSZ/YSZ/LSM-YSZ single cells

6.1 Introduction

To move one step closer to investigation of the lifetime of a real Solid Oxide Fuel Cell, in this chapter the focus is moved from the symmetrical cell to the corresponding single cell: anode supported Ni-YSZ/YSZ/LSM-YSZ. An advantage is that single cells can be operated under current, like a real SOFC. The disadvantage is that more materials and processes are involved, making interpretation of the results more difficult. Previously the value of testing symmetrical cells, with a thick electrolyte compared to the electrolyte in single cells was questioned by Primdahl et al. [1]. Apart from the fact that symmetrical cell can only be tested at OCV (otherwise one of the electrodes would start functioning as an anode), the symmetrical cell also has a thick (100-200 μm) electrolyte, unlike the single cell, which has an electrolyte of only 10-20 μm.

The aim of this chapter is to study four questions regarding single cell testing:

1. To what extent can LSM-YSZ/YSZ/LSM-YSZ symmetrical cells be compared with Ni-YSZ/YSZ/LSM-YSZ single, anode supported cells, at OCV?
2. How comparable is the degradation of anode supported Ni-YSZ/YSZ/LSM-YSZ single cells tested at OCV and under current?
3. What is the influence of decreasing the pO_2 if the supplied cathode gas on the degradation of the anode supported Ni-YSZ/YSZ/LSM-YSZ single cell?
4. Does the quality of air supplied on the cathode side of the anode supported Ni-YSZ/YSZ/LSM-YSZ single cell, have any influence on the degradation of the cell? This question is investigated by exchanging the 21 % oxygen in nitrogen environment by compressed air.

6.2 Experimental

Cell preparation. Two batches of four anode supported Ni-YSZ/YSZ/LSM-YSZ cells were prepared. Both batches were prepared by screen printing 4x4 cm^2 LSM-YSZ inks onto 5x5 cm^2 Ni-YSZ/YSZ half cells, drying and sintering at 1050 °C for 2 hours. Subsequently LSM contact layers were printed onto the cells. Half cells were nominally identical for both batches, but the LSM-YSZ screen-printing inks were slightly different. The LSM-YSZ composition was the same, but different solvents/dispersants/binders

were used. Therefore, the microstructure of the cathode is likely to be different for each of the batches, and performances of different batches are not entirely comparable. Batch 1 was printed with the same ink, and at the same time, as the symmetrical cells discussed in Chapter 4.

Cell characterisation. The cells were tested in alumina test houses in a Fuelcon rig. Current collection plates were applied, a nickel plate at the anode side, a gold plate at the cathode side. Ni-YSZ and LSM gas distribution plates were applies at the anode and cathode side, respectively. Finally standard glass-ceramic composite seals [2] were applied. Gas tightness was achieved by heating the cell in air to 1000 °C, at a heating rate of 1 °C/min and adding 10 kg of weight on top of the cell. At 1000°C the anode side of the cell was reduced, first in humidified 9 % hydrogen in nitrogen, then in 100 % hydrogen. After sealing of the cell and reduction of the anode the temperature was decreased to the testing temperature, 750°C. The test rig and method is described in detail in [3].

Impedance spectra were recorded using the built-in impedance analyser of the Fuelcon rig, from 0.21 to 82541 Hz, at 15 points per decade. The recorded impedance spectra were evaluated by applying the Kramers Krönig method, using KKtest [4]. Analysis of the spectra was performed using Zview 2. Further analysis of the impedance spectra was carried out using ADIS [5]. In some cases dc characteristics of the cell were also investigated by recording IV curves.

An overview of the cell tests performed using the different batches is given in Table 6.I.

TABLE 6.I. Overview of batches and cell tests performed. All cells were tested at 750 °C. The anode was supplied with a 25 l/h, 5 % humidified, H_2 flow at the anode side. In test 2.1, a higher anode gas flow of 50 l/h was supplied for some time. The cathode was supplied with a 43 l/h gas flow.

Cell used	**Time (h)**	**Current density**	**Cathode gas**	**IV curves, temperature /gas changes after**
Batch 1				
1.1	a. 400 b. 120 c. 24 d. 210 e. 140 f. 620	a. OCV b. OCV c. 0.5 A/cm^2 d. OCV e. OCV f. 0.5 A/cm^2	21 % O_2 in N_2	a. gas & temperature changes b. - c. - d. gas & temperature changes e. - f. -
1.2	100	OCV	21 % O_2 in N_2	-
1.3	a. 490 b. 500 c. 500 d. 24	a. OCV b. 0.5 A/cm^2 c. 0.5 A/cm^2 d. 0.5 A/cm^2	a. 21 % O_2 in N_2 b. 21 % O_2 in N_2 c. 5 % O_2 in N_2 d. . 21 % O_2 in N_2	a. gas changes, IV curves b. gas changes, IV curves c. - d. -
Batch 2				
2.1	a. 10 b. 800	a. OCV b. 0.5 A/cm^2	a. 21 % O_2 in N_2 b. 21 % O_2 in N_2	a. gas & T changes, IV curves b. gas changes, IV curves
2.2	Performance test			
2.3	a. 100 b. 620 c. 530 d. 700	a. OCV b. OCV c. 0.5 A/cm^2 d. 0.5 A/cm^2	a. 21 % O_2 in N_2 b. 21 % O_2 in N_2 c. 21 % O_2 in N_2 d. Compressed air	a. gas & temperature changes b. gas changes, IV curves c. gas changes, IV curves d. gas changes, IV curves

6.3 Results and discussion

Impedance spectra

The recorded impedance spectra were evaluated using KKtest. The recorded data were noisy, showing an error up to 2%, which meant that DRT

(distribution of relaxation times), as applied on the symmetrical cells in the previous chapters, could not be calculated.

Cell performance

The cell in test 2.2 was tested for cell performance, for comparison with comparable cell tested previously by our group. The ASR values, corrected for fuel utilisation [3]are shown in Table 6.II. The IV curves are shown in Figure 6.1.

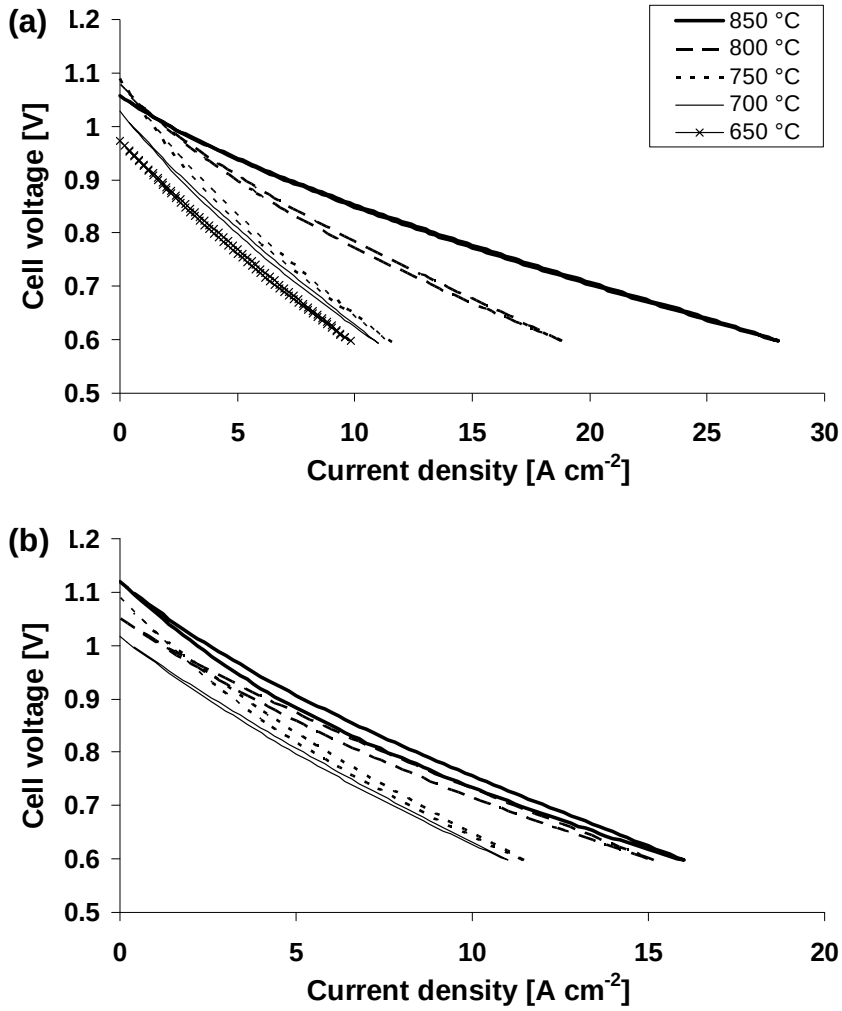

Figure 6.1. IV curves of test 2.2. (a) With changing temperature, cathode: air, anode: H_2 with 4 % H_2O, (b) At 750°C with changing gas conditions: Cathode gas: (-----) and (——): compressed air; (– – –) and (▬▬): O_2. Anode gas: (▬▬) and (----): H_2 with 4 % H_2O; (——) and (– – –): H_2 with 20 % H_2O.

TABLE 6.II. ASR values (corrected) for test 2.2

Anode gas	**H_2, 4% H_2O**	**H_2, 20% H_2O**	**H_2, 4% H_2O**	**H_2, 20% H_2O**
Cathode gas	**Air**	**Air**	**Oxygen**	**Oxygen**
Temperature				
850 °C	0.21 Ωcm^2	0.21 Ωcm^2	0.18 Ωcm^2	0.19 Ωcm^2
750 °C	0.61 Ωcm^2	0.57 Ωcm^2	0.46 Ωcm^2	0.46 Ωcm^2
650 °C	2.27 Ωcm^2	2.08 Ωcm^2	1.84 Ωcm^2	1.59 Ωcm^2

Anode and cathode contributions in the anode supported Ni-YSZ/YSZ/LSM-YSZ single cells

Previous studies [6, 7] have found at least five contributions to the impedance spectra of the Ni-YSZ/YSZ/LSM-YSZ single cell. In Table 6.III the contributions are summarised.

TABLE 6.III. Contributions to the EIS spectra of the single cell [6, 7]

Electrode	**Arc**	$\boldsymbol{F_{summit}}$ **at** 750 °C (Hz)
LSM/YSZ	Cathode I	1800-26100
Ni/YSZ	Anode	1000-1510
LSM/YSZ	Cathode II	100-825
Mostly Ni/YSZ	Diffusion	20-65
Ni/YSZ	Conversion	3-25

By applying gas changes to the single cell, some of the contributions from Table 6.III could be found. When applying gas changes at the cathode side, these should only affect the cathode contributions, and the same goes for the anode gas changes which should only affect the anode contributions. Moreover, it was found that cathode arc I was independent of pO_2, see Chapter 4 [7]. Therefore this arc is not expected to change the impedance spectrum when changing gas compositions. Gas changes of both anode and cathode gas were carried out and the location in the frequency spectrum of the anode and cathode contributions were determined by recording impedance spectra. This was done for several tests (see Table 6.I), and the results were very close for each test. Here, the results from test 2.3 were used. The difference and ADIS plots are shown in Figure 6.2. From this

figure it can be seen that at the applied conditions, anode changes were found at 3 and 200 Hz, while the cathode changes were found at 1 and 300 Hz. The low frequency affected by both anode and cathode gas changes is probably the diffusion. As observed before the diffusion arc was more sensitive for anode gas changes than for cathode gas changes [7]. The anode change at 200 Hz was ascribed to the anode arc. Ramos et al. [7] mention that the frequency of the anode arc decreases with lower H_2O content in the anode gas.

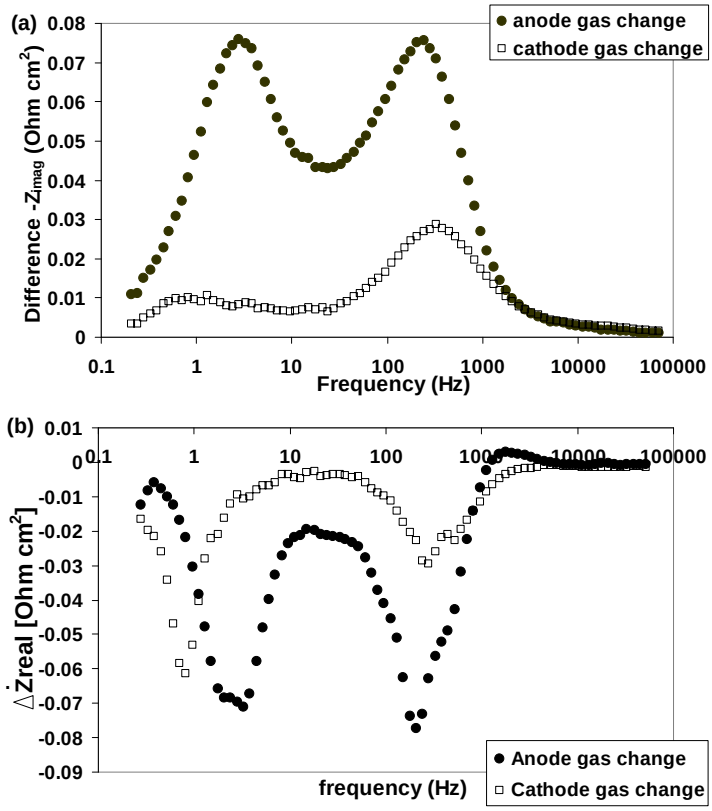

Figure 6.2. (a) Difference plot. (b) ADIS plot. Conditions: gas changes at OCV at 750°C on Ni-YSZ/YSZ/YSZ-LSM single cell; test 2.3. (●) Anode gas change: 25 l/h H_2, 4% humidity to 20% humidity. (■) Cathode gas change: 140 l/h 21% O_2 in N_2 to 100% O_2.

As in this study the H_2O content applied was lower than often applied in literature [6, 7]; 4% in degradation studies, and 20% for the anode gas change, this could explain the low frequency of the anode contribution. Cathode arc II was reflected by the change at 300 Hz. The fact that the anode and cathode contributions were located very close to each other in the

frequency spectrum makes it hard to separate them. Therefore it was not possible to deconvolute the impedance spectra recorded at the chosen conditions of the anode supported Ni-YSZ/YSZ/LSM-YSZ single cells in a reliable way. Accordingly, from hereon R_s is defined as the value of Z_{real} at the highest measured frequency (82541 Hz), and R_p as the value of Z_{real} at the lowest measured frequency (0.21 Hz) minus R_s.

Comparison of the degradation of the LSM-YSZ/YSZ/LSM-YSZ symmetrical cell and anode supported Ni-YSZ/YSZ/LSM-YSZ single cell at OCV

The increase of R_p with time was determined using impedance spectroscopy of a symmetrical cell and a single cell (test 1.1) during operation at 750 °C, at OCV, using 21 % oxygen in nitrogen as the cathode gas. In the period of approximately 280 hours, the polarisation resistance of the symmetrical cell showed an increase of 67 mΩ·cm^2, or 29 %, while the single cell increased by 255 mΩ·cm^2, or 54 %. To determine which of the processes involved in the cell testing are affected by degradation over time, Bode and ADIS plots are shown in Figures 6.3 and 6.4, for the symmetrical and the single cell, respectively. In the case of the symmetrical cell, a process around 200 Hz was mainly affected by degradation over time. As discussed in Chapter 4, this frequency accounts for the co-limited processes of oxygen dissociation and surface diffusion. The very high frequency around 500 kHz was also affected by degradation over time. One possible explanation for this could be slight delamination of the cathode from the electrolyte. However, this seems unlikely as degradation at this frequency was continuous. Therefore, slow degradation of the electrode – electrolyte contacts must have occurred. The impedance spectra for the single cell were recorded up to 82561 Hz only. Therefore it could not be determined if the very high frequency region of the single was also affected by degradation over time. Nonetheless, the intermediate frequency region was affected. From Figure 6.4b it appears that there were two processes affected: one at approximately 300 Hz, and a shoulder appearing at around 100-200 Hz. The latter was possibly the same process as seen at the symmetrical cell: the co-limited process of oxygen dissociation and surface diffusion at the cathode. However, the other process, at 300 Hz was affected to a much greater extent. As this process was not observed for the symmetrical cell, it will be ascribed to charge transfer between Ni and YSZ in the anode [7]. It appears possible to compare degradation of a symmetrical cell with a single cell, however, the

affected process overlapped severely. Therefore, to be able to draw a final conclusion, different testing conditions should be chosen, where the frequencies of the processes are expected to be shifted further apart, for example with a higher humidity at the anode.

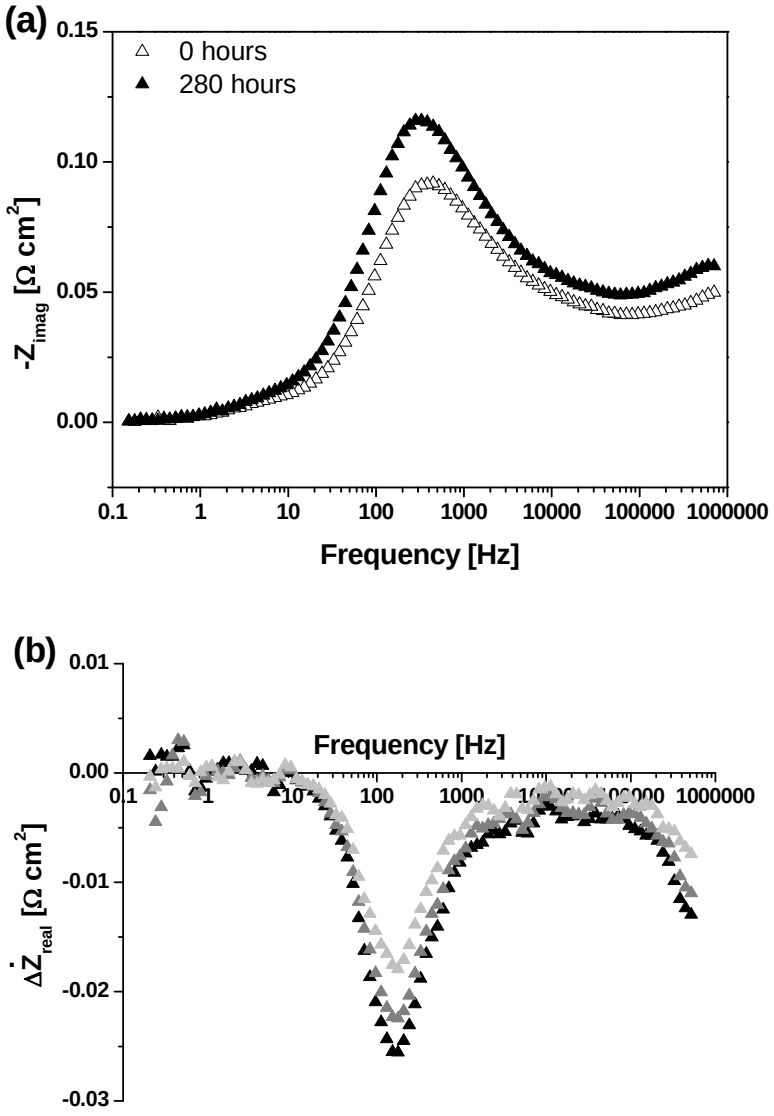

Figure 6.3. Symmetrical LSM-YSZ/YSZ/LSM-YSZ cells (a) Bode and (b) ADIS plots of impedance spectra, corrected for inductance (▲) 280-0 hours, (▲) 189 – 0 hours, (▲) 95 – 0 hours. Conditions: 750 °C, 6 l/h in 21 % O_2 in N_2, OCV, 280-0 hours.

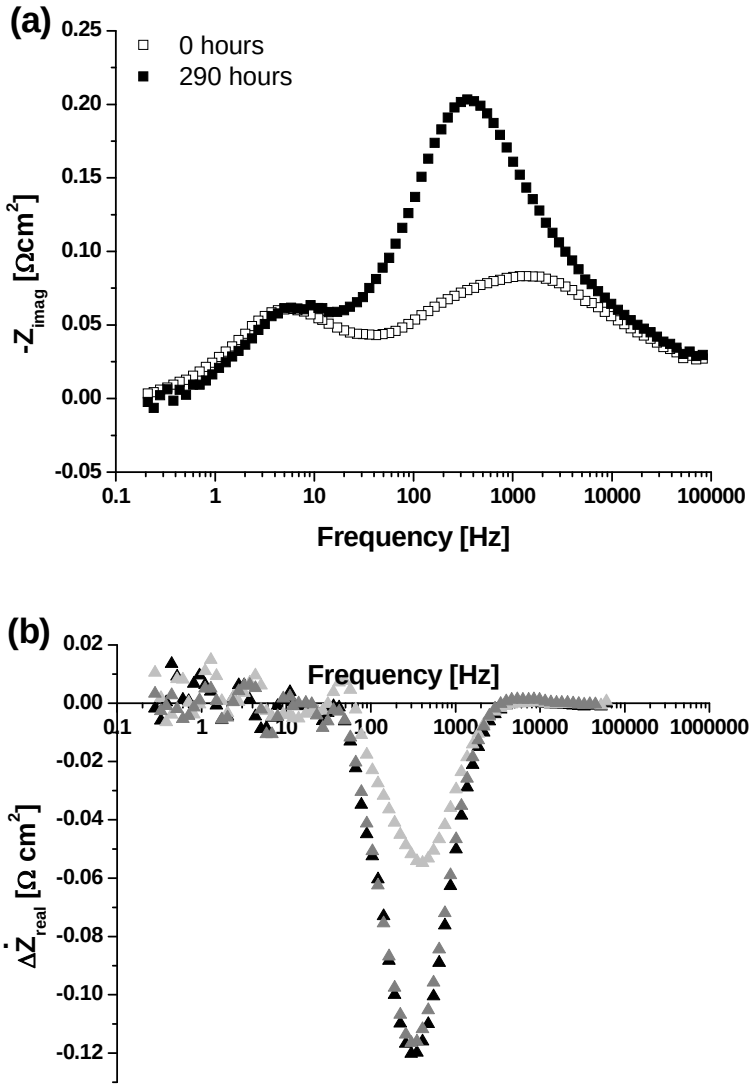

Figure 6.4. Anode supported single Ni-YSZ/YSZ/LSM-YSZ cell; Test 1.1 (a) Bode and (b) ADIS plots of impedance spectra, corrected for inductance: (▲) 290-0 hours, (▲) 146 – 0 hours, (▲) 73 – 0 hours. Conditions: 750 °C, 43 l/h 21 % O_2 in N_2 at the cathode, 25 l/h H_2 (4 % humidified) at the anode, OCV, 290-0 hours.

Furthermore, testing a symmetrical cell with Ni-YSZ anodes on both sides of the electrolyte at the same testing conditions could help determine the anode processes affected by degradation over time.

Comparison of the degradation of the anode supported Ni-YSZ/YSZ/LSM-YSZ single cell at OCV and at 0.5 A/cm^2

Single cell 1.3 was first tested at OCV for 500 hours, after which a current of 0.5 A/cm^2 was started. The results from test 1.3 are shown in Figure 6.5. As expected the ASR of the cell decreased significantly when starting the current [8]; the ASR decreased from 0.92 Ω·cm^2 at OCV to 0.46 Ω·cm^2 at 0.5 A/cm^2. Moreover, while at OCV the cell was degrading significantly from 0.58 Ω·cm^2 to 0.92 Ω·cm^2 during the first 500 hours, at 0.5 A/cm^2 the cell resistance was almost stable. At 0.5 A/cm^2 the cell even activated slightly, from 0.46 Ω·cm^2 to 0.44 Ω·cm^2 in the first 24 hours under current. Afterward it degraded slightly again, back to 0.46 Ω·cm^2 over 450 hours.

However, the cell voltage did not show the same trend; the cell voltage showed a small increase at OCV of 24 mV/1000 hours, a small increase when starting the 0.5 A/cm^2 current, followed by a decrease of 59 mV/1000 hours. It is unclear why the measured cell voltage did not behave according to the increase in cell resistance.

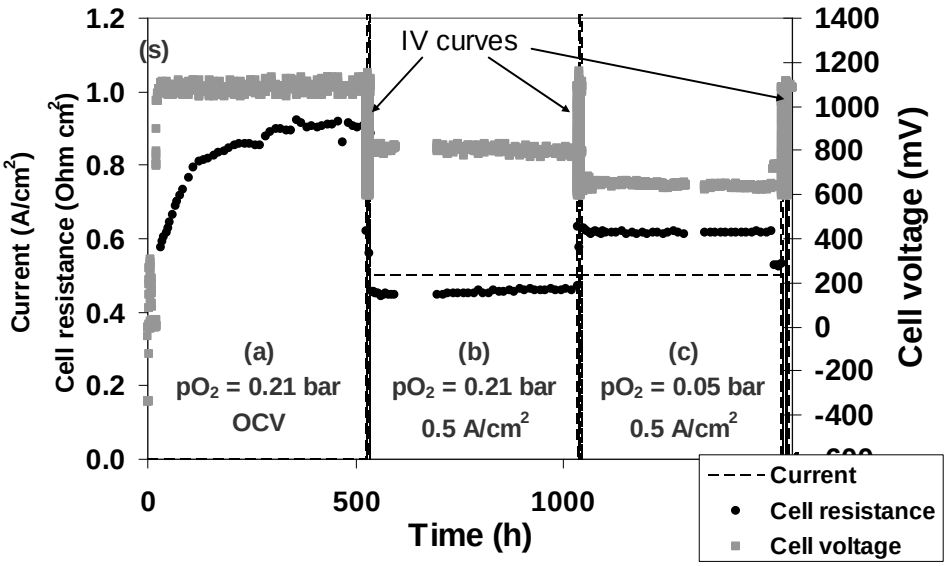

Figure 6.5. History of cell test 1.3. Conditions: 25 l/h H_2 (4 % humidified) on anode side; 43 l/h on cathode side. (s) start-up period. (a) 750°C, OCV, 21% O_2 in N_2 on cathode. (b) 750°C, 0.5 A/cm2, 21% O_2 in N_2 on cathode; (c) 750°C, 0.5 A/cm2, 5% O_2 in N_2 on cathode. IV curves and EIS recordings at different gas compositions.

Comparison of the degradation of the anode supported Ni-YSZ/YSZ/LSM-YSZ single cell at 0.5 A/cm^2 at a pO_2 at the cathode of 0.21 and 0.05 bar

The cell of test 1.3 was finally subjected to harsher conditions by decreasing the pO_2 of the cathode gas from 0.21 to 0.05 bar, see Figures 6.5 and 6.6. By doing this the cell voltage decreased, and the ASR increased. The trend of degradation was very similar at either pO_2; a short activation period of 50 hours was observed, after which the ASR of the cell is stable.

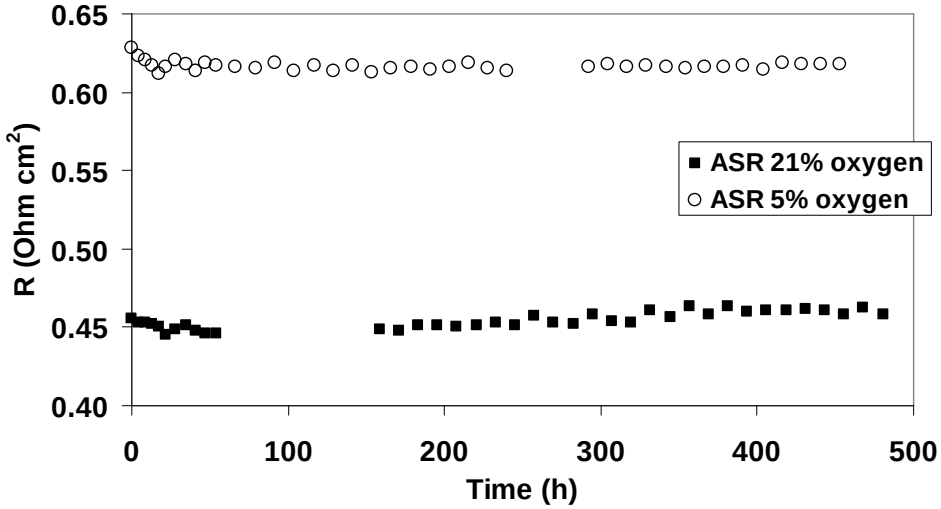

Figure 6.6. Development of ASR under different cathode gas compositions, test 1.3. (■) ASR cathode gas: 21 % O_2 in N_2; (○) ASR cathode gas: 5 % O_2 in N_2. Other conditions: 750°C, 0.5 A/cm^2, 43 l/h at the cathode, 25 l/h H_2, 4 % humidified, at the anode.

The influence of the quality of the cathode gas on the degradation of the anode supported Ni-YSZ/YSZ/LSM-YSZ single cell

Limited degradation was observed at 0.5 A/cm^2 applying a cathode gas of 21 % O_2 in N_2. When changing the cathode gas to compressed air however, the cell resistance started to degrade. This was observed in test 2.3; the development of the ASR is shown in Figure 6.7.

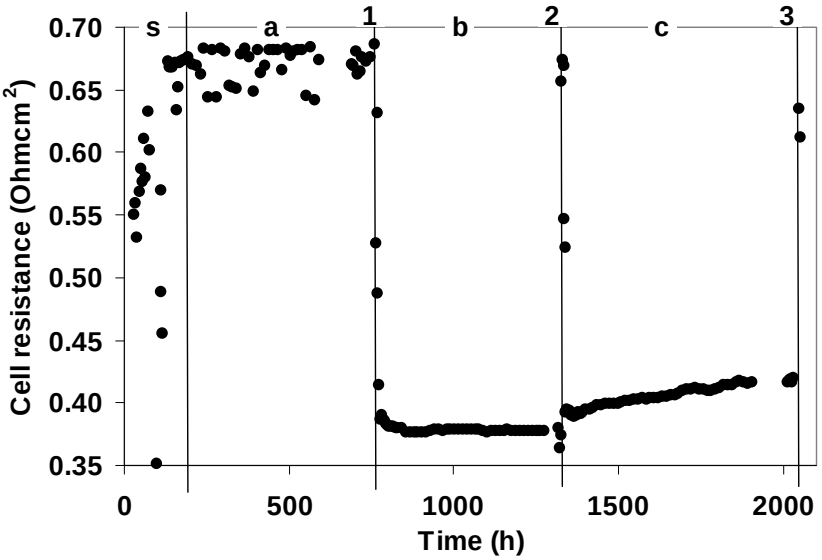

Figure 6.7. Development of cell resistance with time in cell test 2.3. Conditions: 25 l/h H_2 (4 % humidified) on anode side; 43 l/h mixture of 21 % O_2 in N_2 or compressed air on cathode side. (s) start-up period including testing at 850-650°C at different gas compositions. (a) 750°C, OCV, 21 % O_2 in N_2 on cathode. (b) 750°C, 0.5 A/cm^2, 21 % O_2 in N_2 on cathode. (c) 750°C, 0.5 A/cm^2, compressed air. (1), (2) and (3) IV curves and EIS data at different gas compositions.

Both in the case of 21 % O_2 in N_2 and compressed air at the cathode at 0.5 A/cm^2, a short period (up to 100 hours) of decreasing cell resistance occurred. Afterwards in the case of 21 % O_2 in N_2 the cell resistance stabilised, while in the case of compressed air the cell resistance started to increase. In Figure 6.8 the development of R_s and R_p with both gasses is shown. It was found that R_s and R_p showed a similar trend as did the total cell resistance. The increase of the cell resistance observed in the case of compressed air was caused by impurities in compressed air that are not present in the oxygen in nitrogen mixture. Furthermore, the increase should affect the cathode and/or cathode-electrolyte interface only, as the anode conditions were not changed in this experiment. To investigate which processes in the cathode were affected by impurities, a difference plot of Z_{imag} at different times during the test with compressed air is shown in Figure 6.9a, along with the corresponding ADIS plot in Figure 6.9b.

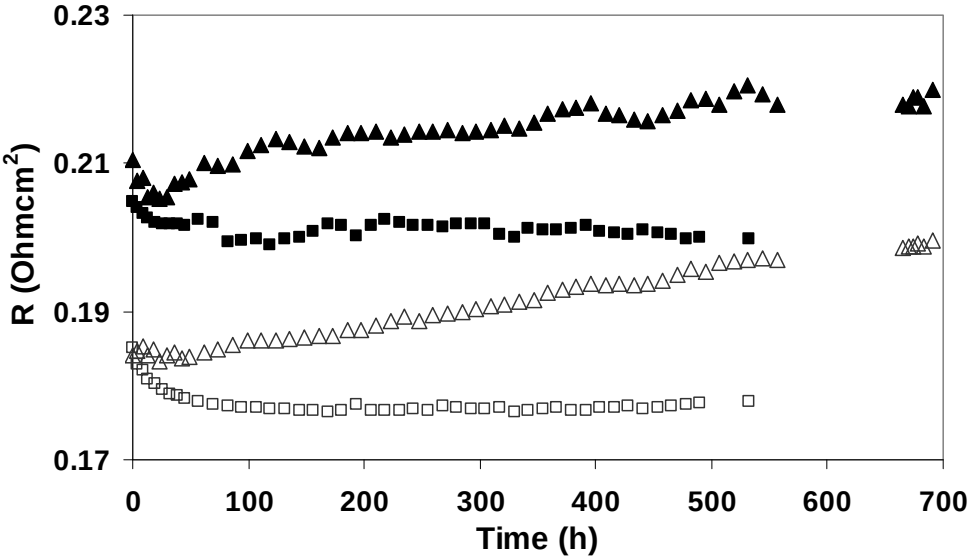

Figure 6.8. Development of R_s and R_p. (□) R_s 21 % O_2 in N_2; (■) R_p 21 % O_2 in N_2; (Δ) R_s compressed air; (▲) R_p compressed air. Conditions: 750°C, 0.5 A/cm^2, 43 l/h air at the cathode, 25 l/h H_2, 4 % humified, at the anode.

Three frequencies appeared to be affected by impurities in compressed air: a small effect was observed around 1 Hz, while a more significant effect was observed at 200 Hz and at 20-30 kHz. The process at 200 Hz was observed to cause a relatively quick change, during the first 100 hours, after which it did not change further. To confirm that only the cathode and/or cathode-electrolyte was affected by changing the cathode gas from 21 % oxygen in nitrogen to compressed air, both cathode and anode gas changes were carried out before and after the period in compressed air. The impedance response was thereby recorded at OCV in 21 % oxygen in nitrogen and in pure oxygen, with the anode gas being 4 % humidified hydrogen. Afterwards the cathode gas was kept at 21 % oxygen in nitrogen and the impedance spectra were recorded with 4 % humidified hydrogen, and 20 % humidified hydrogen. The resulting difference plot is shown in Figure 6.10. It was observed that, unexpectedly, the anode response was also changing during the period in compressed air. The low frequency response at 3 Hz has not changed, but the response at around 100 Hz was affected. Confirmed by the gas changes was that the cathode was mainly affected at around 100 Hz. It is unclear why the anode response changed during the

period at compressed air, while it had not changed during the period at 21 % oxygen in nitrogen.

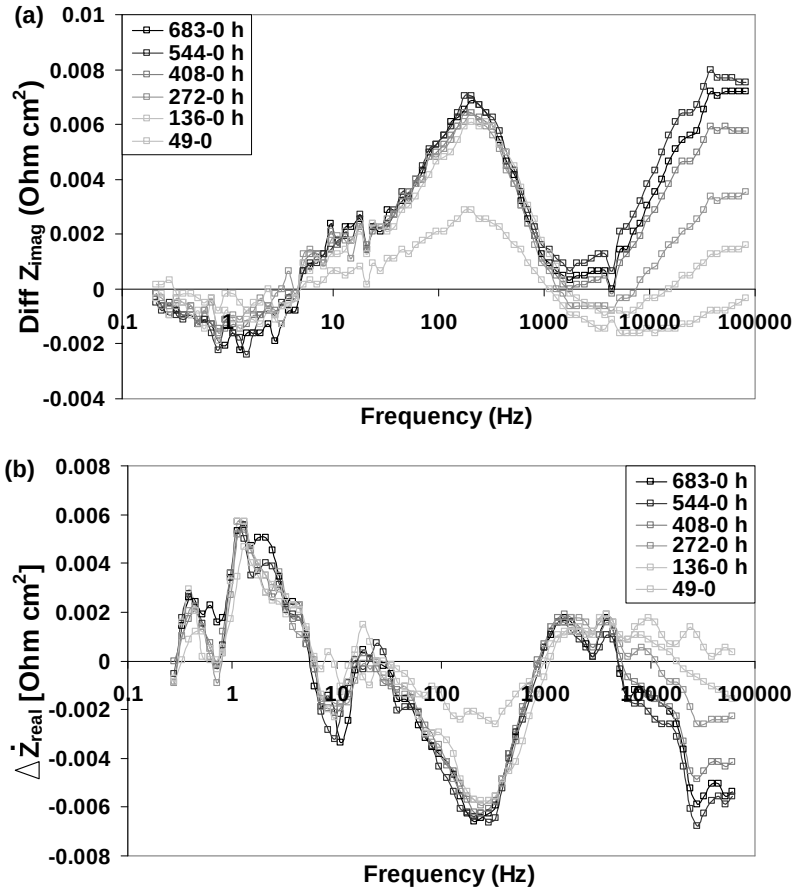

Figure 6.9. (a) Difference plot. (b) ADIS plot. Development of the change of Zimag with time. 750°C, 0.5 A/cm^2, 43 l/h compressed air at the cathode, 25 l/h H_2 at the anode.

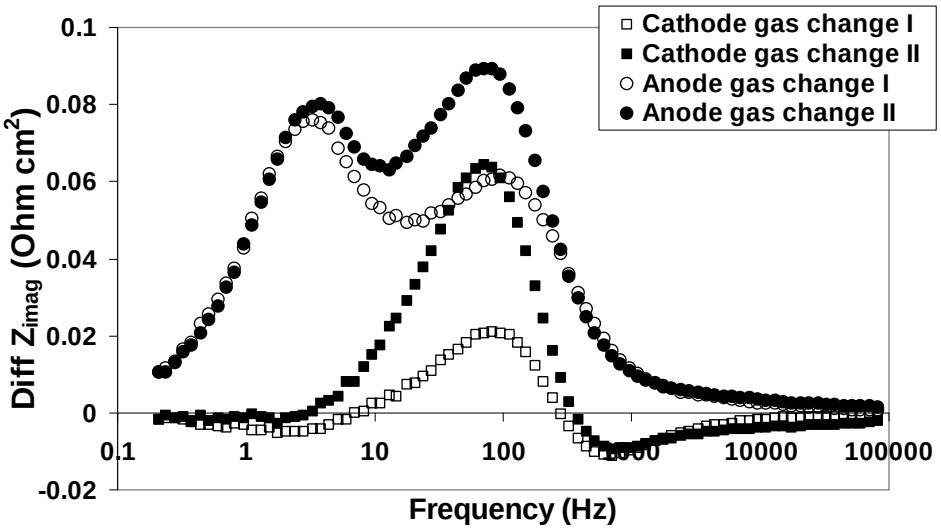

Figure 6.10. Difference plot. Difference for gas changes at OCV before and after degradation period at 750°C, 0.5 A/cm^2, 43 l/h compressed air at the cathode, 25 l/h H_2 at the anode. (□/■) cathode gas change oxygen – air; (○/●) anode gas change 4% humidity – 20% humidity.

6.4 Conclusion

The chosen testing conditions for the single cell testing led to overlapping cathode and anode contributions of the impedance data in the frequency domain. Therefore it was not possible to deconvolute any of the impedance spectra obtained reliably.

At OCV the results for the LSM-YSZ/YSZ/LSM-YSZ symmetrical cell and the anode supported Ni-YSZ/YSZ/LSM-YSZ single cell appeared comparable, at least the location of the contributions in the frequency spectrum. However, the anode and cathode contributions were overlapping at the chosen operation conditions, making quantitative comparison impossible. Comparing the single cell at OCV and under current (0.5 A/cm^2) led to the conclusion that the behaviour of the single cell is very different at OCV than under current. While at OCV a significant increase of the cell resistance with time was observed, under current a slight decrease of the cell resistance was observed during the first 100 hours, after which a slight increase occurred. So even if the symmetrical and single cell lead to comparable results at OCV, the symmetrical cell cannot predict all of the behaviour of the single cell under current. As SOFCs will always be run under current in practice, this led to the conclusion that the symmetrical cell may be of limited value for generating quantitative information about

degradation rates for single cells. Nonetheless, symmetrical cell testing will still be valuable for qualitative investigation on stability trends and sensitivity to impurities.

Harshening the testing conditions of the anode supported Ni-YSZ/YSZ/LSM-YSZ cell by decreasing the pO_2 of the cathode gas to 0.05 led to an immediate increase of the cell resistance. However, it did not affect the degradation of the cell with time.

Impurities in air did have a significant effect on degradation of the cell, as seen before for the symmetrical cells. However, changing the cathode gas composition, from 21 % oxygen in nitrogen to compressed air, appeared to have caused degradation of both the anode and the cathode contributions, which could not be explained.

6.5 References

1. S. Primdahl, P. V. Hendriksen, P. H. Larsen, B. Kindl and M. Mogensen, **16**, 932 (2001).

2. J. G. Larsen, P. H. Larsen and C. Bagger, **10/191432**(US 6828263) (2004).

3. M. Mogensen and P. V. Hendriksen, in *High Temperature Solid Oxide Fuel Cells - Fundamentals, Design and Applications*, S. C. Singhal and K. Kendall, Editors, p. 261, Elsevier, Oxford (2003).

4. B. A. Boukamp, *J. Electrochem. Soc.,* **142**(6), 1885 (1995).

5. S. H. Jensen, A. Hauch, P. V. Hendriksen, M. Mogensen, N. Bonanos and T. Jacobsen, *J. Electrochem. Soc.,* **154**(12), B1325 (2007).

6. R. Barfod, M. Mogensen, T. Klemensø, A. Hagen, Y. -. Liu and P. V. Hendriksen, *J. Electrochem. Soc.,* **154**(4), B371 (2007).

7. T. Ramos, J. Hjelm, M. Wandel, A. Hagen and M. Mogensen, *ECS Trans.,* **13**(26), 235 (2008).

8. S. Koch, M. Mogensen, P. V. Hendriksen, N. Dekker and B. Rietveld, *Fuel Cells,* **6**, 117 (2006).

9. S. Koch, P. V. Hendriksen, M. Mogensen, Y. -. Liu, N. Dekker, B. Rietveld, B. de Haart and F. Tietz, *Fuel Cells,* **6**, 130 (2006).

CHAPTER 7

General discussion, conclusions and outlook

7.1 General discussion and conclusions

LSM-based cathodes are still among the preferred cathodes for SOFCs, and therefore remain of major scientific and technological importance. Many factors play a role when searching for the optimal LSM-YSZ cathode, including composition, preparation method and operating conditions. The focus of this PhD thesis was the investigation of degradation of the LSM-YSZ cathode of the anode supported Ni-YSZ/YSZ/LSM-YSZ solid oxide fuel cell, at realistic operating conditions. Realistic operating conditions were explored here by first testing with relatively pure and dry oxidant gas supplied to the cathode, while subsequent controlled steps towards less pure oxidant gas were taken, to investigate the influence of successively more realistic operation conditions on the degradation of the LSM-YSZ cathode.

Development of an equivalent circuit for the YSZ/LSM-YSZ half-cell of the SOFC can shed light on the processes contributing to the polarisation resistance. Moreover, when applying the equivalent circuit to EIS data from long term experiments, information can be gathered on which processes are affected by degradation of the SOFC over time. When these processes are known, efforts to improve the SOFC can be focussed on the processes with the largest contribution, or the easiest to improve. To develop an equivalent circuit, the primary condition that has to be met is to ensure high quality of the EIS data; no change of the testing system should take place during measuring, a sufficiently large frequency spectrum should be covered, with as many data point as possible. Secondly, EIS spectra have to be recorded on the same sample at different conditions; at least at varying temperature and atmospheres. Even when these conditions are met, it can still be hard to deconvolute the EIS spectra, as the frequency of appearance of some of the processes might overlap. In this PhD study, the use of DRT (distribution of relaxation times) data analysis method has proven very helpful, as the spectrum resulting through DRT transformation separated the overlapping processes to some extent and the shape of the peaks yields information about which type of circuit element is suitable for description of the process. A suitable, physically meaningful, equivalent circuit was identified for the LSM-YSZ/YSZ/LSM-YSZ symmetrical cell, which describes the processes contributing to the polarisation resistance, and fits the observed impedance response over a wide range of experimental conditions well. Deconvolution of impedance data into process specific contributions using the identified

equivalent circuit was carried out as a function of time, yielding process specific cathode degradation kinetics. In an effort to extend the validity of the equivalent circuit to the cathode of full cells, long term experiments were carried out both at OCV and at current. However, the EIS data quality proved of insufficient quality for equivalent circuit development. Moreover, anode and cathode processes overlapped to such an extent that the processes were not separable. Therefore, different operating conditions, or different microstructures should be applied. This will lead to shifting of the frequency of the processes, possibly enabling separation.

Nonetheless, the general features and main relaxation frequencies of the cathode on a symmetrical cell is reflected in response observed in the full cell, as indicated by similarities in the change in impedance response due to oxygen partial pressure variations and cathode side degradation.

When applying current to the single cells the EIS spectra changed significantly and degradation decreased to a minimum. This is expected as the formation of water at the anode side of the SOFC decreases the polarisation resistance of the processes at the anode. Since deconvolution of the spectra was not possible, we were unable to determine if the increased current density had also influenced the polarisation resistance of the cathode. Symmetrical cell testing is very valuable when considering initial screening of new materials or microstructures, ranking them by performance, however from this study we are unable to conclude whether or not symmetrical cell testing of the cathode also has a predictive value for long term single cell testing.

The atmosphere in which the SOFC cathode is operated influences the degradation speed. Part of this degradation was shown to be caused by humidity in the air and possibly impurities in air. By drying and cleaning the air degradation could be prevented to some extent. Therefore, to extend the lifetime of the SOFC, it might be worthwhile to dry and/or clean the air before it entering the SOFC. Whether or not this is an attractive route depends on economics; weighing the costs of the filter against the prolongation of the SOFCs lifetime. Also the lifetime and operational costs of such a filter should be considered.

As has been shown previously [1, 2], the microstructure, layer thickness, and relative perfection of the functional ceramic layer that constitutes the cathode, is of great importance to its performance, impedance characteristics and durability. Cathodes with varying amounts of macroscopic flaws and of different microstructure, but otherwise identical compositions, were tested and it was shown that although the same processes limit the performance, their magnitude and characteristic relaxation frequency varies significantly. The microstructure should be optimised, considering both the initial performance and the degradation over time, although the best microstructure for initial performance might not be the best microstructure on the long term, for example caused by faster or more severe sintering. Additionally, when optimising the microstructure for commercial purposed the costs for improving the microstructure should be considered. For example, high time and energy consumption for making the materials finer; or complicated methods for applying the cathode to the electrolyte, are not acceptable from an economical point of view.

7.2 Main conclusions

Some of the major findings of this work are:

- A physically relevant equivalent circuit was identified for the LSM-YSZ/YSZ/LSM-YSZ symmetrical cells studied in this work, and was used to deconvolute impedance data recorded during ageing of samples under different oxidant gas atmospheres. This approach has improved understanding of the factors influencing the degradation kinetics of processes dominating the polarisation resistance of the LSM-YSZ cathode, and the results indicate that it are the processes at the electrode surface (on the LSM particle surface and at the LSM-YSZ-gas triple phase boundaries) that are most affected by impurities in air.
- Degradation of the LSM-YSZ cathode was partially prevented by drying/cleaning of the applied air. Humidity, possibly along with impurities in air, is a major cause of degradation at the LSM-YSZ cathode.
- Optimisation of the LSM-YSZ electrode performance is very important, in particular since a strong link between cathode overpotential and degradation rate was shown previously. Thus, better performing LSM-YSZ cathode should lead to lower degradation rates for this electrode. Further, as impurities have been shown to affect the degradation rate of

7.3 Outlook

Several issues could be investigated further, for example:

- The microstructure of the cathode material used in this PhD thesis was chosen not optimal from a technological point of view. For increased performance the microstructure of the cathode material should be optimised, since in the current microstructure many holes were present, and some lumps of LSM and YSZ were found. A better and finer mixing of LSM, YSZ and pores could lead to larger triple phase boundary and therefore an improved performance of the cathode. Also the contacting with the electrolyte should be improved.
- Long term experiments with single SOFCs should be repeated, under conditions yielding improved resolution of the different overlapping processes in the impedance spectrum of the full cells, for example by carrying out experiments at more varying conditions, for example at a higher humidity at the anode, to avoid overlap of the anode and cathode processes in the impedance data. This way the impedance data can be deconvoluted and understanding of the different processes and their degradation can be improved.
- It became clear that impurities in air are one of the causes of degradation of the cathode. One of these impurities is water. The applied air could be analysed to discover which other impurities are present. Furthermore, controlled addition of impurities to clean oxidant gas is a methodology which could be applied to establish the lifetime limiting effect of various impurities on the LSM-YSZ cathode.

7.4 References

1. S. P. Jiang, *J. Mater. Sci.*, **43**, 6799 (2008).

2. M. J. Jørgensen, S. Primdahl, C. Bagger and M. Mogensen, *Solid State Ionics*, **139**, 1 (2001).